2017

Flexural demand of columns in Special Moment Frames

Michailina Hadjiyiangou
Iowa State University

Flexural demand of columns in Special Moment Frames

by

Michailina Hadjiyiangou

A thesis submitted to the graduate faculty

in partial fulfillment of the requirements for the degree of

MASTER OF SCIENCE

Major: Civil Engineering (Structural Engineering)

Program of Study Committee:
Jiehua J. Shen, Major Professor
An Chen
Jeramy C. Ashlock

Iowa State University

Ames, Iowa

2017

TABLE OF CONTENTS

LIST OF TABLES

LIST OF FIGURES

LIST OF SYMBOLS

a	Horizontal distance from column face to RBS location
A_g	Gross cross sectional area
b	Length of RBS cut
b_f	Width of beam flange
c	Depth of cut at RBS center
d	Section depth
E	Young modulus of elasticity
F_u	Minimum specified ultimate strength
F_y	Minimum specified yield stress
F_{yb}	specified minimum yield stress of beam, ksi
F_{yc}	specified minimum yield stress of column, ksi
g	Acceleration due to gravity on earth
H	Story height
I_X	Moment of inertia about x-axis.
I_Y	Moment of inertia about y-axis.
M_{pt}	Plastic moment capacity of the smaller column (on the top of the column splice).
M_s	Bending moment at column splice level.
M_{uv}	additional moment due to shear amplification from the location of the plastic hinge to the column centerline based on LRFD load combinations, kip-in. (N-mm)
P_{uc}	required compressive strength using LRFD load combinations, including the amplified seismic load, kips (N)
P_s	Tensile axial force at column splice level, equal to AgFy.
P_{ty}	Nominal tensile strength of the smaller column (on the top of the splice).
r_X	Radius of gyration about x-axis.
r_Y	Radius of gyration about y-axis.
R_y	Ratio of expected yield stress to minimum specified yield stress
S_1	One second period spectral acceleration
S_s	Short period spectral acceleration
S_X	Section modulus about x-axis.
S_Y	Section modulus about y-axis.
t_f	Thickness of flange.
t_{bf}	Thickness of beam flange.
t_w	Thickness web.
T	Natural period of vibration
Z_b	plastic section modulus of the beam, in^3
Z_c	plastic section modulus of the column, in^3
Z_X	Plastic modulus about x-axis.
Z_Y	Plastic modulus about y-axis.
Z_{RBS}	Plastic modulus of RBS
Δ_i	Story drift at level i
δ_i	Story drift at level i
θ_i	Inter-story drift ratio at level i
ϕ	Resistance factor

ACKNOWLEDGEMENTS

Foremost I would like to express my sincere appreciation for my advisor Dr. Shen whose mentoring and encouragement made this thesis possible. The door to Professor Shen's office was always open for advice whenever I had a question and I am very thankful I had the opportunity to work with him.

I would also like to gratefully acknowledge Dr. Seker as my second mentor. Without his participation and insights, this work could not have been successfully conducted.

Finally, I must express my very profound gratitude to my father Panayiotis, my mother Georgia and to Stylianos for providing me with unfailing support and continuous encouragement. This accomplishment would not have been possible without them.

ABSTRACT

This study investigates the flexural demand in columns in the following contexts: the demand on the column splice, the flexural demand distribution (bending moment diagram) shape, and the moment distribution at beam-column joints. Incremental dynamic analysis (IDA) was carried out for a 15-story special moment frame subjected to 20 different ground motions. A newly developed demand-chain concept was employed together with IDA in assessing the seismic demand on column splices and strong column-weak beam mechanism, based on inelastic deformation demand on beam-to-column joints at three performance levels, the immediate occupancy (IO) level, the life safety (LS) level and the collapse prevention (CP) level at 2%, 4% and 6% of story drift ratio (SDR) respectively. The demand on column splice was evaluated in terms of peak normalized axial ratio, peak flexural ratio, and maximum combined axial and flexural demand-to-capacity ratio. This investigation concludes, with a combined IDA and demand-chain concept, that the flexural demand on the splice can reach as high as the nominal strength of the smaller section when the structure is subjected to the design earthquake. This study also presents systematically single curvature deformation patterns in the columns in contrast to the perfect double curvature (PDC) assumption used in code-based design of steel moment frames. Furthermore, this work reveals that plastic hinges may occur in the columns near beam-to-column joints when the frame is subjected to the life safety (LS) level of earthquake ground motions. This finding presents a challenge to the current methodology used in enforcing strong column-weak beam behavior in earthquake-resistant moment frames.

CHAPTER 1. INTRODUCTION

Seismic demand of steel moment frames has drawn the attention of researchers, mainly after the 1994 Northridge earthquake. The aforementioned incident revealed extensive and severe damage at welded moment connections (see Figure 1.1.1) and consequently led to in-depth investigations of the beam-to-column connections. Following the earthquake hazards, the Federal Emergency Management Agency (FEMA) sponsored a detailed investigation on steel moment frames conducted by SAC Steel Joint Venture which enlightened the seismic behavior of the moment frames [8]. This comprehensive study resulted in a revision of seismic provisions and introduced new design concepts. One of the revisions of AISC 341 [2, 3] suggested that the welded column splice connections should be formed as complete-joint-penetration (CJP) connections, in contrast to pre-Northridge column splices formed as partial-joint-penetration welded connections (PJP) as shown in Figures 1.1.2 and 1.1.3.

Shaw and Kanvinde [10] investigated the feasibility of PJP welded column splices used in the special and intermediate moment frame (SMF, IMF), as opposed to CJP welded connections suggested by current standards. To evaluate the seismic behavior of the connection, several PJP welded column splices were subjected to cyclic loading in their study, and the overall response along with the flexural demand of the splices were observed. The results suggested that the seismic performance of specimens was sufficient and PJP welds utilization in SMF could be efficient and cost-effective compared to CJP welds.

Additional investigation on column splices was conducted by Galasso et al. [9] by introducing a probabilistic seismic demand analysis (PSDA) framework to analyze the nonlinear dynamic results of 4- and 20-story steel moment frames. Assessment of the

demand was succeeded by performing IDA analysis and fragility assessment of selected pre-Northridge column splices with Partial-Joint-Penetration (PJP) welds in addition to methods of current practice for column splices. The results revealed that pre-Northridge welded column splices presented high risk of fracture in contrast to post-Northridge connections that displayed lower fracture risk.

Shen et al. [11] presented the first assessment study on seismic demand on column splices by introducing a new demand-chain concept for the first time. The demand on columns was calculated in terms of peak axial and flexural demand of the column splices in 4-, 9- and 20-story steel moment frames. These structures were subjected to a set of 20 ground motions. The excitations were classified into three categories based on the seismic response, from moderate damage to collapse prevention level. The outcomes indicated that the flexural demand of the splice reached 90% of the nominal capacity of the small column when the overall response of the frame was near collapse. Moreover, when the frame experienced severe damage, single curvature moment diagrams and plastic hinge formation in columns were observed in moderate to high-rise structures. The beam-to-column connection was also implemented as plastic hinge rotation (PHR) and correlated with the column splice demand. Findings revealed that when the plastic hinge rotation was equal to the expected capacity of 0.05 to 0.07 rad, the column splice demand appeared to reach the nominal capacity of the small column. The work presented in Shen et al. [11] has been used as a major reference in the seismic design code since its publication. Shen et al. divided 20 ground motions into three performance levels in their evaluations, successfully leading to developing the new demand-chain concept. However, each performance level was represented by a limited number of ground motion intensities. Further research in empowering the new demand-chain concept is to combine

it with incremental dynamic analysis (IDA) from deterministic evaluation to the combined deterministic and probabilistic assessment. The IDA is capable of introducing ever-increasing ground motion intensities, but has not been able to provide structure-specific evaluations.

Further research on the influence of various span lengths in column splice demand was conducted by Akbas et al. [5]. Various steel moment frames were utilized for the assessment with building configurations similar to the one used by Shen et al. [11]. The nonlinear analyses revealed that the seismic demand on column splices is influenced by the span length, while the overall response of the frame was not significantly affected. Additionally, increased demand was observed in frames with unequal span dimensions.

The aforementioned studies provided information to better understand the behavior and mechanisms of column splices in steel moment frames when subjected to seismic loads. However, IDA has not been implemented for a thorough investigation on the flexural demand, the bending moment diagram shape, and the moment distribution of joints. The progressive seismic response of a structure derived from dynamic pushover analysis could provide a comprehensive understanding of demand on column splices at several performance levels. IDA utilization for demand assessment offers the ability to establish correlations between the overall response of the structure and the intensifying flexural demand on column splices. The outcomes of previous studies indicate that the demand on column splices approaches the nominal capacity when beam-to-column connections reach the maximum rotation. Therefore the strong-column-weak beam (SCWB) requirement should be taken into consideration when interpreting the results.

This thesis presents a comprehensive evaluation of the flexural demand on column splices with the implementation of IDA to assess the overall response of a steel special

moment frame at three performance levels. The parameter employed for the IDA plot was the story drift ratio (SDR) in order to assess the overall response of the frame. First performance level was defined as immediate occupancy (IO) at 2% of SDR where the structure sustained minor damage to nonstructural and structural members, followed by the life safety (LS) level at which structural and nonstructural elements are expected to experience extended damage defined at 4% of SDR. Life safety is the expected performance level when the frame is subjected to the design earthquake, at which the behavior of the structure is not elastic and plastic hinge formation in structural members is initiated. The last performance level was specified as the collapse prevention (CP) level when the structure undergoes 6% of SDR and structural members are expected to sustain severe damage in addition to failure of nonstructural elements.

The objective of this study is to investigate the seismic demand on the column splices and establish the interrelation between the plastic hinge formation and the bending moment diagrams as the intensity of the ground motion is gradually increasing. Furthermore, the flexural demand on the columns and the design SCWB ratio will be evaluated to check the conservatism of current standards and the efficiency of the ratio in seismic behavior of steel moment frames. In addition, this study has demonstrated how the demand-chain concept and IDA can be combined successfully for the combined deterministic and probabilistic seismic performance evaluation.

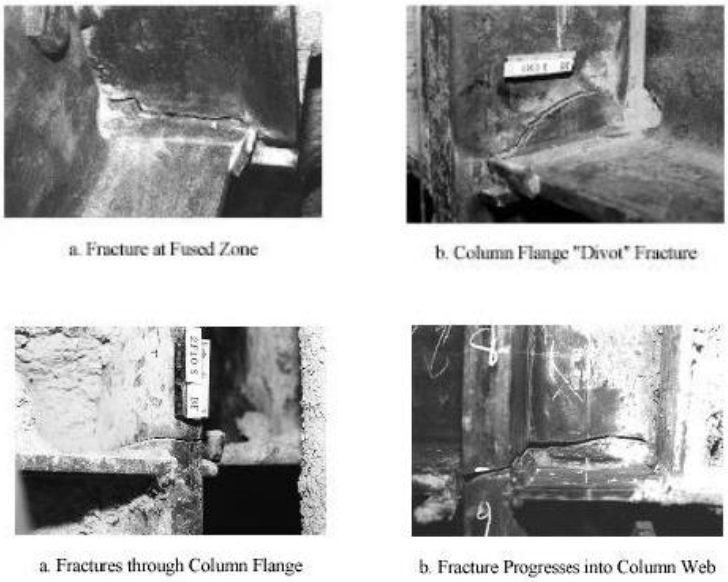

Figure 1.1.1. Failures of moment connections (1994 Northridge)

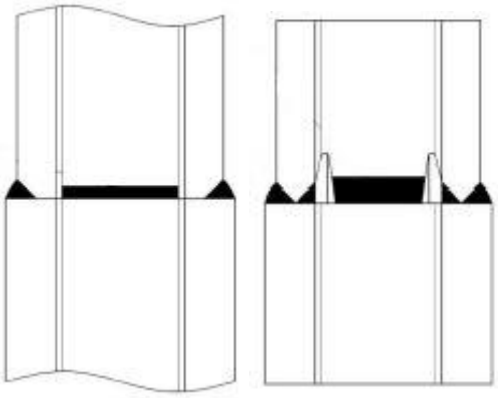

Figure 1.1.2. Pre-Northridge (left) and Post-Northridge column splice (right)

Figure 1.1.3. Post-Northridge welded column splice

CHAPTER 2. ANALYTICAL MODEL

2.1 Design of the 15-story special moment frame

For the purpose of this study, a 15-story Special Moment Frame (SMF) was designed based on seismic provisions in ANSI/AISC 341-16, ANSI/AISC 358-16 and ASCE 7-10 [1, 3, 4]. The building plans and elevation of the frame are similar to the one used by Shen et al. [11] and are given in Figure 2.1.1 and 2.1.2, respectively. The 15-story building represents moderate to high-rise buildings and it consists of two moment frames in the East-West direction and two braced frames in the North –South direction, as shown in Figure 2.1.1. The building plan is symmetrical with dimensions of 150 ft x 125 ft. For this study, only the moment frame design will be presented. The moment frame consists of five bays spaced at 25 ft and it includes two levels below seismic base with story height of 12 ft for the two basement levels, 18 ft for the first level and 13 ft for the upper levels. The columns below seismic base at B1 and B2 levels are pinned to the ground and horizontal displacement is not allowable. The columns on the base of the frame are assumed to be pinned at the foundation.

The 15-story office building was located in downtown Los Angeles, with site class D, S_S of 200%g and S1 of 100%g. The frame was designed with dead loads of 96 psf and 83 psf at floor and roof levels, respectively, in addition to live loads of 50 psf and 20 psf at floor and roof levels, respectively. The response modification factor (R) based on ASCE7-10 [4] was 8 for special moment frame, the overstrength factor (Ω_0) was equal to 3 and total base shear on the moment frame based on the seismic design parameters was approximately 1723 kips and it was distributed along the height of the building with proportion to the height and weight of each story level considering the first fundamental mode of the frame. The approximate period of the building according to design

parameters is 1.941 seconds. Column splices are located at the 2nd, 5th, 8th, 11th and 14th level of the frame while for the location of the splice on the column, this study will use the Primary Case from Shen et al. [11], for which the column splice location is 4ft above the floor elevation. The floor system of the building consists of beams which also provide lateral support to the girders, and a concrete slab with a thickness of 4 inches. The composite floor system of the building is to be rigid and serves as a diaphragm, which sustains and transfers loads in the vertical plane in addition to resisting lateral loads in the horizontal plane.

The frame was designed based on four requirements; the story drift limit, the column strength, the beam strength, and the strong column-weak beam (SCWB) requirement. As expected, the design was controlled by the drift limit as it was intended that the frame should be close to the story drift limit of 2% for this study. The same design goal, if applicable, is common in engineering practice since the members have smaller sections hence, the structure is cost effective. Due to the drift-limit-controlled design, the demand-over-capacity ratio of column, beams as well as the strong column-weak beam ratio are overdesigned, as shown in Tables 2.1.2, 2.1.5, 2.1.6 and 2.1.7. The final members are included in Table 2.1.1, and the design story drift limit corresponding to the final sections are displayed in Figure 2.1.3. All the members are wide-flange sections with a minimum yield strength of 50 ksi. The frame was subjected to the equivalent lateral loads in SAP2000, as they were estimated from the seismic parameters, and the story drift limit was calculated. The equation for the story drift ratio and the limit was

$$\delta_x = \delta_{xe} * C_d / I_e$$

$$\Delta_x = \delta_x - \delta_{x-1} \leq \Delta_a = 0.02 * h_{sx}$$

where the deflection amplification factor C_d was equal to 5.5 based on ASCE 7-10 and

the importance factor I_e equal to 1.0 since the structure is an office building, while the story relative displacement δ_{xe} was obtained from the analysis.

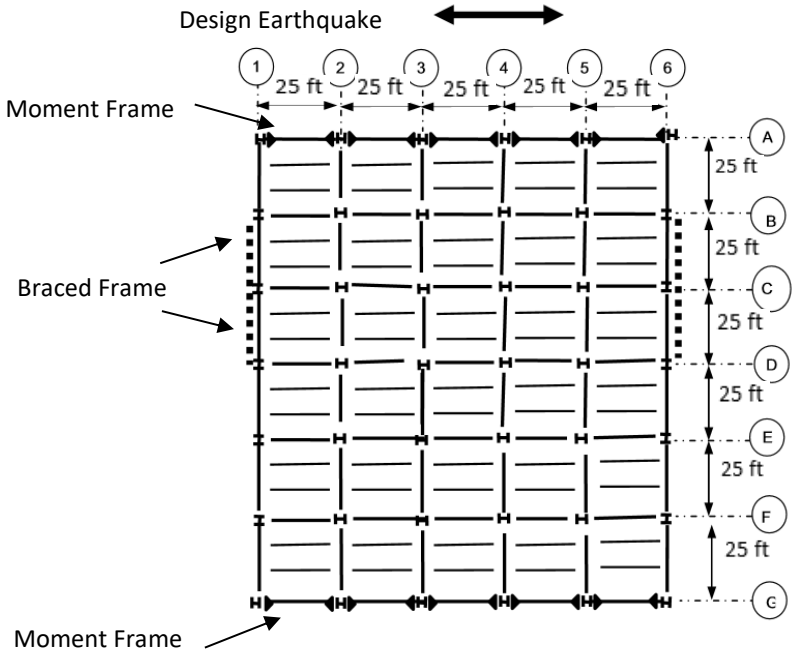

Figure 2.1.1. Building Plan

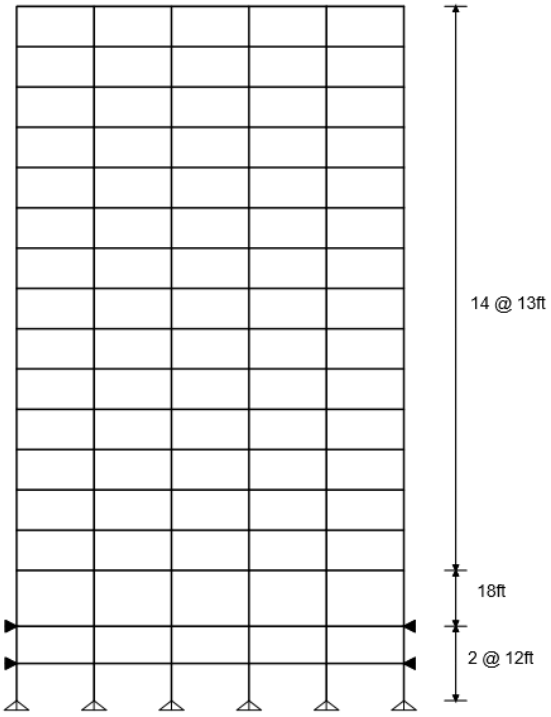

Figure 2.1.2. Moment frame on Line A

Table 2.1.1. Sections of 15-story SMF

Story	Exterior Column	Interior Column	Girder
15	W14X145	W14X176	W24X76
14	W14X145	W14X176	W24X76
13	W14X159	W14x398	W24x162
12	W14X159	W14x398	W24x162
11	W14X159	W14x398	W24x162
10	W14x370	W14x455	W27x194
9	W14x370	W14x455	W27x194
8	W14x370	W14x455	W27x194
7	W14x426	W14x500	W27x235
6	W14x426	W14x500	W27x235
5	W14x426	W14x500	W27x235
4	W14x500	W14x550	W27x235
3	W14x500	W14x550	W27x235
2	W14x500	W14x550	W27x235
1	W14x550	W14x605	W27x258
B1	W14x550	W14x605	W27x258
B2	W14x550	W14x605	W27x258

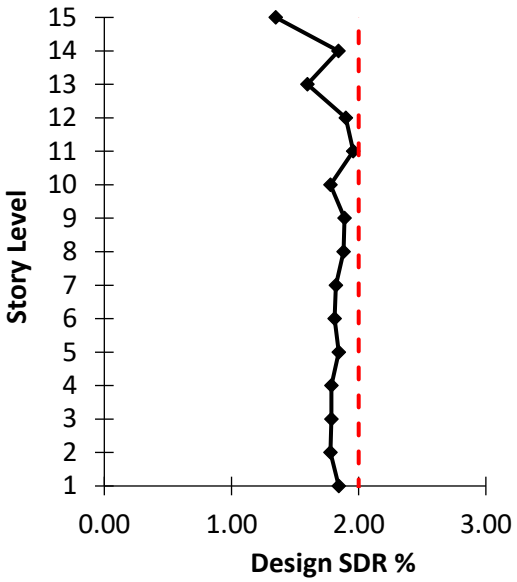

Figure 2.1.3. Story drift ratio of final members

After the drift limit was met, the column strength was checked in terms of the demand over capacity ratio. The columns of the moment frame were treated as sections under combined flexure and axial force. The required strength included the response from both gravity loads and the lateral forces that were calculated in the first analysis according to AISC to design the column with adequate strength and prevent a possible failure. The equations used in the design procedure were:

$$Pr = Pnt + B_2 * Plt$$

$$Mr = B_1 * Mnt + B_2 * Mlt$$

$$When\ pPr \geq 0.2: \quad pPr + bMr \leq 1.0 \qquad Eq.\ (6-1)$$

$$When\ pPr < 0.2: \quad 0.5\,pPr + bMr \leq 1.0 \qquad Eq.\ (6-2)$$

Table 2.1.2 illustrates the check for the first story interior and exterior column of the moment frame. As can be observed the columns are overdesigned.

Table 2.1.2. Column Strength

	Exterior Col 1st floor	Interior Col 1st floor
Section	W14x550	W14x605
B1 / B2	1.0 / 1.148	1.0 / 1.148
Pnt [kips]	502.61	871.83
Plt [kips]	880.87	136.80
Pr [kips]	1513.85	1028.88
Mnt [k-ft]	27.35	-
Mlt [k-ft]	1151.08	1368.39
Mr [k-ft]	1348.79	1570.91
Ky	1.0	1.0
L_b [ft]	18	18
p x10^3 [k]$^{-1}$	0.162	0.147
b x10^3 [k-ft]$^{-1}$	0.202	0.180
pPr	0.245	0.151
Eq. 6-1/6-2	0.517	0.394

Preceding the beam design was the reduced beam section (RBS) design. The beam-to-column connections of the moment frame were important to be designed with adequate strength for seismic design, if the expected lateral forces are greater than the capacity of the connection, unexpected failure can occur. For this study, all the beam-to-column connections were designed as the RBS moment connection according to the prequalified connections in special moment frames according to AISC 358-10, where the section of the beam is reduced by trimming the flange in selected regions away from the beam-column interface in order to control the location of yielding and plastic hinge formation. The beam flange is connected to column flange using complete-joint-penetration (CJP) groove welds as Figure 2.1.4 displays. The beam depth is limited to W36 and the beam weight limit is set to 302 lb/ft in addition to the beam flange thickness limit of 1 ¾ in. There are no limitations for the column depth or weight per foot. The design of the RBS connection was an iterative procedure where the dimensions a, b and c shown in Figure 2.1.4, were estimated so that the factored plastic moment of the beam is lower than the demand. The dimensions should meet the limits as defined in AISC 358-16. For

the calculation of the beam strength, the reduced beam section properties were utilized such as the plastic section modulus at the center of RBS (Z_{RBS}). Tables 2.1.4 and 2.1.5 show the design values for the final sections as they were defined in the design process. All the sections satisfy the flexural strength and the designed reduced beam dimensions are also given in the table. Following, the beam strength requirement was checked for the selected sections as they were defined in the drift limit requirement. All the beams and columns were designed as highly ductile members as specified in AISC 341-16 for special moment frame (SMF). Table 2.1.3 summarize a strength check of the first story level beam for demonstration. The demand is estimated using the same formula utilized in column strength requirement where the B_2 multiplier accounts for the P-Δ effects and is calculated based on the dead and lateral loads of each story level. It is noted that the beam demand over capacity ratio is less than 0.5, the section is overdesigned as column sections.

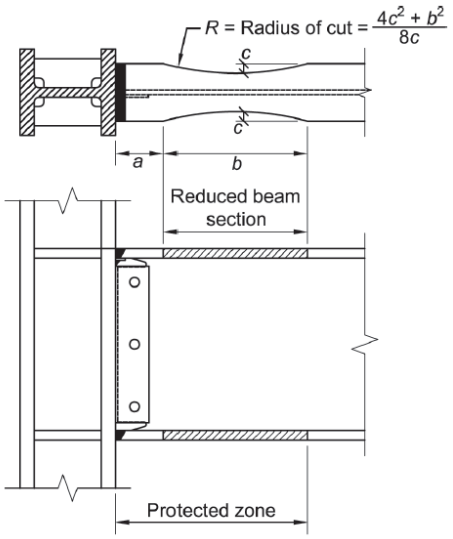

$$0.5b_{bf} \le a \le 0.75b_{bf}$$

$$0.65d \le b \le 0.85d$$

$$0.1b_{bf} \le c \le 0.25b_{bf}$$

Figure 2.1.4. Reduced beam section connection and limits

Table 2.1.3. Beam Strength

Story - Section	1st – W27x258
ϕ	0.9
Zx [in3]	852
Fy [ksi]	50
Mn [k-ft]	3550
Mnt [k-ft]	35.73
Mlt [k-ft]	1135.83
B1	1.00
B2	1.148
ϕMn [k-ft]	3195.00
Mu [k-ft]	1339.66
Mr/Mc	0.419

Table 2.1.4. RBS Design Exterior Span Beam

Section	d_{bf} (in)	t_{bf} (in)	b_{bf} (in)	Z_x (in3)	a (in)	b (in)	c (in)	Z_{RBS} (in3)	C_{pr}	M_{pr} (k-ft)	S_h (in)	L_h (ft)	V_{RBS} (kip)	M_f (k-ft)	$\phi_d * M_{pe}$ (k-ft)	$M_f / \phi_d M_{pe}$
W24X76	23.90	0.68	8.99	200.00	6.20	17.90	1.45	154.21	1.15	812.82	15.15	26.23	67.97	898.63	916.67	0.98
W24X76	23.90	0.68	8.99	200.00	6.20	17.90	1.45	154.21	1.15	812.82	15.15	26.23	69.64	900.74	916.67	0.98
W24x162	25.00	1.22	13.00	468.00	9.00	18.75	2.30	334.55	1.15	1763.34	18.38	25.55	145.49	1986.12	2145.00	0.93
W24x162	25.00	1.22	13.00	468.00	9.00	18.75	2.30	334.55	1.15	1763.34	18.38	25.55	145.49	1986.12	2145.00	0.93
W24x162	25.00	1.22	13.00	468.00	9.00	18.75	2.30	334.55	1.15	1763.34	18.38	25.55	145.49	1986.12	2145.00	0.93
W27x194	28.10	1.34	14.00	631.00	9.00	21.10	2.30	466.05	1.15	2456.48	19.55	25.20	202.29	2786.04	2892.08	0.96
W27x194	28.10	1.34	14.00	631.00	9.00	21.10	2.30	466.05	1.15	2456.48	19.55	25.20	202.29	2786.04	2892.08	0.96
W27x194	28.10	1.34	14.00	631.00	9.00	21.10	2.30	466.05	1.15	2456.48	19.55	25.20	202.29	2786.04	2892.08	0.96
W27x235	28.70	1.61	14.20	772.00	9.50	21.60	2.40	562.65	1.15	2965.63	20.30	25.02	244.36	3379.00	3538.33	0.95
W27x235	28.70	1.61	14.20	772.00	9.50	21.60	2.40	562.65	1.15	2965.63	20.30	25.02	244.36	3379.00	3538.33	0.95
W27x235	28.70	1.61	14.20	772.00	9.50	21.60	2.40	562.65	1.15	2965.63	20.30	25.02	244.36	3379.00	3538.33	0.95
W27x235	28.70	1.61	14.20	772.00	9.50	21.60	2.40	562.65	1.15	2965.63	20.30	24.96	244.93	3379.97	3538.33	0.96
W27x235	28.70	1.61	14.20	772.00	9.50	21.60	2.40	562.65	1.15	2965.63	20.30	24.96	244.93	3379.97	3538.33	0.96
W27x235	28.70	1.61	14.20	772.00	9.50	21.60	2.40	562.65	1.15	2965.63	20.30	24.96	244.93	3379.97	3538.33	0.96
W27x258	29.00	1.77	14.30	852.00	9.65	21.75	2.50	610.77	1.15	3219.29	20.53	24.87	266.19	3674.63	3905.00	0.94
W27x258	29.00	1.77	14.30	852.00	9.65	21.75	2.50	610.77	1.15	3219.29	20.53	24.87	266.19	3674.63	3905.00	0.94
W27x258	29.00	1.77	14.30	852.00	9.65	21.75	2.50	610.77	1.15	3219.29	20.53	24.87	266.19	3674.63	3905.00	0.94

Table 2.1.5. RBS Design Interior Span Beam

Section	d_{bf} (in)	t_{bf} (in)	b_{bf} (in)	Z_x (in^3)	a (in)	b (in)	c (in)	Z_{RBS} (in^3)	C_{pr}	M_{pr} (k-ft)	S_h (in)	L_h (ft)	V_{RBS} (kip)	M_f (k-ft)	ϕ_d*M_{pe} (k-ft)	M_f / $\phi_d M_{pe}$
W24X76	23.90	0.68	8.99	200.00	6.20	17.90	1.45	154.21	1.15	812.82	15.15	26.21	68.01	898.68	916.67	0.98
W24X76	23.90	0.68	8.99	200.00	6.20	17.90	1.45	154.21	1.15	812.82	15.15	26.21	69.68	900.79	916.67	0.98
W24x162	25.00	1.22	13.00	468.00	9.00	18.75	2.30	334.55	1.15	1763.34	18.38	25.41	146.20	1987.20	2145.00	0.93
W24x162	25.00	1.22	13.00	468.00	9.00	18.75	2.30	334.55	1.15	1763.34	18.38	25.41	146.20	1987.20	2145.00	0.93
W24x162	25.00	1.22	13.00	468.00	9.00	18.75	2.30	334.55	1.15	1763.34	18.38	25.41	146.20	1987.20	2145.00	0.93
W27x194	28.10	1.34	14.00	631.00	9.00	21.10	2.30	466.05	1.15	2456.48	19.55	25.16	202.63	2786.59	2892.08	0.96
W27x194	28.10	1.34	14.00	631.00	9.00	21.10	2.30	466.05	1.15	2456.48	19.55	25.16	202.63	2786.59	2892.08	0.96
W27x194	28.10	1.34	14.00	631.00	9.00	21.10	2.30	466.05	1.15	2456.48	19.55	25.16	202.63	2786.59	2892.08	0.96
W27x235	28.70	1.61	14.20	772.00	9.50	21.60	2.40	562.65	1.15	2965.63	20.30	24.98	244.70	3379.58	3538.33	0.96
W27x235	28.70	1.61	14.20	772.00	9.50	21.60	2.40	562.65	1.15	2965.63	20.30	24.98	244.70	3379.58	3538.33	0.96
W27x235	28.70	1.61	14.20	772.00	9.50	21.60	2.40	562.65	1.15	2965.63	20.30	24.98	244.70	3379.58	3538.33	0.96
W27x235	28.70	1.61	14.20	772.00	9.50	21.60	2.40	562.65	1.15	2965.63	20.30	24.93	245.16	3380.36	3538.33	0.96
W27x235	28.70	1.61	14.20	772.00	9.50	21.60	2.40	562.65	1.15	2965.63	20.30	24.93	245.16	3380.36	3538.33	0.96
W27x235	28.70	1.61	14.20	772.00	9.50	21.60	2.40	562.65	1.15	2965.63	20.30	24.93	245.16	3380.36	3538.33	0.96
W27x258	29.00	1.77	14.30	852.00	9.65	21.75	2.50	610.77	1.15	3219.29	20.53	24.84	266.48	3675.14	3905.00	0.94
W27x258	29.00	1.77	14.30	852.00	9.65	21.75	2.50	610.77	1.15	3219.29	20.53	24.84	266.48	3675.14	3905.00	0.94
W27x258	29.00	1.77	14.30	852.00	9.65	21.75	2.50	610.77	1.15	3219.29	20.53	24.84	266.48	3675.14	3905.00	0.94

Subsequently, in the design process the strong column-weak beam (SCWB) requirement was to be satisfied. As defined in AISC 341-16 [3], the moment ratio at all joints of the structure should be greater than 1.0. The flexural strength of the beam is defined as the moment at the location of the reduced beam section (RBS) to comply with the prequalified connections [1] based on AISC 341-16 [3]

$$\frac{\Sigma M^*_{pc}}{\Sigma M^*_{pb}} > 1.0$$

where

ΣM^*_{pc} = the sum of the nominal flexural strengths of the columns above and below the joint to the beam centerline with a reduction for the axial force in the column.

$$\Sigma M^*_{pc} = \Sigma Z_c \left(F_{yc} - P_{uc} / A_g \right)$$

ΣM^*_{pb} = the sum of the expected flexural strengths of the beams at the plastic hinge locations to the column centerline.

$$\Sigma M^*_{pb} = \Sigma \left(1.1 R_y F_{yb} Z_{RBS} + M_{uv} \right)$$

When ensured that the column is stronger than the girder, the failure mechanism of the frame was defined. The intentional yielding and plastic hinge formation in the beams was desirable so that the column yielding takes longer and protects the structure from possible column failure. A summary of the SCWB requirement is displayed in Tables 2.1.6 and 2.1.7.

Table 2.1.6. Strong column-weak beam check at exterior joints

Joint level	Column									Beam	$\frac{\Sigma M_{pc}}{\Sigma M_{pb}}$
	Top				Bottom				ΣM_{pc}	ΣM_{pb}	
	Section	Z_c (in^3)	A_g (in^2)	$M_{pc,top}$	Section	Z_c (in^3)	A_g (in^2)	$M_{pc,bot}$			
15	-	0	0	0	W14X145	260.0	42.7	1083.33	1083.33	905.21	1.20
14	W14X145	260.0	42.7	1083.33	W14X145	260.0	42.7	1083.33	2166.67	908.35	2.39
13	W14X145	260.0	42.7	1083.33	W14X159	287.0	46.7	1195.83	2279.17	2000.39	1.14
12	W14X159	287.0	46.7	1195.83	W14X159	287.0	46.7	1195.83	2391.67	2000.39	1.20
11	W14X159	287.0	46.7	1195.83	W14X159	287.0	46.7	1195.83	2391.67	2000.39	1.20
10	W14X159	287.0	46.7	1195.83	W14x370	736.0	109.0	3066.67	4262.50	2830.10	1.51
9	W14x370	736.0	109.0	3066.67	W14x370	736.0	109.0	3066.67	6133.33	2830.10	2.17
8	W14x370	736.0	109.0	3066.67	W14x370	736.0	109.0	3066.67	6133.33	2830.10	2.17
7	W14x370	736.0	109.0	3066.67	W14x426	869.0	125.0	3620.83	6687.50	3440.45	1.94
6	W14x426	869.0	125.0	3620.83	W14x426	869.0	125.0	3620.83	7241.67	3440.45	2.10
5	W14x426	869.0	125.0	3620.83	W14x426	869.0	125.0	3620.83	7241.67	3440.45	2.10
4	W14x426	869.0	125.0	3620.83	W14x500	1050.0	147.0	4375.00	7995.83	3451.06	2.32
3	W14x500	1050.0	147.0	4375.00	W14x500	1050.0	147.0	4375.00	8750.00	3451.06	2.54
2	W14x500	1050.0	147.0	4375.00	W14x500	1050.0	147.0	4375.00	8750.00	3451.06	2.54
1	W14x500	1050.0	147.0	4375.00	W14x550	1180.0	162.0	4916.67	9291.67	3758.71	2.47
B1	W14x550	1180.0	162.0	4916.67	W14x550	1180.0	162.0	4916.67	9833.33	3758.71	2.62
B2	W14x550	1180.0	162.0	4916.67	W14x550	1180.0	162.0	4916.67	9833.33	3758.71	2.62

Table 2.1.7. Strong column-weak beam check at interior joints

Joint level	Column									Beam	$\frac{\Sigma M_{pc}}{\Sigma M_{pb}}$
	Top				Bottom				ΣM_{pc}	ΣM_{pb}	
	Section	Z_c (in^3)	A_g (in^2)	$M_{pc,top}$	Section	Z_c (in^3)	A_g (in^2)	$M_{pc,bot}$			
15	-	0	0	0	W14X176	320	51.8	1333.33	1333.33	1812.82	0.74
14	W14X176	320	51.8	1333.33	W14X176	320	51.8	1333.33	2666.67	1819.15	1.47
13	W14X176	320	51.8	1333.33	W14x398	801	117.0	3338	4670.83	4044.02	1.15
12	W14x398	801	117.0	3338	W14x398	801	117.0	3338	6675.00	4044.02	1.65
11	W14x398	801	117.0	3338	W14x398	801	117.0	3338	6675.00	4044.02	1.65
10	W14x398	801	117.0	3338	W14x455	936	134.0	3900	7237.50	5680.40	1.27
9	W14x455	936	134.0	3900	W14x455	936	134.0	3900	7800.00	5680.40	1.37
8	W14x455	936	134.0	3900	W14x455	936	134.0	3900	7800.00	5680.40	1.37
7	W14x455	936	134.0	3900	W14x500	1050	147.0	4375	8275.00	6900.96	1.20
6	W14x500	1050	147.0	4375	W14x500	1050	147.0	4375	8750.00	6900.96	1.27
5	W14x500	1050	147.0	4375	W14x500	1050	147.0	4375	8750.00	6900.96	1.27
4	W14x500	1050	147.0	4375	W14x550	1180	162.0	4916.67	9291.67	6915.54	1.34
3	W14x550	1180	162.0	4916.67	W14x550	1180	162.0	4916.67	9833.33	6915.54	1.42
2	W14x550	1180	162.0	4916.67	W14x550	1180	162.0	4916.67	9833.33	6915.54	1.42
1	W14x550	1180	162.0	4916.67	W14x605	1320	178.0	5500.00	10416.67	7534.47	1.38
B1	W14x605	1320	178.0	5500.00	W14x605	1320	178.0	5500.00	11000.00	7534.47	1.46
B2	W14x605	1320	178.0	5500.00	W14x605	1320	178.0	5500.00	11000.00	7534.47	1.46

Furthermore, the panel zone thickness was checked according to current specifications so that if the column web thickness does not satisfy the requirement, doubler plates should be added to the column to ensure the rigid zone has adequate stiffness. For this study, as shown in Tables 2.1.8 and 2.1.9, no doubler plates were needed for the selected sections. The panel zone was determined by AISC 341-16 [3] with the dimensions illustrated in Figure 2.1.5 :

$$t \geq (d_z + w_z)/90$$

where

d_z = d-2t_f of the deeper beam at the connection (in)

t = thickness of column web or doubler plate (in)

w_z = width of the panel zone between column flanges (in)

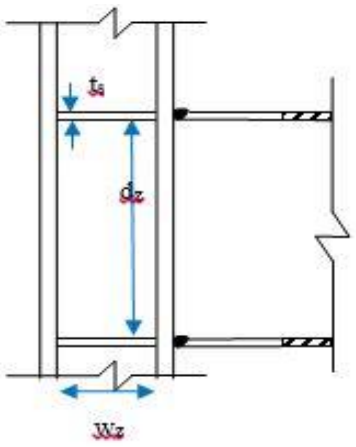

Figure 2.1.5. Panel zone

Table 2.1.8. Panel Zone Checks of Exterior Joints

	Exterior Column			Beam					
Joint	**Section**	**d_c (in)**	**t_{cf} (in)**	**Section**	**d_b (in)**	**t_{bf} (in)**	**$(d_z+w_z)/90$ (in)**	**t_{cw} (in)**	**Doubler Plate**
15	W14X159	15,0	1,190	W21X62	21,0	0,615	0,36	0,75	No
14	W14X159	15,0	1,190	W21X62	21,0	0,615	0,36	0,75	No
13	W14X159	15,0	1,190	W24x162	25,0	1,220	0,39	0,75	No
12	W14X159	15,0	1,190	W24x162	25,0	1,220	0,39	0,75	No
11	W14X159	15,0	1,190	W24x162	25,0	1,220	0,39	0,75	No
10	W14x370	17,9	2,66	W27x194	28,1	1,340	0,42	1,66	No
9	W14x370	17,9	2,66	W27x194	28,1	1,340	0,42	1,66	No
8	W14x370	17,9	2,66	W27x194	28,1	1,340	0,42	1,66	No
7	W14x426	18,7	3,04	W27x235	28,7	1,610	0,42	1,88	No
6	W14x426	18,7	3,04	W27x235	28,7	1,610	0,42	1,88	No
5	W14x426	18,7	3,04	W27x235	28,7	1,610	0,42	1,88	No
4	W14x500	19,6	3,50	W27x235	28,7	1,610	0,42	2,19	No
3	W14x500	19,6	3,50	W27x235	28,7	1,610	0,42	2,19	No
2	W14x500	19,6	3,50	W27x235	28,7	1,610	0,42	2,19	No
1	W14x500	19,0	3,50	W27x258	29,0	1,770	0,42	2,19	No
B1	W14x500	19,0	3,50	W27x258	29,0	1,770	0,42	2,19	No
B2	W14x500	19,0	3,50	W27x258	29,0	1,770	0,42	2,19	No

Table 2.1.9. Panel Zone Checks of Interior Joints

	Interior Column			Beam					
Joint	**Section**	**d_c (in)**	**t_{cf} (in)**	**Section**	**d_b (in)**	**t_{bf} (in)**	**$(d_z+w_z)/90$ (in)**	**t_{cw} (in)**	**Doubler Plate**
15	W14X193	15,5	1,440	W21X55	21,0	0,615	0,360	0,89	No
14	W14X193	15,5	1,440	W21X55	21,0	0,615	0,360	0,89	No
13	W14x398	18,3	2,850	W24x162	25,0	1,220	0,391	1,77	No
12	W14x398	18,3	2,850	W24x162	25,0	1,220	0,391	1,77	No
11	W14x398	18,3	2,850	W24x162	25,0	1,220	0,391	1,77	No
10	W14x455	19,0	3,210	W27x194	28,1	1,340	0,422	2,02	No
9	W14x455	19,0	3,210	W27x194	28,1	1,340	0,422	1,66	No
8	W14x455	19,0	3,210	W27x194	28,1	1,340	0,422	1,66	No
7	W14x500	19,6	3,500	W27x235	28,7	1,610	0,423	2,19	No
6	W14x500	19,6	3,500	W27x235	28,7	1,610	0,423	2,19	No
5	W14x500	19,6	3,500	W27x235	28,7	1,610	0,423	2,19	No
4	W14x550	20,2	3,820	W27x235	28,7	1,610	0,423	2,38	No
3	W14x550	20,2	3,820	W27x235	28,7	1,610	0,423	2,38	No
2	W14x550	20,2	3,820	W27x235	28,7	1,610	0,423	2,38	No
1	W14x550	20,2	3,820	W27x258	29,0	1,770	0,422	2,38	No
B1	W14x550	20,2	3,820	W27x258	29,0	1,770	0,422	2,38	No
B2	W14x550	20,2	3,820	W27x258	29,0	1,770	0,422	2,38	No

2.2 Earthquake ground motions

The moment frame was designed based on a seismic design concept according to which the structure should undergo a ductile response regardless of the type of ground excitation. For the purpose of this study, an ensemble of 20 ground motions with 10% Probability of Exceedance in 50 years (10%PE) was selected in order to cover a wide range of ground motion types. The 20 ground motion records were selected from PEER Ground motion database and they are scaled to be compatible with site class D in Los Angeles area, with design spectrum parameters S_S=2.0g, S_1=1.0g and T_L=12.0 sec. The elastic response spectra of the ground motions and the target spectrum are illustrated in Figure 2.2.1. The selected time histories are composed of 10 events with two components each, the fault normal (FN) component and the fault parallel (FP) component. Each component was applied separately on the structure for each time-history analysis. PGA varies from 0.512g up to 1.566g as shown in Table 3.2.1 with more information on the selected ground motions. Figures 2.2.2 displays the time histories of the 20 ground motions used in this study including the original scale factor. Comparison of GM01, GM02, GM17 and GM19 was conducted in order to demonstrate the variation of the selected excitations used in this study. GM02, GM17 and GM19 ground excitations were selected after the first analyses, based on the response of the structure, and GM01 was selected for comparison between different components of the same event (Northridge, 1994). The correlation of these ground excitations was in terms of response spectra, duration and intensity. Figure 2.2.3 displays the response spectra of the four selected records for clarification. The peak ground acceleration of GM01, GM02, GM17 and GM19 is 0.979g, 0.578g, 0.512g and 1.566g respectively.

Table 2.2.1. Ground motions used in this study

ID No.	NGA#	Component	Scale Factor	Event	Year	Mag	Duration (seconds)	PGA (g)	PGV (in/sec)
GM01	1085	FN	1.1675	Northridge	1994	6.69	40	0.979	5.35
GM02		FP						0.578	3.60
GM03	1489	FN	2.8835	Chi-Chi-Taiwan	1999	7.62	90	0.810	5.08
GM04		FP						0.718	6.50
GM05	1515	FN	2.5841	Chi-Chi-Taiwan	1999	7.62	90	0.643	5.71
GM06		FP						0.513	5.02
GM07	1009	FN	3.8019	Northridge	1994	6.69	55.33	1.041	4.84
GM08		FP						0.985	3.68
GM09	726	FN	6.5733	Superstition Hills	1987	6.54	21.89	0.817	2.03
GM10		FP						1.059	4.61
GM11	179	FN	1.9573	Imperial Valley	1979	6.53	39	0.699	6.00
GM12		FP						0.929	3.09
GM13	802	FN	2.3023	Loma Prieta	1989	6.93	39.955	0.835	5.03
GM14		FP						0.866	3.92
GM15	779	FN	1.0816	Loma Prieta	1989	6.93	25.005	1.021	4.13
GM16		FP						0.581	3.07
GM17	722	FN	4.8465	Superstition Hills	1987	6.54	21.98	0.512	2.72
GM18		FP						0.669	6.31
GM19	1148	FN	7.2093	Kocaeli-Turkey	1999	7.51	30	1.566	5.72
GM20		FP						1.098	10.94

Note: NGA # - Sequential number in PEER Strong Ground Motion Database

Table 2.2.2. Spectral Accelerations Corresponding to Fundamental Period (T_1=2.491 sec)

GMs	Sa (T1)	GM Scale Factor
GM01	0.454783	1.1675
GM02	0.927671	1.1675
GM03	0.374193	2.8835
GM04	0.282124	2.8835
GM05	0.391273	2.5841
GM06	0.384503	2.5841
GM07	0.539317	3.8019
GM08	0.274894	3.8019
GM09	0.332888	6.5733
GM10	0.586398	6.5733
GM11	0.610186	1.9573
GM12	0.326335	1.9573
GM13	0.455528	2.3023
GM14	0.273208	2.3023
GM15	0.510062	1.0816
GM16	0.273876	1.0816
GM17	0.211755	4.8465
GM18	0.653012	4.8465
GM19	0.279130	7.2093
GM20	0.565932	7.2093

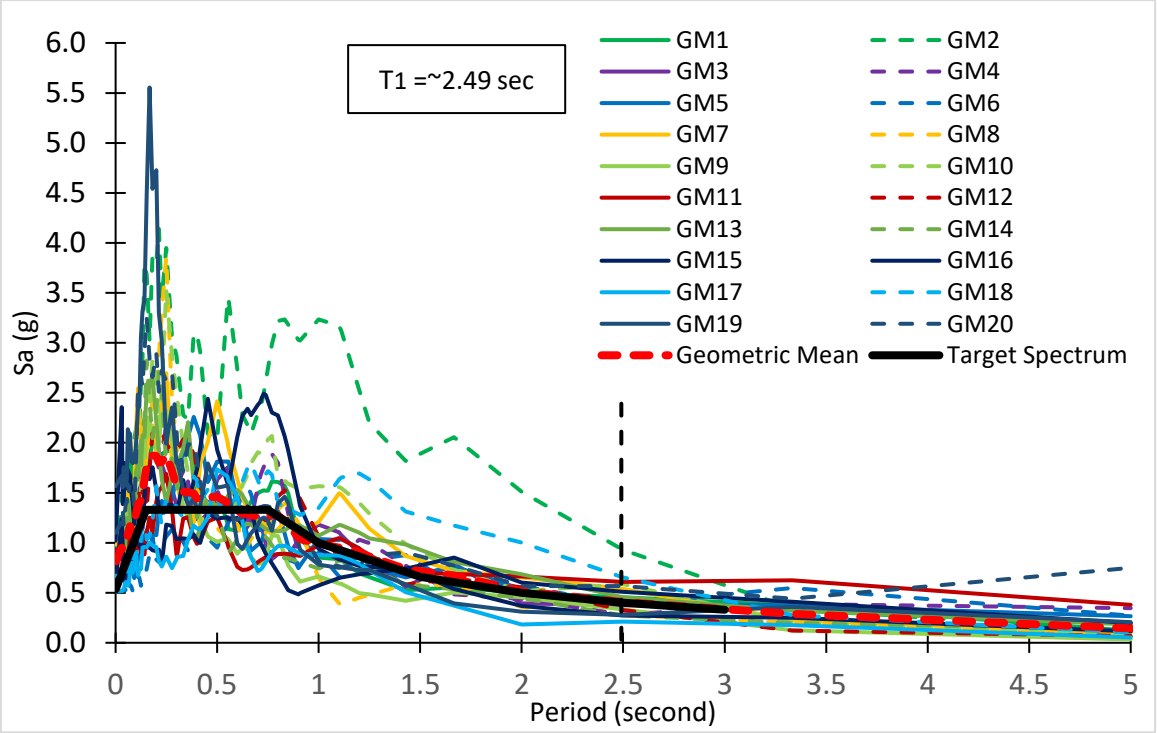

Figure 2.2.1. Response spectra of ground motions

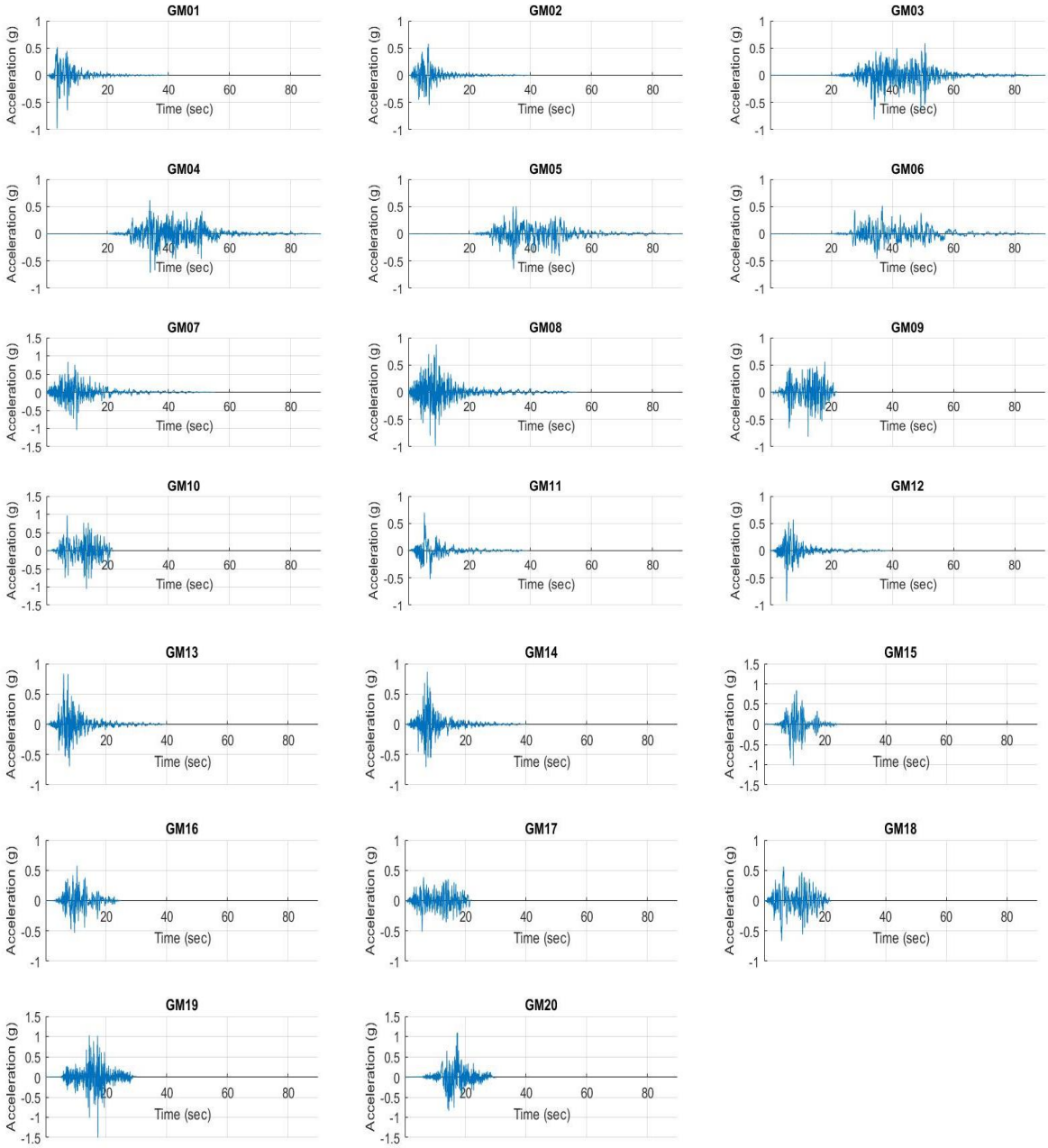

Figure 2.2.2. Time histories of ground motions

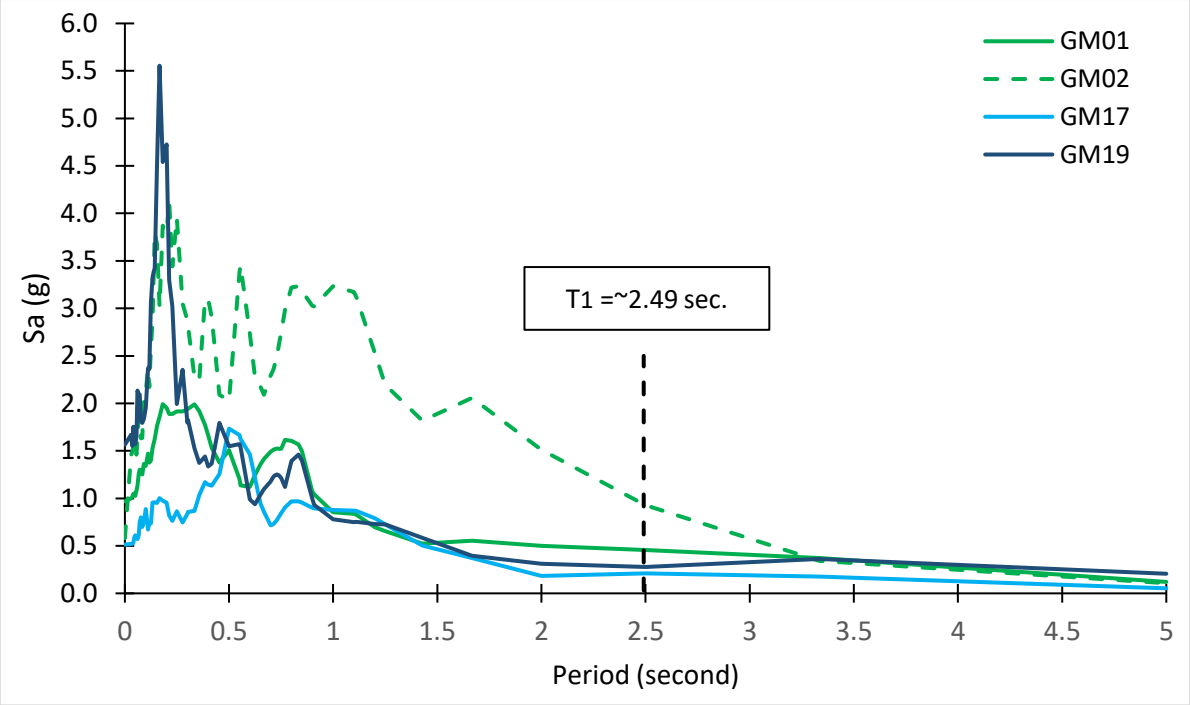

Figure 2.2.3. Response spectra of GM01, GM02, GM17 and GM19

Initial comparison of the fault normal (FN) component and the fault parallel (FP) component of Northridge 1994 shows that the two recorded ground motions have the same intensity pattern, which is a short period of a few seconds during which the peak ground acceleration occurs, as shown in Figure 2.2.2. In contrast with the PGA of each component, when analyzing the response spectra, it is noted that for structures with shorter first period, the fault parallel component has higher values of ground acceleration. Moreover, although GM01 has larger value of PGA, it is observed that for the structure of this study with first fundamental period of 2.49 seconds, the ground motion with name GM02 has a significant drop in the ground acceleration. During the plastic response of the frame where the fundamental period of the frame can shift to a longer period, the response of the structure will vary under these two ground excitations. The difference in the ground acceleration in addition to the significant drop can be interpreted in terms of energy, therefore it can be said that the required energy to force the frame to reach 4% of story drift ratio (SDR) for GM01 is

greater than the energy required from ground motion GM02. Additional comparison was conducted for GM02, GM17 and GM19 with duration of 40 sec, 21.98 sec and 30 sec respectively. Although ground motions GM02 and GM17 have approximately similar PGA's of 0.578g and 0.512g respectively, when analyzing the recorded time history there is a divergence in the pattern of the excitation. Ground motion GM02 has a period of approximately 10 seconds of peaks in contrast with GM17, where during the 21.89 seconds of the excitation, a pattern of peaks is observed with constant frequency. GM19 follows a pattern between GM02 and GM17, it has a period of peaks with constant frequency in addition to a 10 second period where the peak ground acceleration occurs. GM19 has higher peak ground acceleration (PGA) than the other two ground excitations while the response spectrum of this excitation after 1 sec is similar to GM17, however after 3 seconds the ground acceleration is increasing in contrast with the spectra of the other ground motions. As it will be demonstrated in the following chapters, the response of the structure differs under each excitation.

2.3 Numerical model in SAP2000

Succeeding the finalization of the sections with the design process, the analytical numerical model was developed. For the numerical model and analyses, SAP2000 was utilized in this study. Initially, as it was mentioned in previous sections for the design process the moment frame was modeled in order to finalize member sizes, and it was the base for the analytical model which included the column splice locations and plastic hinges at the column end and at the RBS region. The final numerical model of the 15-story frame is illustrated in Figure 2.3.1. The special moment frame was modeled as a 2D frame with all the columns and beams modeled as line elements which define the centerline of the section. In order to account for P-Δ effects, additional columns were introduced in to the model in order to

sustain dead load appertaining to the frame, without any contribution to the overall lateral response of the structure, also known as dummy columns. Lumped masses were assumed at each story level assigned to one of the interior joints of the level, calculated as shown in Table 2.3.2.

The column splice is located 4 ft above the beam-to-column connection (see figure 2.3.2) at story levels 2, 5, 8, 11 and 14 with the locations summarized in Table 2.3.1. After expanding the sections up to the column splice location in the model, the drift ratio is estimated and compared with the design drift ratio, Figure 2.3.3. As expected, the drift ratios in both cases are similar, with a small decrease in the ratio after modeling the column splice locations due to the increased stiffness. The larger section contributes to the stiffness of that level and was not considered in the calculations during the design process, hence the story drift was decreased.

For the nonlinear dynamic time history analyses, plastic hinges were assigned at the RBS locations as shown in Table 2.3.3, the relative locations are determined based on the RBS dimensions shown in previous sections. Moreover, plastic hinges were also assigned at the column end at dc/2 in the numerical model. Figure 2.3.4 illustrates a detail of the panel zone and the plastic hinges assigned to the model. The moment-rotation interaction curves of the beam plastic hinges account for the nonlinearity of the material by a bilinear plot. Engelhardt et al. [7] conducted a study on RBS connections used in special moment frames by testing several specimens of two-sided moment connections under cyclic load as suggested by AISC. The evaluation of the moment connection was in terms of story drift angle and ductility, in addition to the failure modes of the connection and the dissipated energy. Based on the overall response and specifically on specimen 1C with balanced strength of panel zone and composite slab, test results showed that the moment connection undergo yielding followed

by local buckling until fracture of the flange occurred. Total story drift angle of 0.05 radians was reached and the strength of the connection was decreased to 80% of the capacity following the bottom flange fracture. Further investigation on one-sided moment connection was conducted by Lee et al. [6] and Yu et al. [13] with test results similar to previous studies. The RBS strength after yielding, increases at 1.2 of normalized moment ratio until 4% of SDR. Based on previous studies, several moment-rotation (M-θ) curves were investigated to achieve the best results based on real test data. Figures 2.3.5 and 2.3.6 display two of the cases investigated as a parametric study to define the final moment-rotation relationship for the plastic hinges assigned on RBS locations. The first plot was based on previous studies although the analyses showed that the negative stiffness after 0.04 radians causes numerical problems in SAP2000. Figure 2.3.6 illustrates the final moment-theta interaction modeled for the RBS plastic hinges. Appendix B summarizes the parametric study results for the cases under investigation at 4% and 6% of SDR including plastic hinge maps and deformed shapes of the frame.

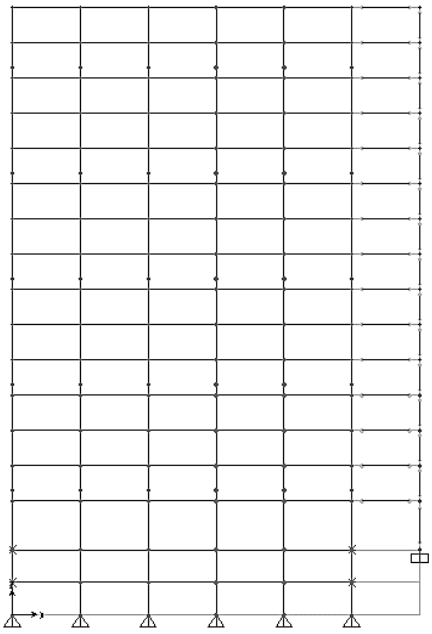

Figure 2.3.1. Moment frame model

Table 2.3.1. Column Splice location

Level	Beam Section	db [in]	Splice location from CL [ft]
14	W24X76	23.9	5.329
11	W24x162	25.0	5.375
8	W27x194	28.1	5.504
5	W27x235	28.7	5.529
2	W27x258	29.0	5.542

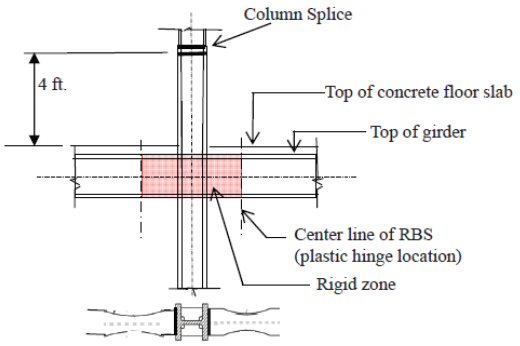

Figure 2.3.2. Column splice location

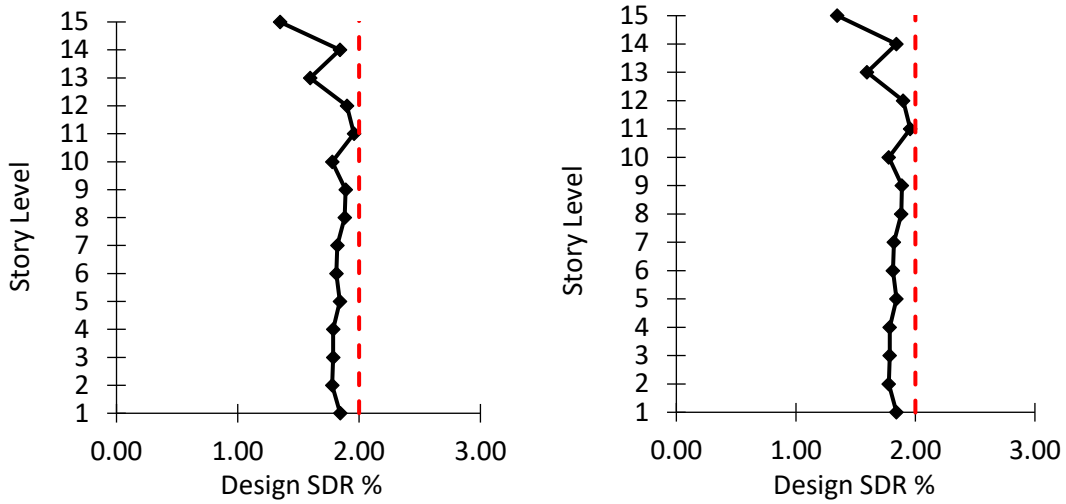

Figure 2.3.3. Design (left) and actual (right) story drift ratio

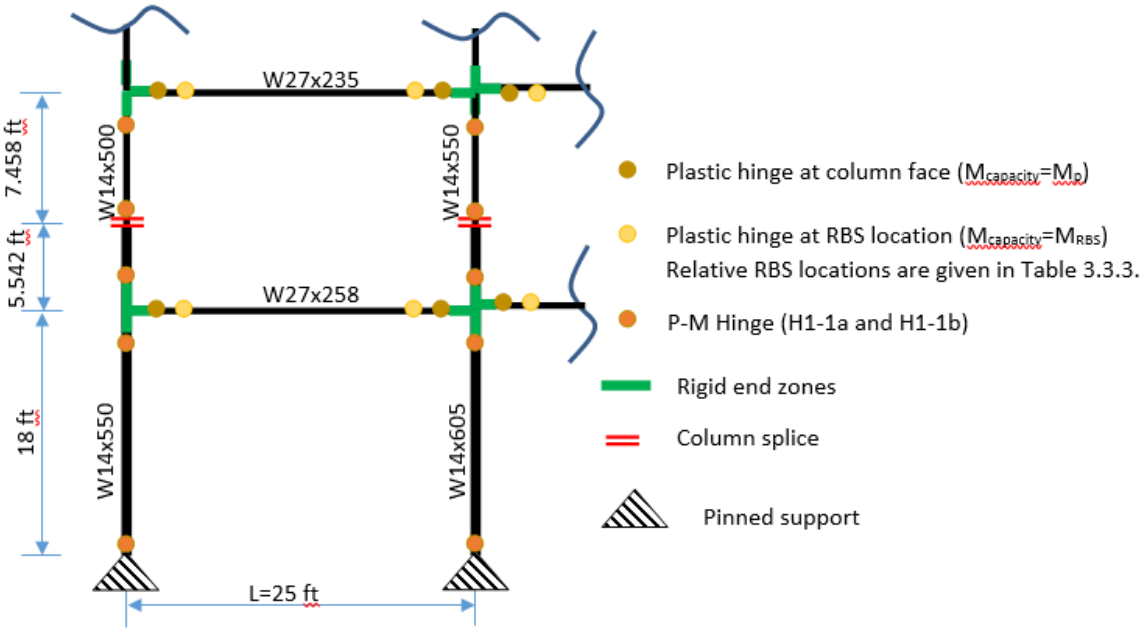

Figure 2.3.4. Plastic hinge and rigid zone assignments

Table 2.3.2. Lumped mass

Story level	Mass as weight (kips)
15	778.125
1-14	900

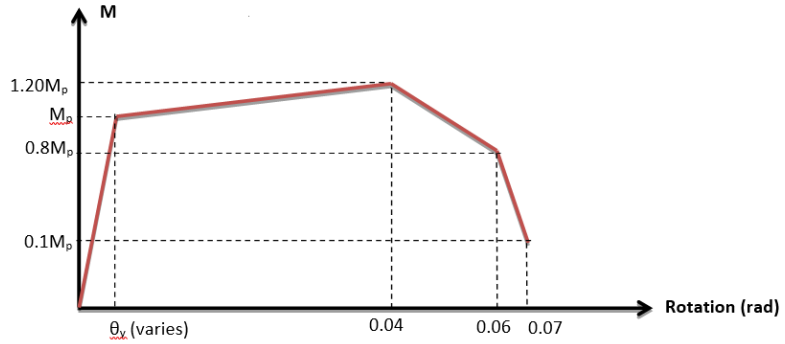

Figure 2.3.5. Initial moment-theta interaction curve

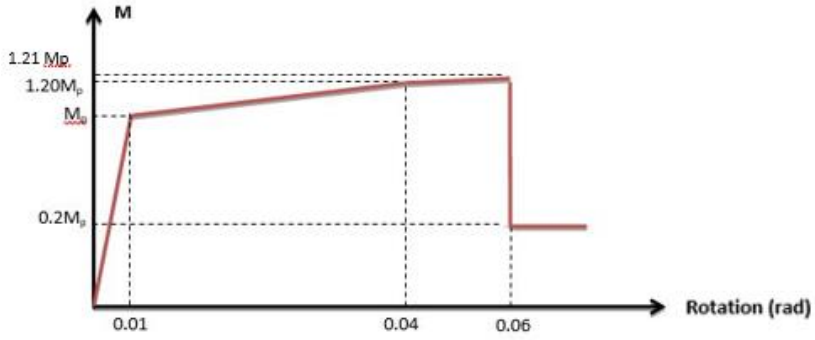

Figure 2.3.6. Final moment-theta interaction curve

Table 2.3.3. Nominal Moment Capacity and Location of RBS for Numerical Model

Beam Section	Mrbs (k-ft)	Relative Locations			
		Exterior Span		Interior Span	
		Left	Right	Left	Right
W24X76	642.5	0.0752	0.9242	0.0758	0.9242
W24X76	642.5	0.0752	0.9242	0.0758	0.9242
W24x162	1393.9	0.0863	0.9083	0.0918	0.9083
W24x162	1393.9	0.0863	0.9083	0.0918	0.9083
W24x162	1393.9	0.0863	0.9083	0.0918	0.9083
W27x194	1941.9	0.0950	0.9032	0.0968	0.9032
W27x194	1941.9	0.0950	0.9032	0.0968	0.9032
W27x194	1941.9	0.0950	0.9032	0.0968	0.9032
W27x235	2344.4	0.0988	0.8997	0.1003	0.8997
W27x235	2344.4	0.0988	0.8997	0.1003	0.8997
W27x235	2344.4	0.0988	0.8997	0.1003	0.8997
W27x235	2344.4	0.1003	0.8987	0.1013	0.8987
W27x235	2344.4	0.1003	0.8987	0.1013	0.8987
W27x235	2344.4	0.1003	0.8987	0.1013	0.8987
W27x258	2544.9	0.1021	0.8967	0.1033	0.8967
W27x258	2544.9	0.1021	0.8967	0.1033	0.8967
W27x258	2544.9	0.1021	0.8967	0.1033	0.8967

Furthermore, modal analysis was performed on the moment frame to determine the dynamic properties of the structure. The response of the frame is directly related to the properties as were predefined through the design process and the selected sections. For the purposes of the modal analysis, the mass was assumed to be lumped at the level of each story as shown in Table 2.3.2 and the damping ratio is taken as 5% for all modes. The fundamental periods of the first six modes of the moment frame as well as the modal participating mass ratios were determined after the modal analysis as shown in Table 2.3.4. As it is observed, the actual period of the structure for the first mode is 2.491 seconds while the estimated period corresponding to the first mode defined during the design process was 1.941 seconds. This difference in the fundamental period is important since it will define the seismic forces attracted to the structure based on the response spectra of the ground excitations.

Table 2.3.4. Fundamental periods and modal participating mass ratio

Mode	Period [sec]	Modal participating mass ratio
1	2.491	0.718
2	0.920	0.100
3	0.549	0.034
4	0.388	0.017
5	0.293	0.010
6	0.228	0.006

The structure utilized in this research is a 15-story special moment frame, hence it was expected that higher mode shapes and damping would influence the inelastic response of the frame. Therefore, the Rayleigh damping should be taken under careful consideration for the numerical model. A parametric study was conducted to investigate the impact of damping coefficient on the response of the structure and to identify which mode combination would be the most suitable for the analytical model so that the demand assessment was based on a model with realistic parameters. The combinations of mode shapes and damping coefficients

are illustrated in Figure 2.3.5. The parametric study was conducted prior the finalization of the numerical model and 2% and 5% of damping was taken into considerations as shown and linear as well as nonlinear analyses were performed for each case. The analysis indicated that the peak displacement of the frame occurred at the combination of first and third mode, in both 2% and 5% of damping. Moreover, between the two main cases of damping, maximum response occurred at 2% as expected due to the lower energy dissipation. For this thesis, the damping was taken as 5% for all modes so that the model includes realistic structure parameters. Refer to Appendix A for figures and results from the comparison of mode shapes.

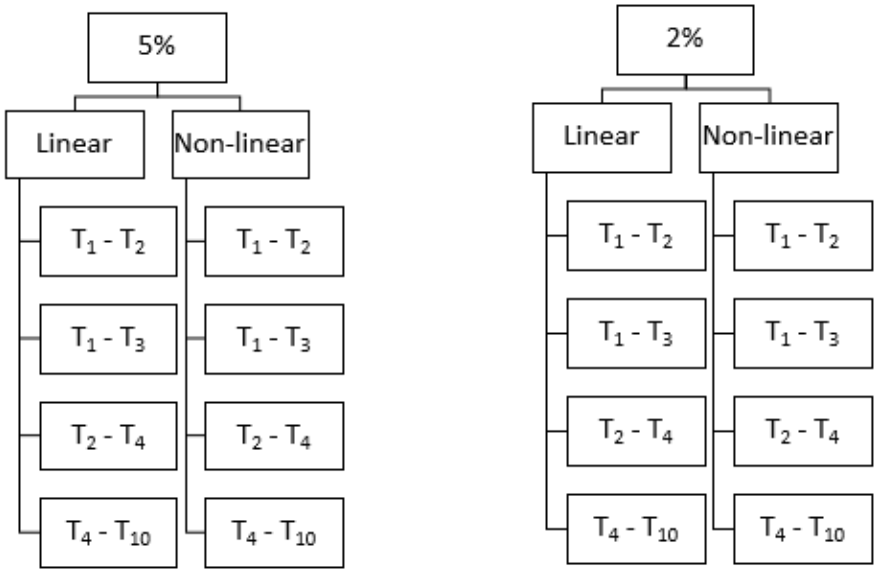

Figure 2.3.5. Cases under investigation for damping coefficient

2.4 Incremental dynamic analysis

Researchers studied several methodologies over the years to evaluate seismic performance of structures. Incremental dynamic analysis (IDA) is a sophisticated method for performance based evaluation of structural response, also adopted by Federal Emergency Manage Assessment (FEMA). Vamvatsikos et al. [12] conducted a study on IDA with several structures including a 20-story moment frame and various ground excitations. The parameter

utilized for the IDA curve was the maximum interstory angle and correlation of the demand and capacity of the frames was evaluated on several performance levels. This study followed the methodology summarized in the aforementioned research and the constant parameter utilized for the IDA plots was the peak story drift ratio of the 15-story special moment frame. Nonlinear time-history analysis was performed on the frame with a set of 20 ground motions and each excitation scaled to specific levels of intensity so that the structure undergo different performance levels until collapse. The evaluation of the flexural demand will be based on the seismic demand on the column splice in terms of peak axial tensile demand (P_s), peak bending moment demand (M_s) and peak combined tensile forces and bending moment at the column splice level. The overall response of the special moment frame as peak story drift ratio and plastic hinge rotation, was to be evaluated and correlation of the frame response and the demand at the column splice at three performance levels will be discussed. Initially, the incremental dynamic analysis of the structure was completed and the ground acceleration $S_a(g)$ versus the peak story drift of the 15-story special moment frame was plotted to identify the performance levels. This study focused on three performance levels as defined in FEMA [8] and were expressed in terms of story drift ratio (SDR). First level was immediate occupancy (IO) at 2% of SDR, second was the life safety (LS) performance level at 4% of SDR and final level included in this study was the collapse prevention (CP) level at 6% of SDR. Illustration of the IDA curve for ground motion GM01 is included in this section and the IDA of the 20 ground excitations is to be discussed in the following sections.

Initially, the fundamental period of the structure was defined and used in the response spectra (see Figure 2.2.3) to estimate the ground acceleration corresponding to the first mode, $S_a(T1)$ which was equal to 0.45g for GM01, a value close to the peak ground acceleration (PGA). The response spectrum was based on the original factors, therefore the

next step was to run the nonlinear time-history analysis on the frame with the original scale factor and define the peak story drift ratio. Hence, the first point of the IDA curve was estimated. The next scale factor was calculated using a linear formula considering that the response spectrum is elastic in terms of scale factor. For example, the original factor of GM01 was 1.167 which corresponds to 0.45g, hence the formula to estimate the scale factor corresponding to S_a(T1) of 0.50g was:

$$SF_{0.50g} = (1.167*0.5)/0.45 = 1.283$$

Table 2.4.1. IDA scale factor for GM01

GM	Sa (T1)	GM Scale Factor
Original GM01	0.45	1.167
GM01	0.45	1.167
	0.5	1.283
	0.55	1.412
	0.58	1.491
	0.6	1.540
	0.65	1.668

This procedure was repeated for all the ground motions and analyses for all scale factors were performed. Through the analyses the peak story drift ratios were extracted by selecting the maximum value of relative displacement of each level. Figure 2.4.1 displays the time history of the story drift ratio for all the 15 levels of the moment frame from which the peak SDR was defined at approximately 3.8% corresponding to the second story. It can be observed that the response pattern of the frame is consistent at all story levels.

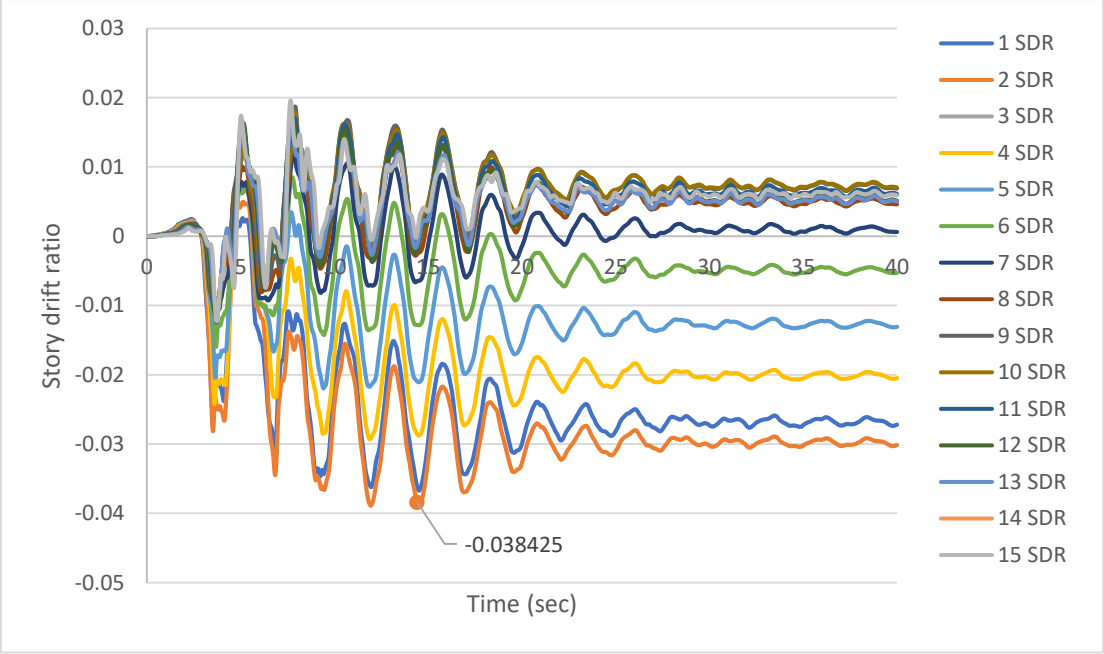

Figure 2.4.1. Story drift ratio time history for GM01

CHAPTER 3. SEISMIC DEMAND ON THE COLUMN SPLICES IN THE 15-STORY FRAME UNDER GM01

3.1 Dynamic properties of the frame: Modes and periods of vibration

The dynamic properties of the frame have an impact on the seismic response of the structure, hence it was important to define these properties by performing modal analysis on the 15-story special moment frame as discussed in previous sections. The first twelve fundamental modes of the frame were defined from the numerical model and were under investigation for Rayleigh damping as mentioned. The fundamental periods of the first, second, third and fourth modes were 2.491sec, 0.920sec, 0.549sec and 0.388sec respectively. All the mode shapes are illustrated in Figures 3.1.1, 3.1.2, 3.1.3 and 3.1.4. In the following sections, it will be demonstrated that the response of the structure beyond elastic behavior is mainly affected by higher modes and the deformed shape is similar to the mode shapes.

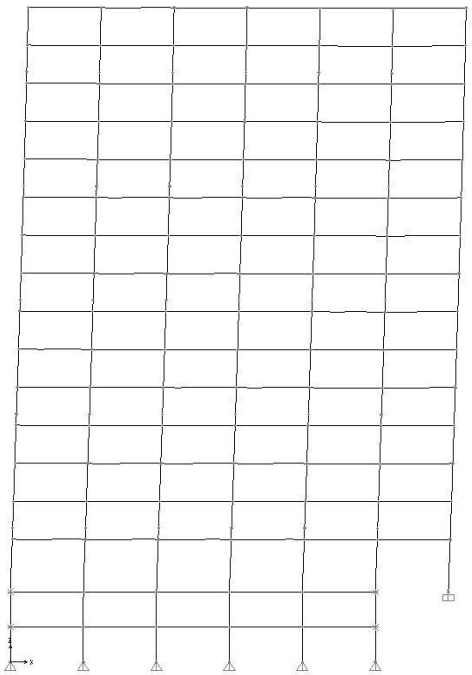

Figure 3.1.1. 1st mode, T_1=2.491 sec

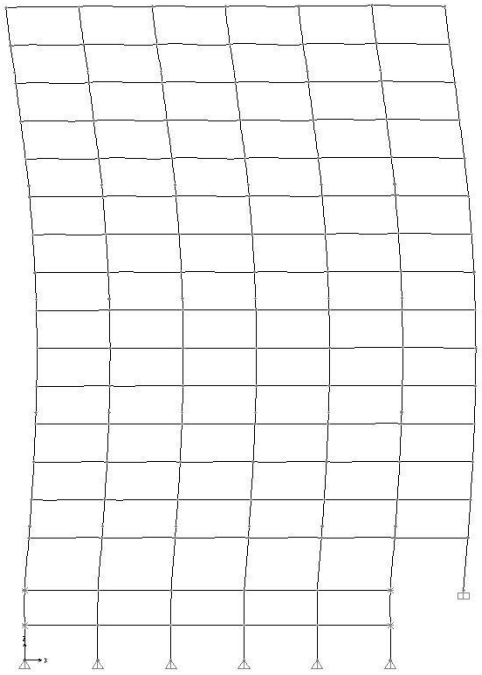

Figure 3.1.2. 2nd mode, T_2=0.920 sec

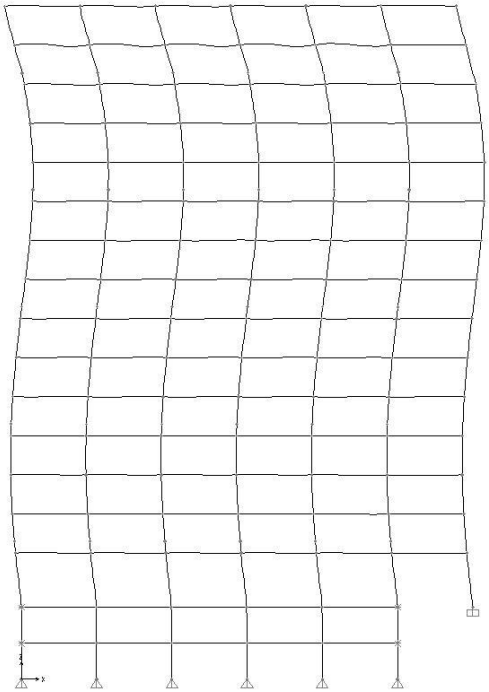

Figure 3.1.3. 3rd mode, T_3=0.549 sec

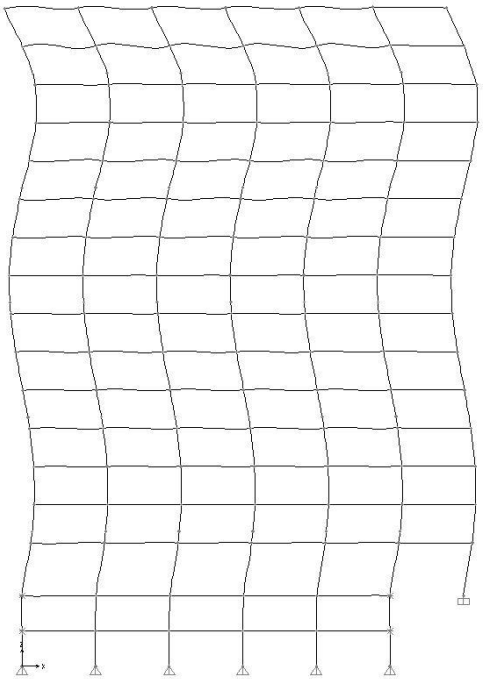

Figure 3.1.4. 4th mode, T_4=0.388 sec

3.2 Identification of the peak tension forces in the column splice, Ps

The first term to be estimated is the tensile axial force demand of the column splice. The notation adopted for this study is following Shen et al [11] notation, therefore the peak axial tensile force at the column splice level is noted as P_s and it was normalized by the nominal capacity of the smaller column on top of the column splice, P_{ty}. To identify the peak value, the time history of the axial force of the column splices locations were extracted, normalized and the peak absolute value of each splice was calculated in order to estimate the maximum tensile demand of the frame. For illustration, Figure 3.2.1 shows the response of the structure in terms of axial force demand of 14th story exterior column splices, it is observed that for these two splices the absolute peak P_s/P_{ty} ratio is approximately 0.057. The procedure was time consuming considering that the 15-story moment frame includes thirty column splices hence, the peak values of P_s were extracted using SAP2000, normalized and

locating the peak value. As it is observed, the maximum value is negative which indicates that the splice is in compression. Following the procedure described, the peak axial tensile demand ratio of the moment frame under GM01 for a story drift ratio of 2% estimated was 0.374. The analyses results indicated that all the column splices were under compression for all the cases set in the model and the demand over capacity ratio is not affected by the ground motion, on the contrary the axial force demand is relatively constant as it will be discussed in the following chapters. Additionally, the ground acceleration versus the peak P_s/P_{ty} ratio was plotted with the peak exterior and the maximum value for interior column splices at each level of the frame as demonstrated in Figure 3.2.2 under GM01 for story drift ratios of 2%, 4% and 6%. It can be observed that the frame peak axial demand-to-capacity ratio corresponds to the 2nd story exterior column splice. Furthermore, the exterior column ratios are higher than the interior column ratios.

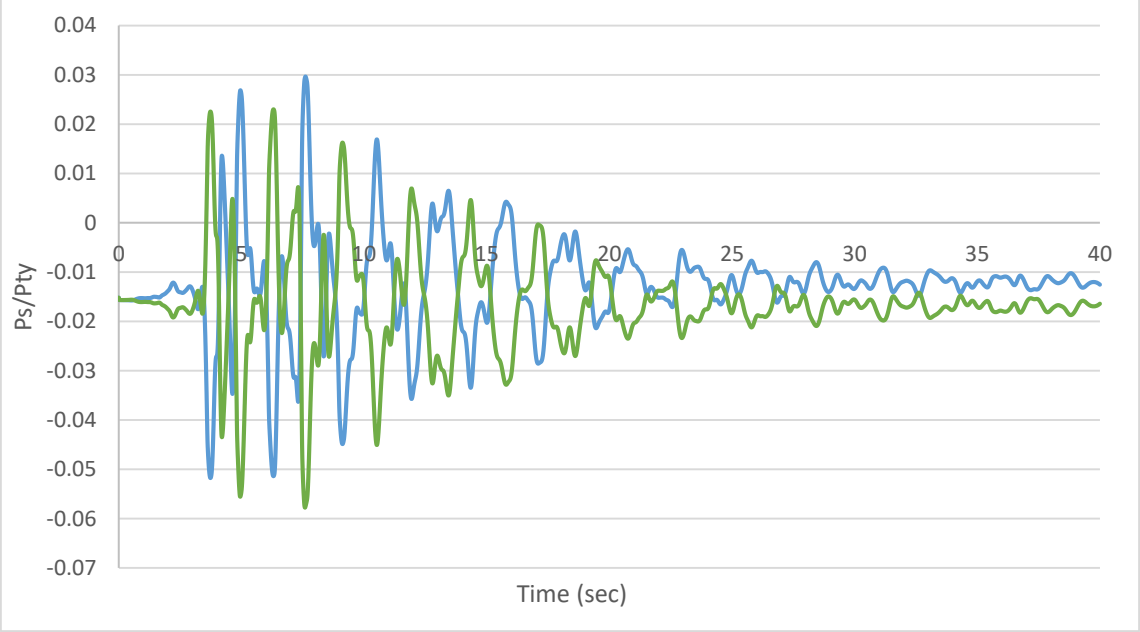

Figure 3.2.1. Normalized axial force time history response of 14th floor exterior column splices under GM01 at 2% SDR

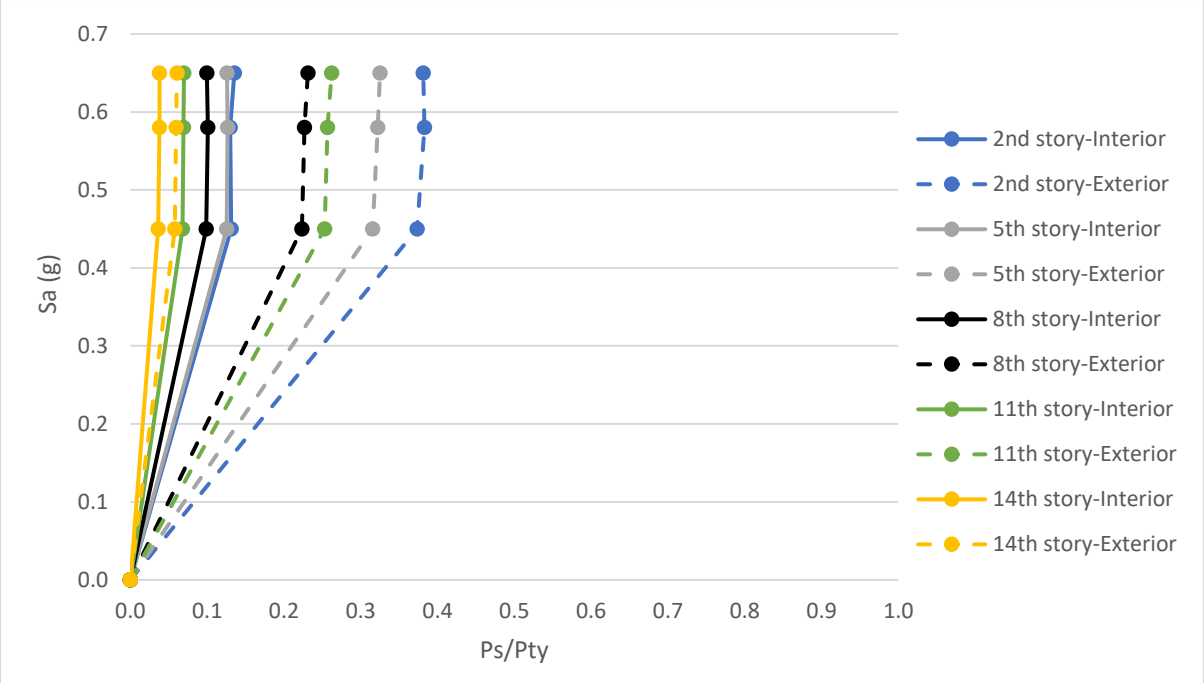

Figure 3.2.2. Splice Locations: Sa(g) vs. Ps/Pty under GM01

3.3 Identification of the peak bending moment in the column splice, Ms

The second term estimated for the seismic demand evaluation was the peak bending moment of the column splice and plastic moment ratio M_s/M_{pt}. With similar procedure as the identification of the axial tensile force, the time history of the moment demand on the splices was extracted from SAP2000, normalized and then the absolute value was taken to find the maximum value of the ratio. The demand ratio is important to the investigation of the demand on the splice location specifically and in combination with the IDA curve and the performance levels, the correlation between the overall response of the frame and the splice demand can be established. In contrast with the axial force demand, it was observed from the analyses results that the bending moment demand varies under each ground excitation and as expected is increasing in proportion to the story drift ratio of the structure. The bending moment demand over capacity ratio of the 14th story exterior column splices under GM01 corresponding to the axial tensile force plotted in the previous section is illustrated in

Figure 3.3.1. As it can be observed, the column splice response is almost identical for the two exterior locations investigated in the plot. The peak normalized flexural ratio of the two exterior column splices at 14th story is approximately equal to 0.510 as it was calculated and displayed on the plot. As mentioned, this process was time consuming thus the peak values of the moment demand were extracted from SAP2000 and the demand over capacity ratio was calculated. In the next chapter, the flexural demand of the frame is summarized for the twenty ground motions. Moreover, the ground acceleration was plotted with the peak flexural demand/capacity ratio for each column splice level as demonstrated in Figure 3.3.2 under GM01 for the overall response of the frame at 2%, 4% and 6% of SDR. It is observed that the frame peak M_s/M_{pt} ratio is correlated to the 14th story interior column splice and that the interior column ratios are greater than the exterior column ratios.

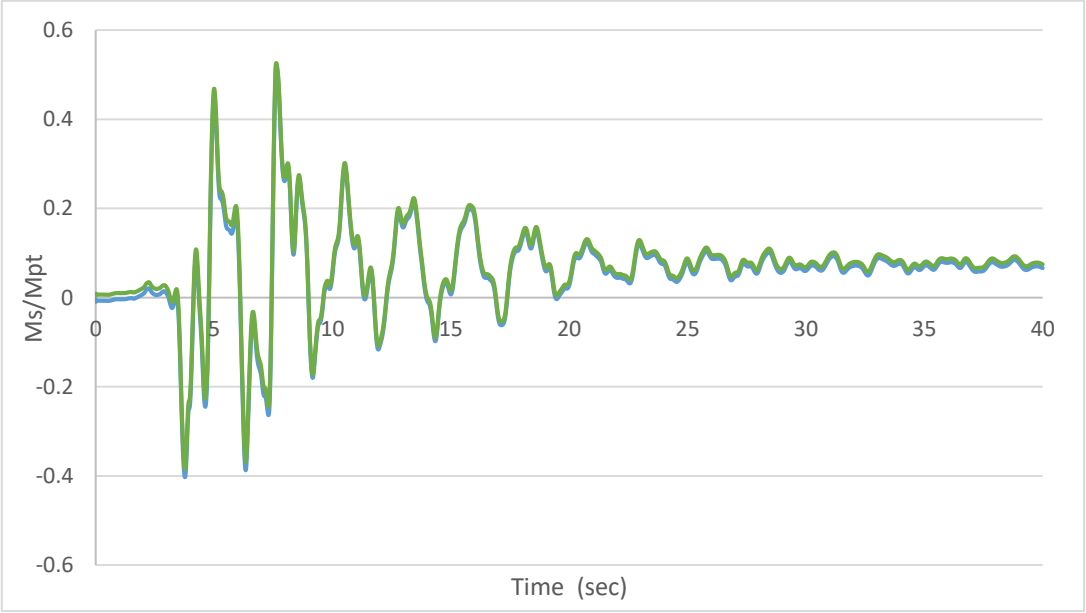

Figure 3.3.1. Normalized bending moment time history response of 14th floor exterior column splices under GM01 at 2% SDR

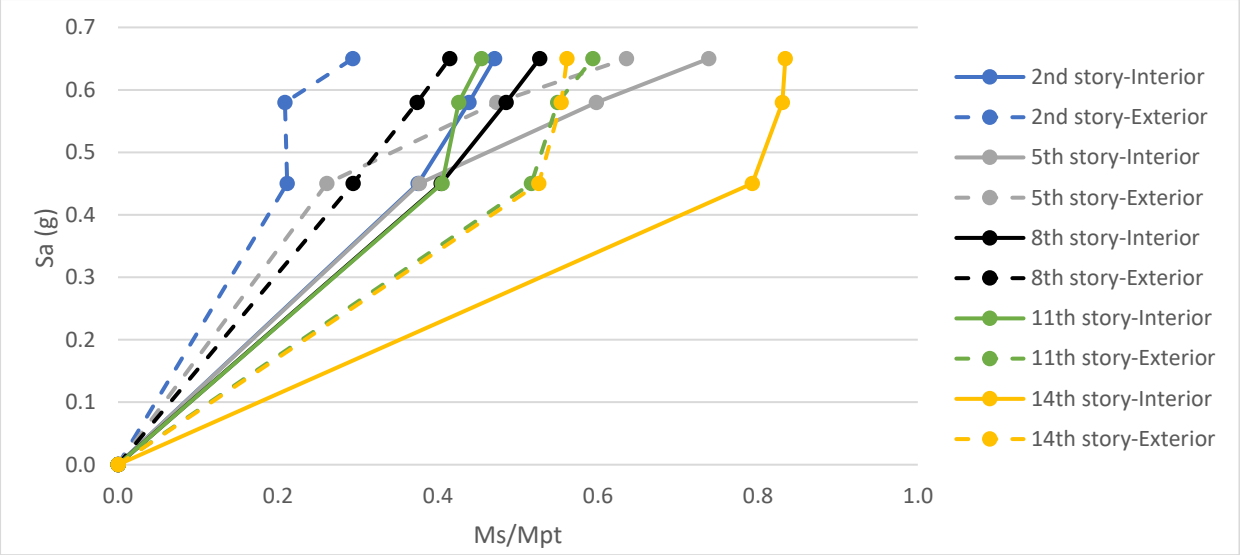

Figure 3.3.2. Splice Locations: Sa(g) vs. Ms/Mpt under GM01

3.4 Identification of the peak combination of bending moment and axial tensile force

Assessment of the demand on the splices was mainly established by the peak combined axial and flexural demand of the frame. To estimate the maximum ratio, the time histories of both axial tensile force and bending moment were calculated from the nonlinear time history analyses and extracted as described in the previous sections. The axial force P_s of the splice was normalized by the capacity, P_{ty}, of the small section and likewise the flexural demand-to-capacity ratio was calculated separately with the demand of the splice location M_s and the capacity of the smaller column M_{pt}. The axial and flexural demand was combined as time histories from sections 3.2 and 3.3 resulting to the combined demand of the exterior column splices located at 14th story as shown in Figure 3.4.1. It is observed that although the axial response of the splices was not identically the same, the combined axial and flexural ratio comply with the normalized bending moment time history of the frame. Despite the importance of the axial force on the welded connection, the influence on the combined demand in limited due to constant axial demand for all ground motions. The peak combined axial and moment ratio is the maximum absolute value when comparing the response of all

the column splice locations for specific scale factor of ground excitation. For demonstration, the peak $P_s/P_{ty} + M_s/ M_{pt}$ ratio for exterior column splices at level 14 is approximately 0.54. Overall response and comparison is following in the next chapter.

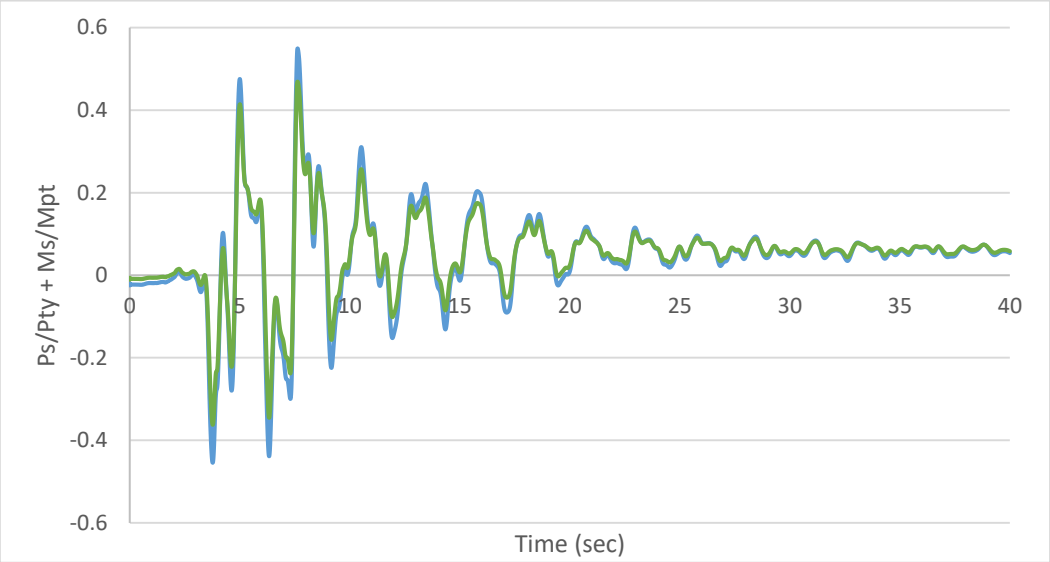

Figure 3.4.1. Combined axial and flexural demand time history of 14th floor exterior column splices under GM01 at 2% SDR

3.5 Identification of the maximum plastic hinge rotations in beams

The plastic hinge rotation (PHR) in beams is directly related to the story drift ratio. Due to the displacement of the frame, it is expected that the beam will rotate proportionally to maintain the 90-degree angle at the beam-to-column interface. For evaluation, the peak plastic hinge rotation was determined after each analysis with similar procedure to peak axial and flexural demand. The PHR time history of hinges was extracted and the maximum absolute value was to be defined. Considering that the 15-story special moment frame is consisted of 75 beams with two plastic hinges assigned at each beam, this procedure would be extremely time consuming, therefore the envelope of plastic hinge rotation was determined through SAP2000 and the peak absolute value was determined.

CHAPTER 4. SEISMIC DEMAND ON THE COLUMN SPLICES IN THE 15-STORY FRAME UNDER 20 GROUND MOTIONS

4.1 Peak response patterns in the moment frame and column splice

Assessment of the demand was a combination of the seismic behavior of the frame, the demand on column splices and the plastic hinge rotation. The column splice demand and the plastic hinge rotation at beam ends was evaluated at specific performance levels as defined earlier, utilizing the incremental dynamic analysis of the 15-story special moment frame. Initially the IDA curves evaluate the seismic response at increasing levels of ground motion intensity as shown in Figure 4.1.1. It can be observed that an outlier curve corresponding to ground motion GM02 exceeds the ground acceleration range of 0.37g and 1.2g that represents the set of ground excitations. GM02 curve requires more than 3.0g for the frame to experience 6% of SDR in contrast with the minimum value of 0.37g correlated to GM04. For discussion, GM02 will be excluded from the IDA plot nevertheless the results of demand corresponding to this ground excitation are not excluded. Figure 4.1.2 illustrates the IDA curves excluding the ground motion GM02 and it is noted that:

- While the ground acceleration is increasing, the story drift ratio is linearly increasing until approximately 2% of SDR.
- From Figures 4.1.3 – 4.1.5, it is observed that the response under different ground excitations varies. Some of the curves are smoother than others due to the nature of the excitation.
- The peak SDR in most of the cases was the story drift angle corresponding to higher stories for elastic response until 2% of SDR while the second story of the moment frame experienced the peak SDR ratio when the structure undergoes inelastic behavior.

For better understanding and assessment of the overall response of the structure, the plastic hinge maps of the frame at 1%, 2%, 3%, 4% and 6% of SDR with the corresponding bending moment diagrams were plotted for GM02. Figures were utilized to evaluate the response of the frame under elastic behavior and gradually to plastic hinge formation until the 15-story SMF experienced 6% of story drift ratio. Appendix C includes plastic hinge maps and bending moment diagrams at several time steps such as at the peak SDR, at the first plastic hinge formation in columns and at the end of the excitation. The results correlate to ground motion GM02 and the observations from the figures in Appendix C are:

- The moment diagrams revealed different moment diagram shapes that were categorized for the purpose of this study as they are illustrated in Figure 4.1.6. The first category was defined as the Perfect Double Curvature (PDC), the elastic BMD utilized in design with point of inflection (PI) near mid-height of the column. The second type was specified as the Upper Triangle Double Curvature (UTDC) as shown in figure 4.1.6b with point of inflection below the mid-height of the column. Next pattern was the Lower Triangle Double Curvature (LTDC) where point of inflection for the column is located above mid-height. Last type of moment diagram shape is the Perfect Single Curvature (PSC) describing the frame mechanism when no axial force is observed in the beams and the columns of the frame from top to base is responding as a cantilever (see Figure 4.1.6d).
- Two of the patterns observed in seismic response of the frame implicate column splice formation. When UTDC occurs, plastic hinge forms on the top of the column while at the case of LTDC plastic hinge formation was observed on the bottom of the column.
- The displacements of the frame at 1%, 2% and 3% of SDR comply with the first mode shapes. For 4% and 6% of story drift, higher modes mainly influence the response of the frame.

- At 1%, 2% and 3% of SDR when peak story drift occurs, perfect double curvature (PDC) was observed on columns.
- In all cases of SDR, at the end of excitations at 40 seconds, single curvature was observed in the moment diagrams. While SDR is increasing, the number of columns experiencing single curvature is rising as it is demonstrated, especially in the lower story levels. At 1% of SDR, single curvature is observed on 14^{th} story and by the time structure reach 3% of SDR, plastic hinge formation occurred on the interior column splice of 14^{th} story and the bottom of exterior columns on the same level. Additional plastic hinge forms on the top of column on 12^{th} story.
- At 4% of SDR, plastic hinges formed on the bottom of 1^{st} story columns with the LTDC bending moment pattern. Additional plastic hinges formed on the top of the 5^{th} story under the UTDC moment diagram shape and on the column splice location on 14^{th} story. The column splice plastic hinge was also indicated by the peak M_s/M_{pt} results at 4% of SDR as shown in Figure 4.3.2. At the end of excitation, massive single curvature was observed at the lower levels of the frame.
- When the overall response of the frame was near collapse prevention at 6% of SDR, similar behavior was observed with plastic hinge formation under LTDC and UTDC bending moment patterns. Furthermore, at the columns of 2^{nd} up to the 5^{th} story, plastic hinge formation was initiated on the top of the columns with the joints to develop plastic hinges: two in the beams and one on the bottom column of the joint. The inelastic action in three joint members was critical with possibility of joint failure if hinge form on the top section. This development could be interpreted with the rotational capacity of the beams. When the beam was not able to develop additional rotation, the plastic hinge was forced to form on the column creating a critical joint.

- At the end of excitation at 6% of story drift ratio the massive single curvature moment diagram and the plastic hinge map indicate various column splices with possibility of plastic hinge formation at any point beyond 6% of SDR.
- The main observation from the response is the plastic hinge formation on the column splices of 14th story. Recall that that the strong column-weak beam ratio determined in design process corresponding to 14th story level joint was 1.47, and the frame sections satisfy the SCWB requirement. In contrast to the high SCWB ratio, the demand exceeded the capacity in splices in addition to the bottom of exterior columns at the same level.
- Plastic hinge formation occurred on the top columns of lower levels although large SCWB ratio was estimated for the selected members. One could believe that the high design ratio would be conservative and inelastic action on columns would be prevented, however the findings indicate that even the overdesigned column sections undergo inelastic behavior.

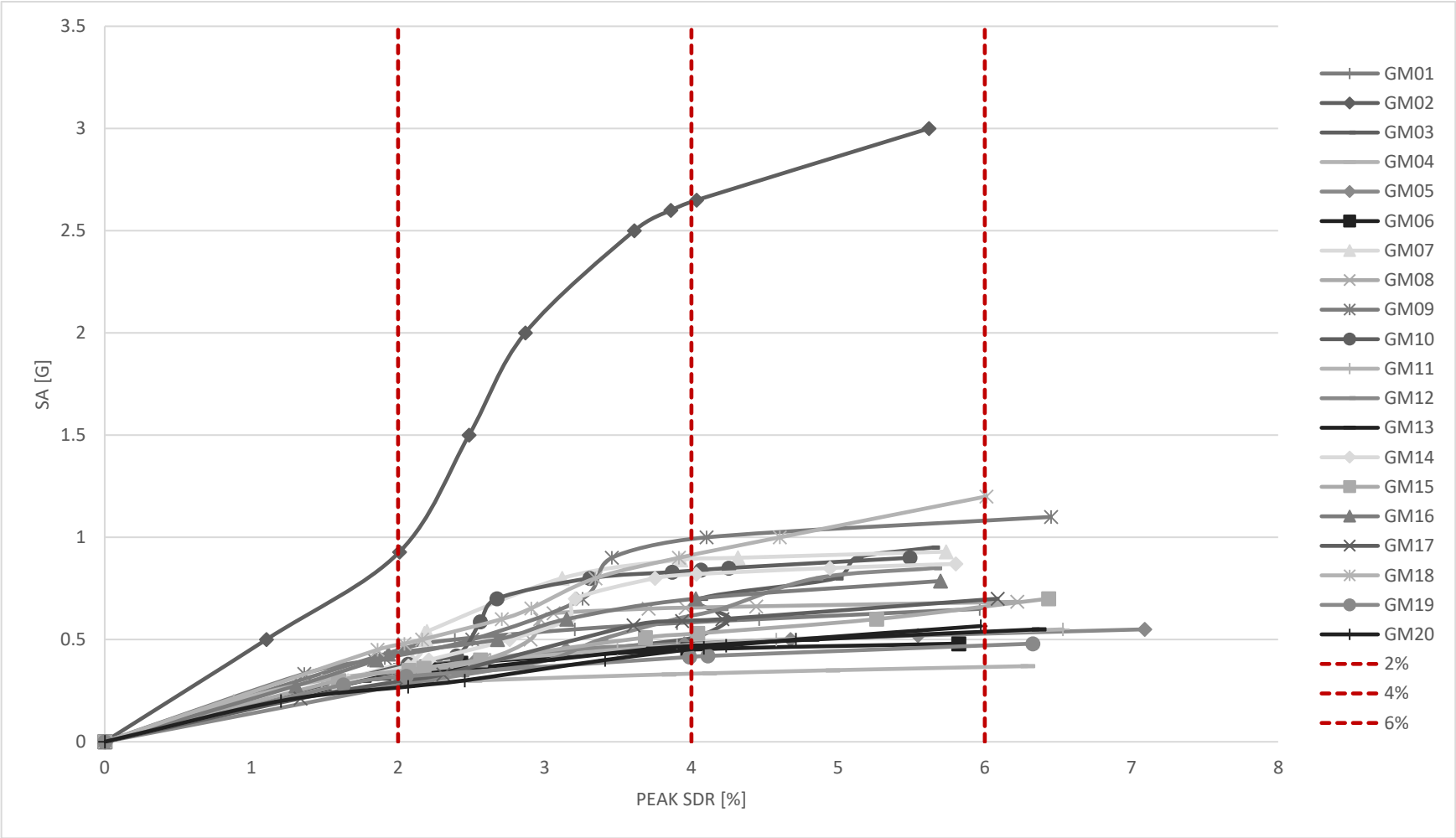

Figure 4.1.1. Incremental dynamic analysis curve of 20 ground motions

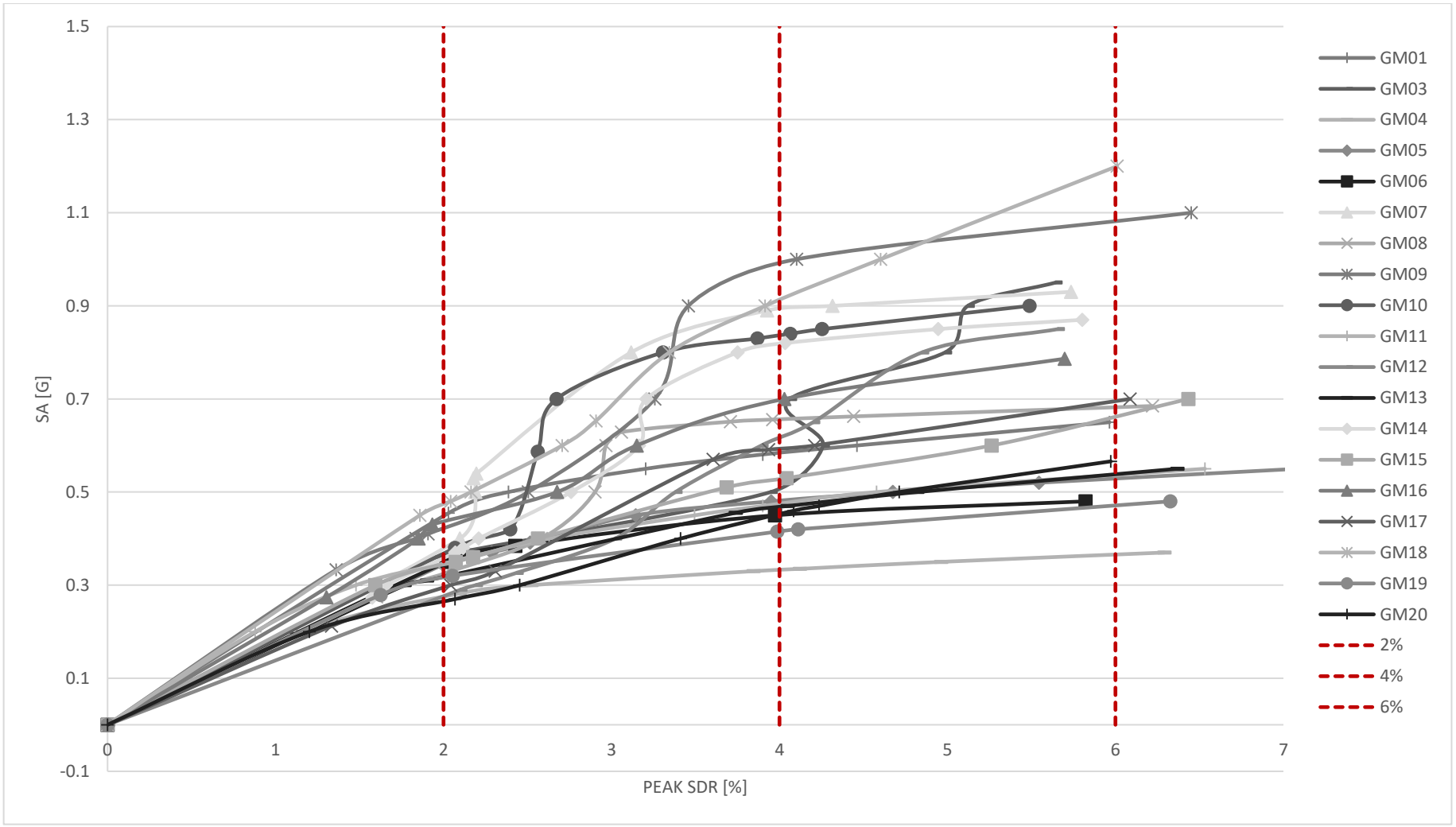

Figure 4.1.2. Incremental dynamic analysis curve of ground motions excluding GM02

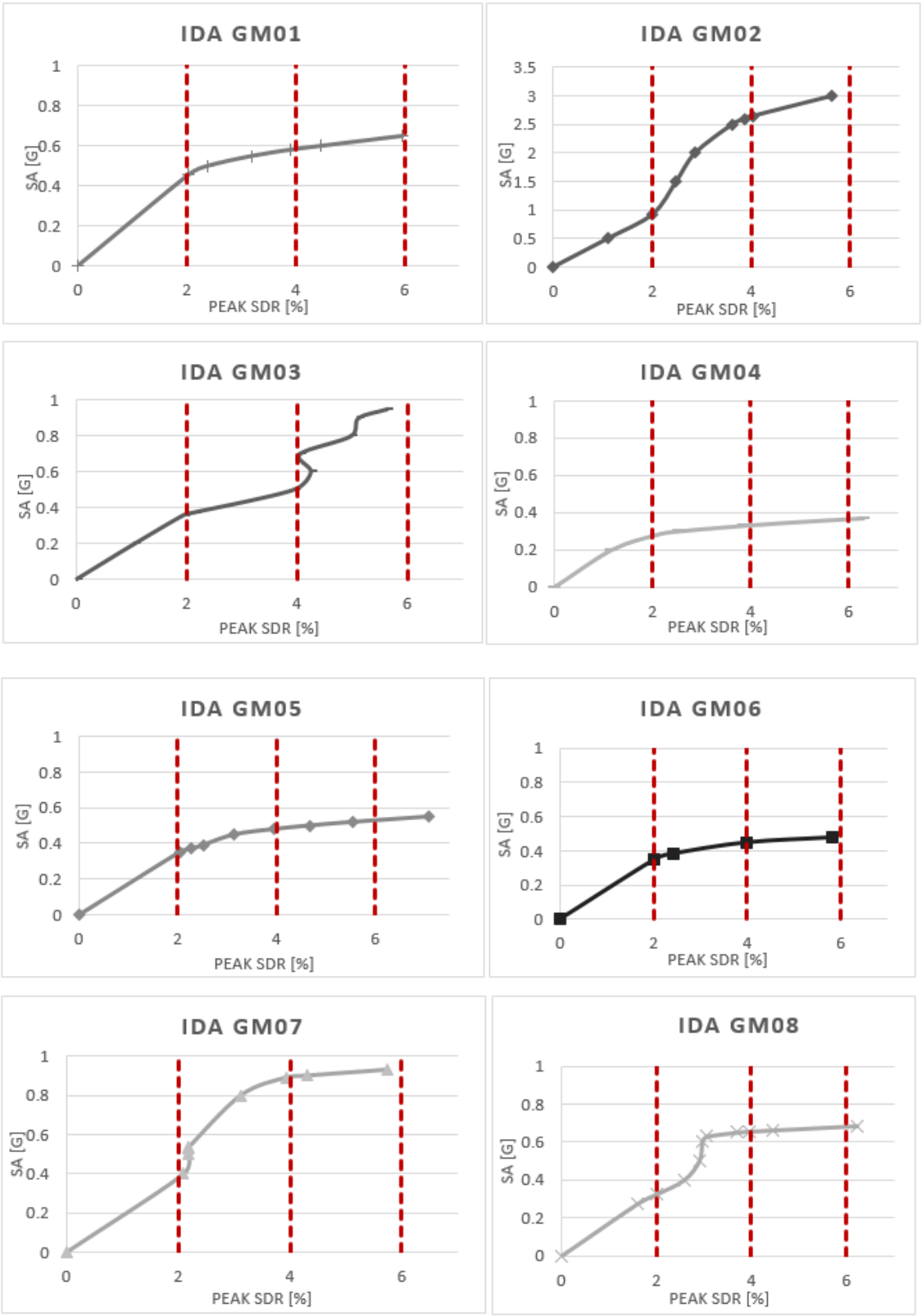

Figure 4.1.3. Incremental dynamic analysis curve of ground motions GM01-08

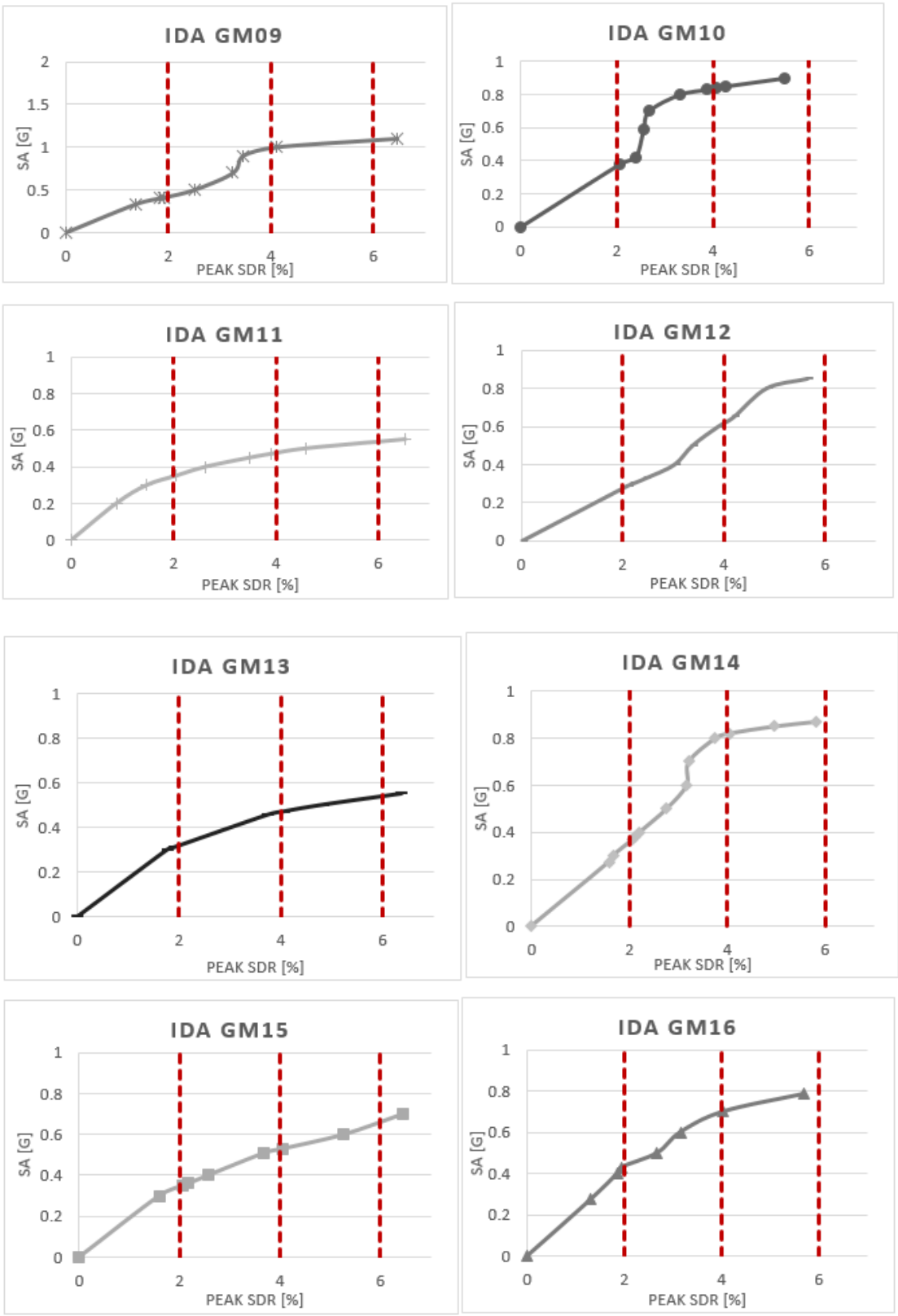

Figure 4.1.4. Incremental dynamic analysis curve of ground motions GM09-16

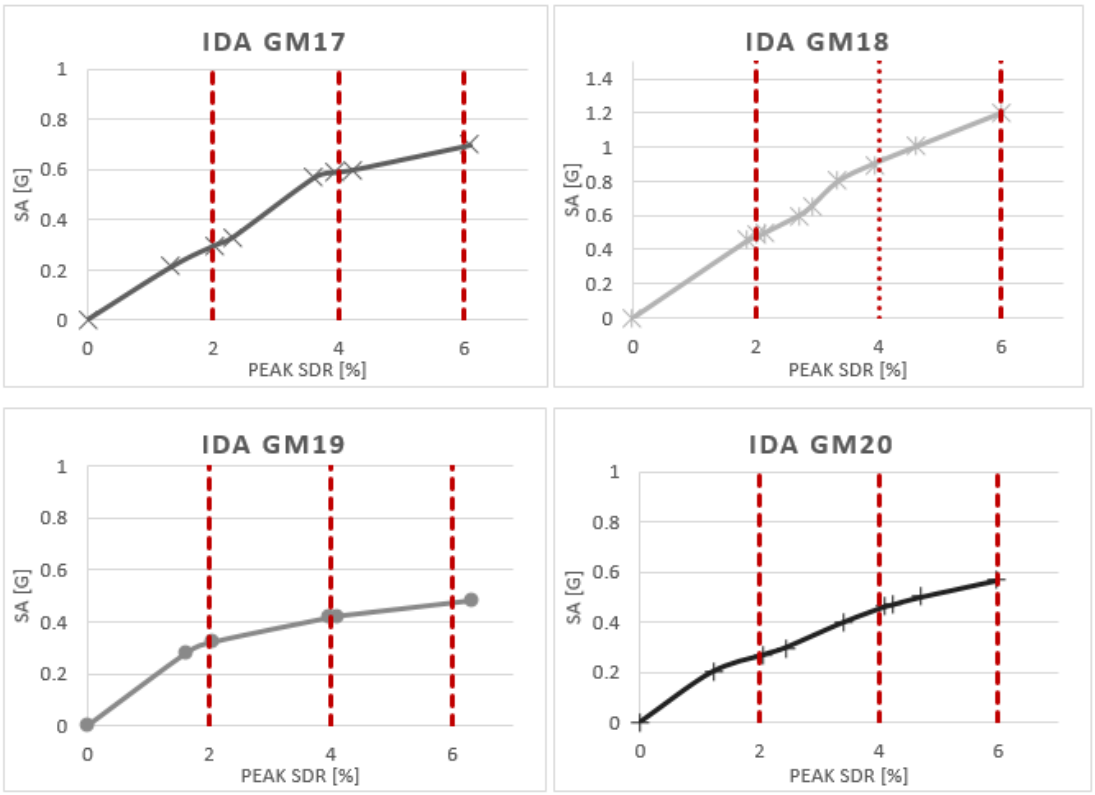

Figure 4.1.5. Incremental dynamic analysis curve of ground motions GM17-20

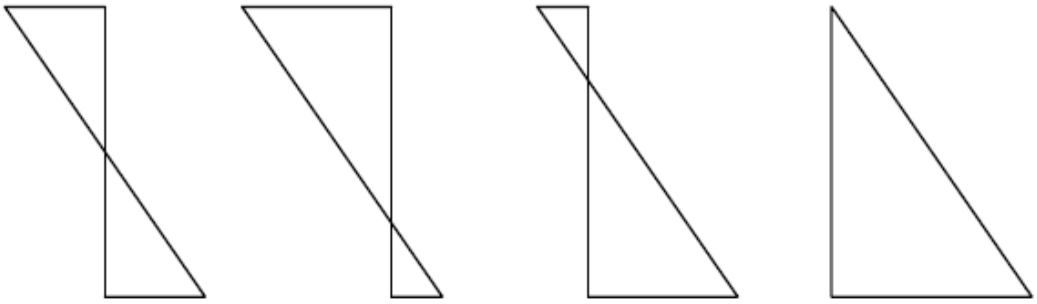

a) PDC b) UTDC c) LTDC d) PSC

Figure 4.1.6. Bending moment patterns

4.2 Peak tension forces in the column splice, P_s

The maximum axial tensile force demand ratio determined normalized by the axial capacity of the smaller column section is demonstrated in Figures 4.2.1, 4.2.2 and 4.2.3 at 2%, 4% and 6% of story drift ratio respectively. Figures represent the absolute values of the estimated ratios although actual values were of negative sign

representing compressive forces. Axial demand was compressive in all ground excitations result. As it can be observed:

- At 2% of story drift ratio, the average axial demand on the column splices with is 0.354 and a small variation under each ground excitation is observed with lowest ratio of 0.282 and maximum of 0.379 at GM20 and GM18 respectively.
- When the frame experienced 4% of story drift ratio, the maximum P_s/P_{ty} is increased compared to 2% of SDR however not significantly. The average of peak axial demand over capacity ratio is 0.390 and the overall demand over the set of twenty ground motions is uniform as shown in Figure 4.2.2.
- The peak P_s/P_{ty} ratio at 6% of SDR is greater than the previous levels with mean of 0.399. As Figure 4.2.3 displays, the demand varies under each ground excitation in contrast with 2% and 4% of SDR, with the lowest ratio to be 0.374 and the highest 0.423 corresponding to GM20 and GM03 respectively.
- In general, it is noted that the peak P_s/P_{ty} ratio is uniform through the ground excitations with a small increase at each performance level.

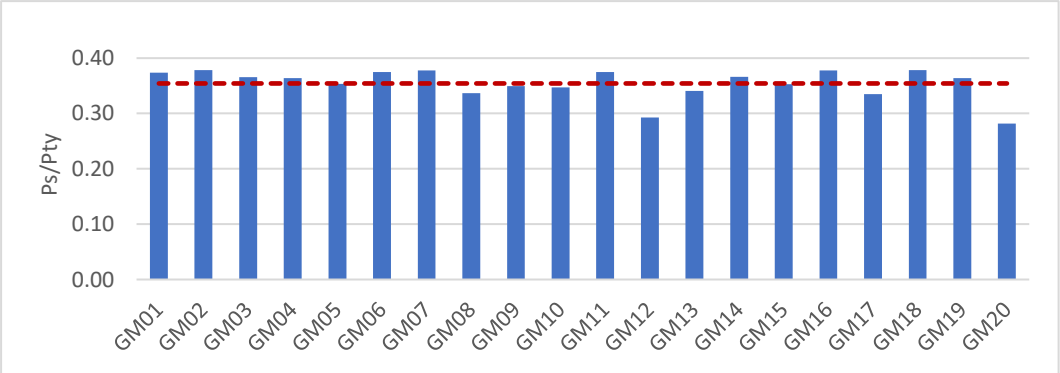

Figure 4.2.1. Axial force demand at 2% of SDR under 20 ground motions

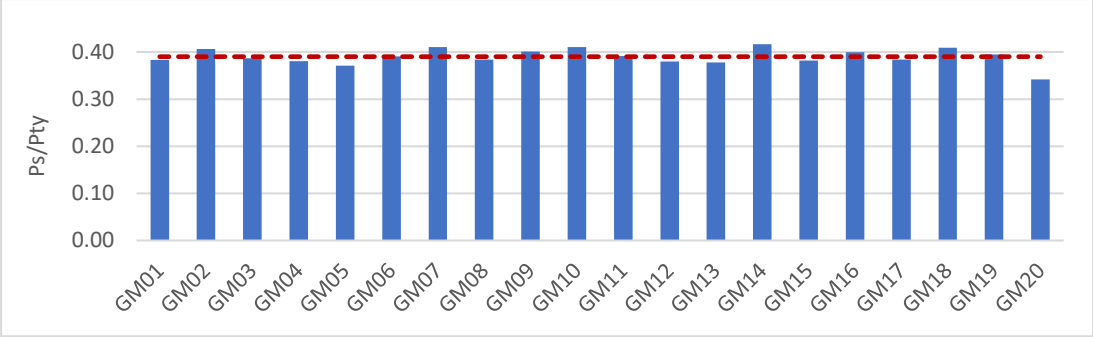

Figure 4.2.2. Axial force demand at 4% of SDR under 20 ground motions

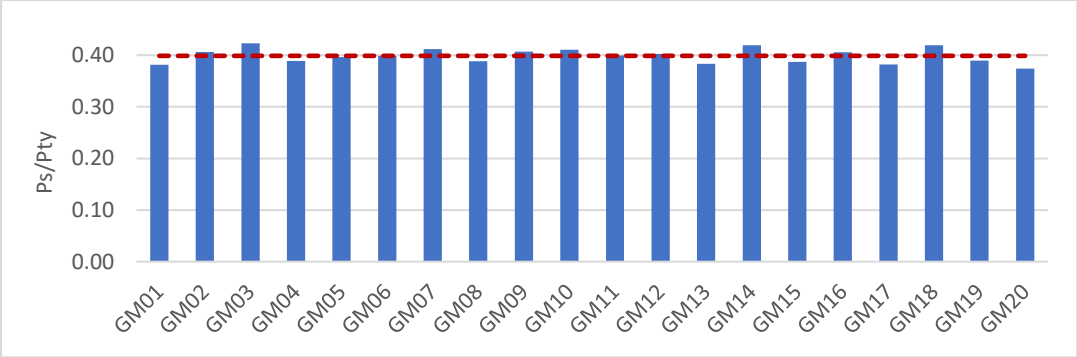

Figure 4.2.2. Axial force demand at 6% of SDR under 20 ground motions

4.3 Peak bending moment in the column splice, M_s

The normalized moment demand on the column splice is demonstrated in Figures 4.3.1, 4.3.2 and 4.3.3 for the three performance levels at 2%, 4% and 6% of SDR respectively. Bending moment is important in assessment of seismic demand of the splice with the parameter to implement the shear forces in the column. The shear force will not be discussed in this thesis due to the correlation with the bending moment forces. Observation from the figures are that:

- When the frame experience 2% of SDR, the mean peak M_s/M_{pt} ratio on the column splice is 0.786 with the response of the structure to vary under each excitation. Additionally, from Figure 4.3.1 it is noted that under GM20 the splice demand corresponds to the lowest value of demand/capacity ratio equal to 0.596.
- Increasing the story drift ratio of the structure to 4%, leads to higher flexural demand/capacity ratio as observed in Figure 4.3.2. The rise is uniform and average

of 0.907 was estimated. In several cases the M_s/M_{pt} ratio exceeds 1.0, which implicates that plastic hinge formation occurred on column splices.

- At 6% of SDR, the peak demand is 94.8% of the small column nominal capacity on average. Simultaneously, the rising ratio causes increase in the plastic hinge formation with 50% of the cases to reach M_s/M_{pt} ratio equal or greater of 1.0.
- For all cases with flexural ratio over 1.0, the plastic hinge map was investigated. The results showed plastic hinge formation at the column splice of 14th story and several plastic hinges forming at the top of columns in the lower levels. Plastic hinge maps will be displayed in the following section.

Figure 4.3.1. Flexural demand at 2% of SDR under 20 ground motions

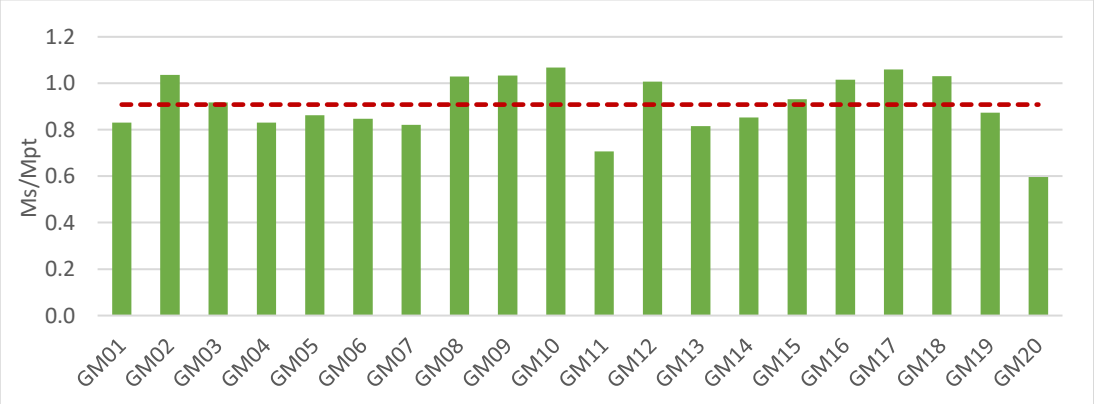

Figure 4.3.2. Flexural demand at 4% of SDR under 20 ground motions

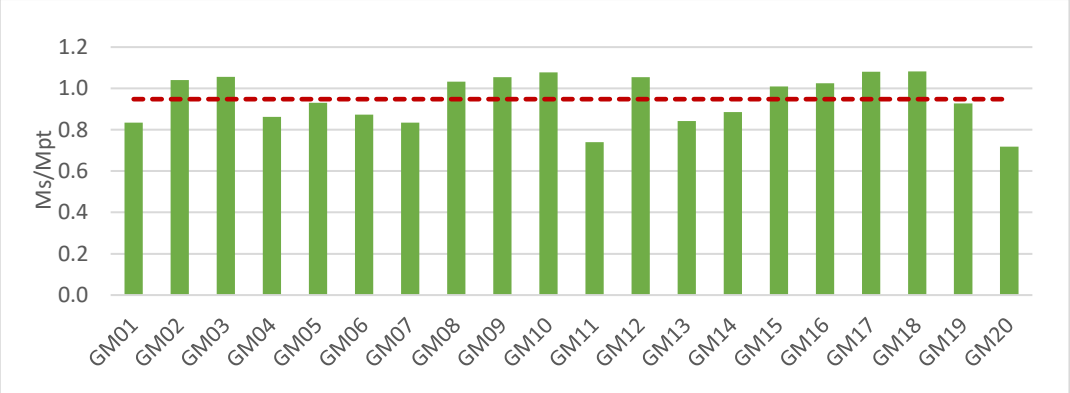

Figure 4.3.3. Flexural demand at 6% of SDR under 20 ground motions

4.4 Peak combination of bending moment and axial tensile force

Finally, the combined axial and flexural demand over capacity ratio was plotted for the ensemble of ground motions as illustrated in Figures 4.4.1, 4.4.2 and 4.4.3 at 2%, 4% and 6% of story drift ratio. From the plots, it can be inferred that:

- The $P_s/P_{ty} + M_s/M_{pt}$ ratio is influenced mainly by the flexural demand-to-capacity ratio as revealed from comparison between the two ratios, similar values were presented in Figure 4.3.1. The axial force influence is not as significant as the bending moment on the column splice.
- As the flexural ratio gradual increases, likewise the combined axial and flexural ratio follows the same pattern. The combined demand rises with uniform increase shown in Figures 4.4.1-4.4.3.
- At 2% of SDR the demand is less than the capacity with average ratio of 0.786 but as SDR gradually rises, the demand exceeds the capacity and plastic hinges are forming on the column splice location.
- By 6% of SDR, 50% of the ground motions the splice demand to go beyond the capacity of the smaller column section.

- When the frame reaches 6% of SDR, the demand approached 98.9% of capacity on average. At this performance level for the case of GM10, the demand is equal to 120% of nominal capacity being the highest combined axial and flexural demand/capacity ratio.

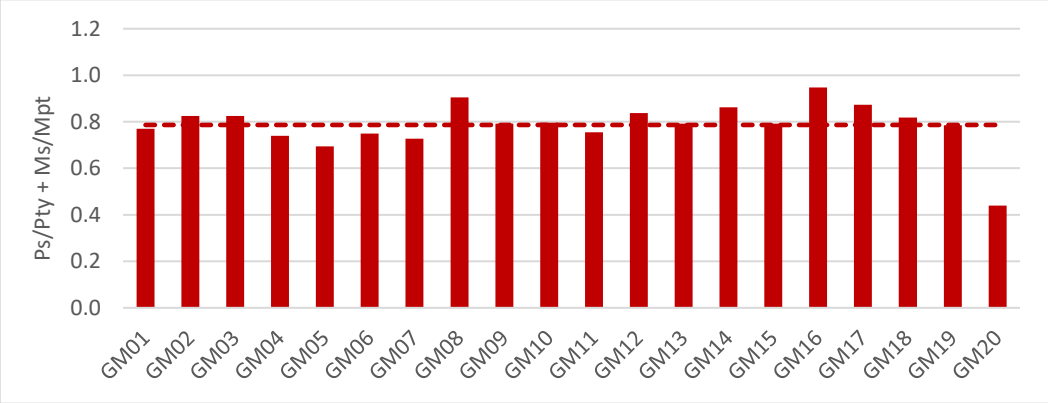

Figure 4.4.1. Combined demand at 2% of SDR under 20 ground motions

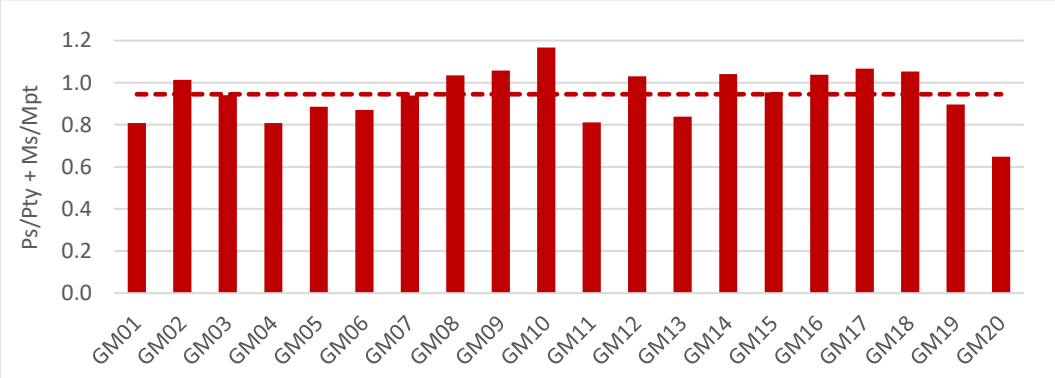

Figure 4.4.2. Combined demand at 4% of SDR under 20 ground motions

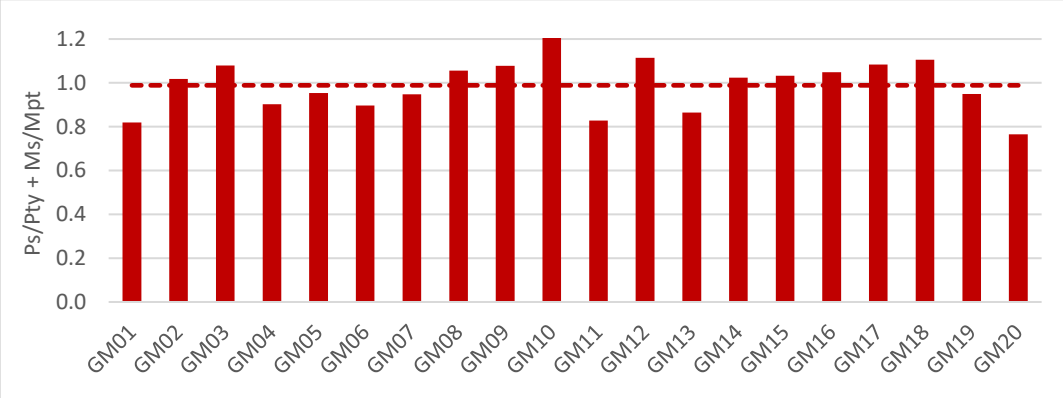

Figure 4.4.3. Combined demand at 6% of SDR under 20 ground motions

4.5 Maximum plastic hinge rotations in beams

Correlation between the plastic hinge rotation at beam ends and story drift ratio is expected. At 2% of story drift ratio is observed that the peak plastic hinge rotation (PHR) has a mean of 0.015 radians as illustrated in Figure 4.5.1. Subsequently, by increasing the SDR to 4%, the plastic hinge rotation at RBS locations is rising to a peak PHR of 0.034 radians on average. However, the RBS plastic hinges do not reach more than 0.04 rad when structure experience a story drift ratio of 6%, with exception ground motions GM09 and GM12. In combination with plastic hinge maps in previous sections, it is observed that the RBS hinges do not go beyond 0.04 radians, forcing plastic hinge formation on top of columns in lower story levels. Joints where plastic hinges were formed on the lower columns, already appear to have plastic hinges in three out of four sections. This mechanism can be critical due to possible failure of the joint if further demand force plastic hinge on the top section of the joint. This mechanism is observed at three consecutive story level joints as shown in figures in Appendix C.

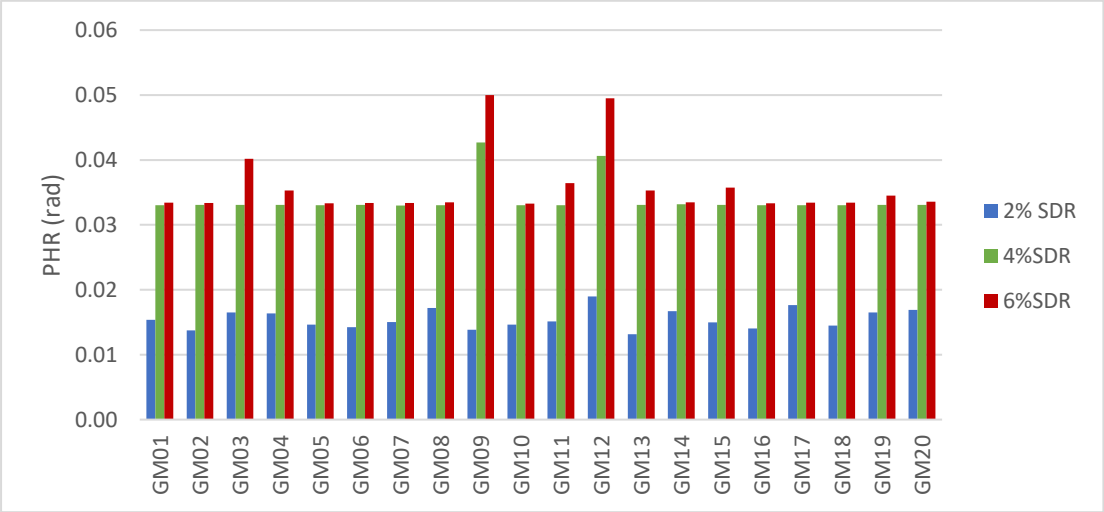

Figure 4.5.1. Peak plastic hinge rotation at beam end under 20 ground motions

CHAPTER 5. OBSERVATIONS AND CONCLUSIONS

This study investigates the flexural demand in columns in the following contexts: the demand on the column splice, the flexural demand distribution (bending moment diagram) shape, and the moment distribution at beam-column joints. Incremental dynamic analysis (IDA) was carried out for a 15-story special moment frame subjected to 20 different ground motions. A newly developed demand-chain concept was employed together with IDA in accessing the seismic demand on column splices and strong column-weak beam mechanism, based on inelastic deformation demand on beam-to-column joints at three performance levels, the immediate occupancy (IO) level, the life safety (LS) level and the collapse prevention (CP) level at 2%, 4% and 6% of story drift ratio (SDR) respectively. The demand on column splice was evaluated in terms of peak normalized axial ratio, the peak flexural ratio, and the maximum combined axial and flexural demand-to-capacity ratio. This investigation concludes, with combined IDA and demand-chain concept, that the flexural demand on the splice can reach as high as the nominal strength of the smaller section when the structure is subjected to the design earthquake. This study also presents systematically single curvature deformation patterns in the columns in contrast to the perfect double curvature (PDC) assumption used in code-based design of steel moment frames. Furthermore, this work reveals that plastic hinges may occur in the columns near beam-to-column joints when the frame was subject to the life safety (LS) level of earthquake ground motions. This finding presents a challenge to the current methodology used in enforcing strong column-weak beam in earthquake-resistant moment frames.

The overall response of the special moment frame was evaluated in terms of story drift ratio implementing incremental analysis and the demand was assessed in three performance levels. The IDA curves indicate that the range of ground acceleration for the ensemble of ground motions utilized was from 0.4g up to 1.2g excluding GM02. The ground acceleration against the story drift ratio is linearly increasing until 2% of SDR at which plastic hinges form at the RBS locations in the beams.

Beyond 4% of SDR it is noted that without significant increase in the ground acceleration, the frame response approaches the collapse prevention level. The decrease of the slope in the curve between 4% and 6% of SDR can be justified by the inelastic behavior and plastic hinge formation within the frame. Plastic hinges initiated at the design level earthquake did not influenced the ductile response of the frame.

The peak axial, flexural and combined demand-to-capacity ratios estimated at three performance levels are summarized in Figures 5.1, 5.2 and 5.3, illustrating the development of the seismic demand on the column splices. As the story drift ratio increases, the demand was gradually rising with uniform tensile axial force ratio P_s/P_{ty} at all performance levels. The increase in axial ratio was not as significant as the flexural demand. The normalized axial ratio initiated at 35.4% for minor structural damage and reached 39.9% near collapse.

The mean of flexural ratio (M_s/M_{pt}) was significantly increased from 75.7% up to 94.8% when structure experienced minor damage to near collapse respectively. In 50% of the ground excitations, the demand exceeded the nominal flexural strength of the small column. The combined axial and flexural demand/capacity ratio is mainly

influenced by the flexural ratio and follows the same pattern over the set of 20 ground excitations.

Moreover, the plastic hinge maps and the bending moment diagrams at various time steps and performance levels revealed four patterns on the seismic response of the 15-story special moment frame, two of which indicate plastic hinge formation on columns. Plastic hinges on column splices were observed beyond 4% of story drift ratio under all 20 ground motions regardless the type of the excitation. Additionally, at the end of excitations, single curvature was observed in several stories in all 20 ground motions.

Plastic hinges were observed at top of columns of lower story levels with the joint forming three plastic hinges out of four intersected sections. Although the strong column-weak beam mechanism was ensured through design with ratios greater than 1.20, the inelastic action on the column was not prevented. On the contrary, critical joint mechanism was observed.

Implementation of incremental dynamic analysis in this study revealed significant information on the flexural demand on columns. The outcomes indicate plastic hinge initiation on the column splices and gradual increase in the demand through various performance levels. However, further investigation with heavy section members will provide in depth understanding of the flexural demand. Finally, the strong column-weak beam (SCWB) requirement should also be incorporated in future research to assess the conservatism of current standard specifications.

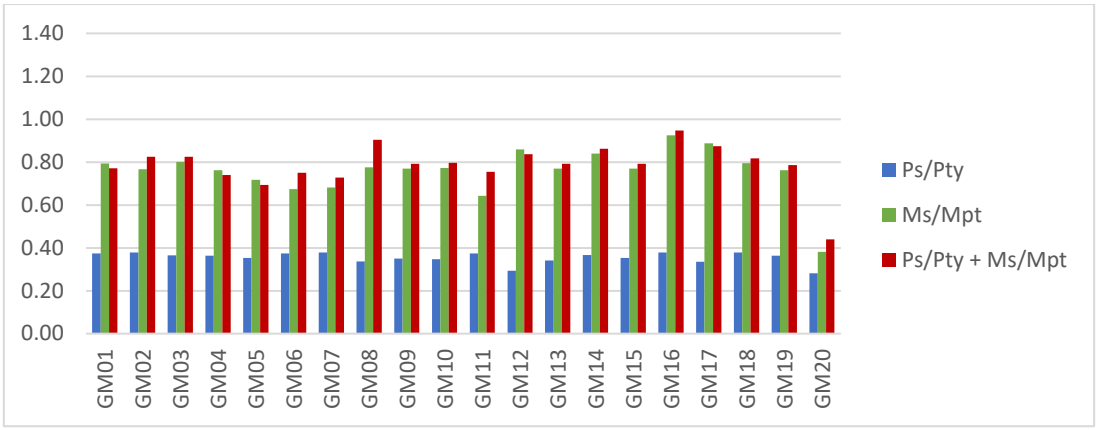

Figure 5.1. Column splice demand at 2% of SDR

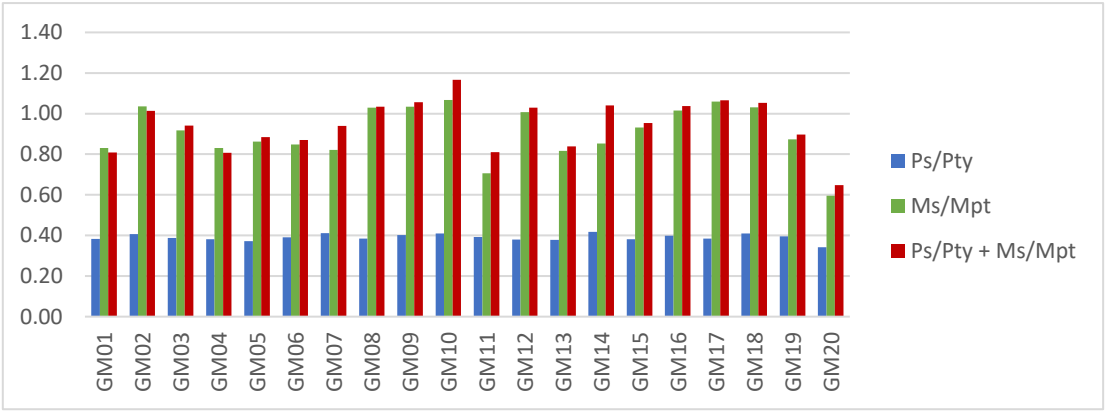

Figure 5.2. Column splice demand at 4% of SDR

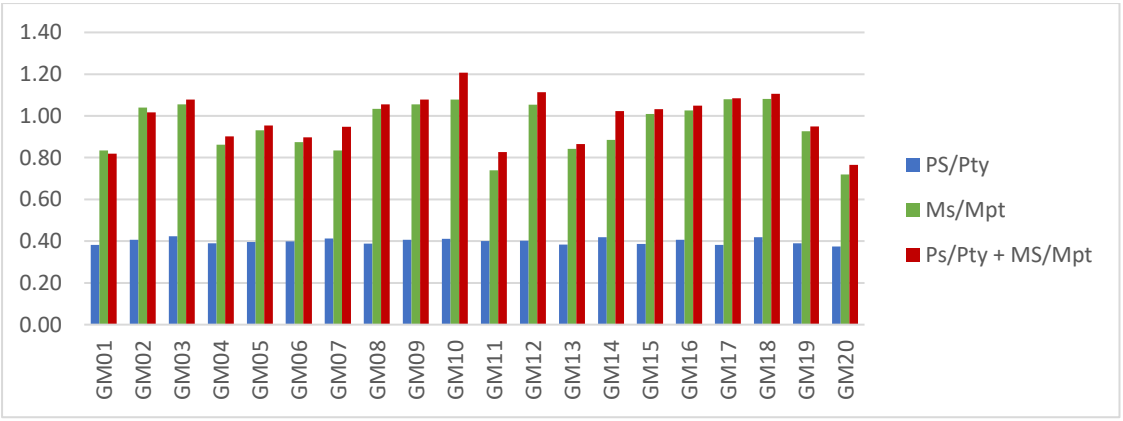

Figure 5.3. Column splice demand at 6% of SDR

Table 5.1. Average normalized demand

	Story Drift Ratio (%)		
	2%	**4%**	**6%**
Ps/Pty	0.354	0.390	0.399
Ms/Mpt	0.757	0.908	0.948
Ps/Pty + Ms/Mpt	0.786	0.945	0.989

REFERENCES

[1] AISC, 2010, *Prequalified Connections for Special and Intermediate Steel Moment Frames for Seismic Applications*, AISC 358-10, American Institute of Steel Construction, Chicago, Illinois.

[2] AISC, 2010, *Seismic Provisions for Structural Steel Buildings*, AISC 341-10, American Institute of Steel Construction, Chicago, Illinois.

[3] AISC, 2016, *Seismic Provisions for Structural Steel Buildings*, AISC 341-16, American Institute of Steel Construction, Chicago, Illinois.

[4] ASCE, 10, *Minimum Design Loads for Buildings and Other Structures*, ASCE 7-10, American Society of Civil Engineers, Virginia.

[5] Akbas, B., Doran, B., Sabol, T.A., Seker, O., Toru, P., Shen, J. "*Effects of various span lengths on seismic demand on column splices in steel moment frames*." Engineering Structures, (2014): 94–105.

[6] Lee, C.H., Jeon, S.W., Kim, J.H and Uang, C.M. (2005). "*Effects of Panel Zone Strength and Beam Web Connection Method on Seismic Performance of Reduced Beam Section Steel Moment Connections.*" Journal of Structural Engineering, 2005, 131(12): 1854-18.

[7] Engelhardt, M. D., Venti, M. J., Fry, G. T., Jones, S. L., and Holliday, S. D. (2000). "*Behavior and design of radius cut reduced beam section connections*." SAC/BD-00/17, SAC Joint Venture, Sacramento, Calif.

[8] FEMA-350, 2000, *Recommended Seismic Design Criteria for New Steel Moment-Frame Buildings*, prepared by the SAC Joint Venture for the Federal Emergency Management Agency, Washington, DC.

- "FEMA 355C: State of the Art Report on Systems Performance of Steel Moment Frames Subject to Earthquake Ground Shaking." Report. 2000. Document.
- "FEMA 355D: State of the Art Report on Connection Performance." Report. 2000. Document.

[9] Galasso, C., Stillmaker, K., Eltit, C., Kanvinde, A.M. (2015). "Probabilistic demand and fragility assessment of welded column splices in steel moment frames." Earthquake Engineering and Structural Dynamics, 2015, 44:1823-1840.

[10] Shaw, S.M., Stillmaker, K., Kanvinde, A.M. (2015). "*Seismic Response of Partial-Joint-Penetration Welded Column Splices in Moment-Resisting Frames*." Engineering Journal, AISC (2015): 87-108.

[11] Shen, J., Sabol, T.A., Akbas, B., Sutchiewcharn, N. (2010). "*Seismic demand on column splices in steel moment frames*." Engineering Journal, AISC (2010): 223-240.

[12] Vamvatsikos, D. and Cornell, C. A. (2002). "*Incremental dynamic analysis*." Earthquake Engineering and Structural Dynamics, 2005, 31(3):491-514.

[13] Yu, Q. S., Gilton, C., and Uang, C.-M. (2000). "*Cyclic response of RBS moment connections: Loading sequence and lateral bracing effects*." SAC/BD-00/22, SAC Joint Venture, Sacramento, Calif.

APPENDIX A: IMPACT OF DAMPING COEFFICIENTS REPORT

Cases:

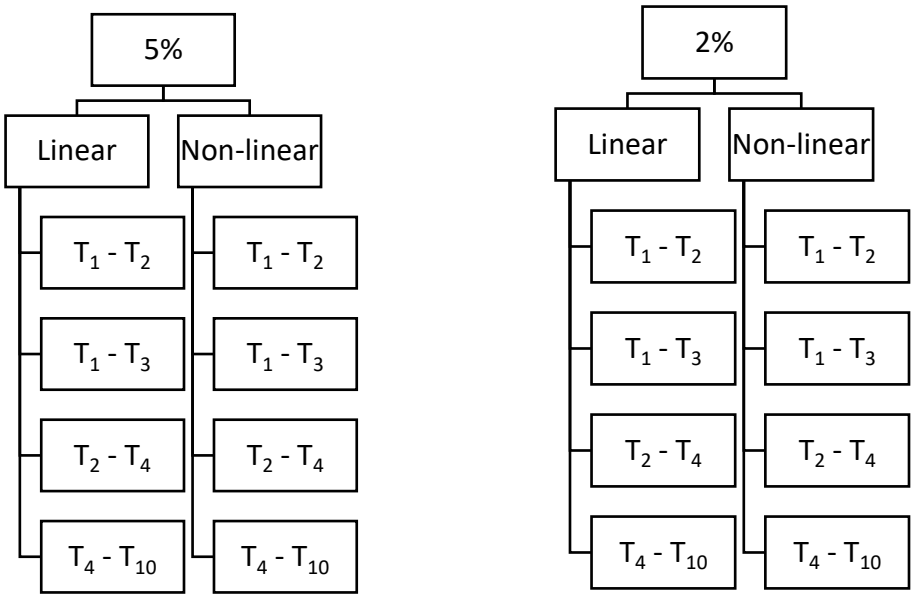

In analyses, the P-Delta effect was not included for all the above cases.

A. Damping ratio 5%

A1. 5% Linear Analysis

The Peak SDR is on the 1st level above the seismic base of the moment frame.

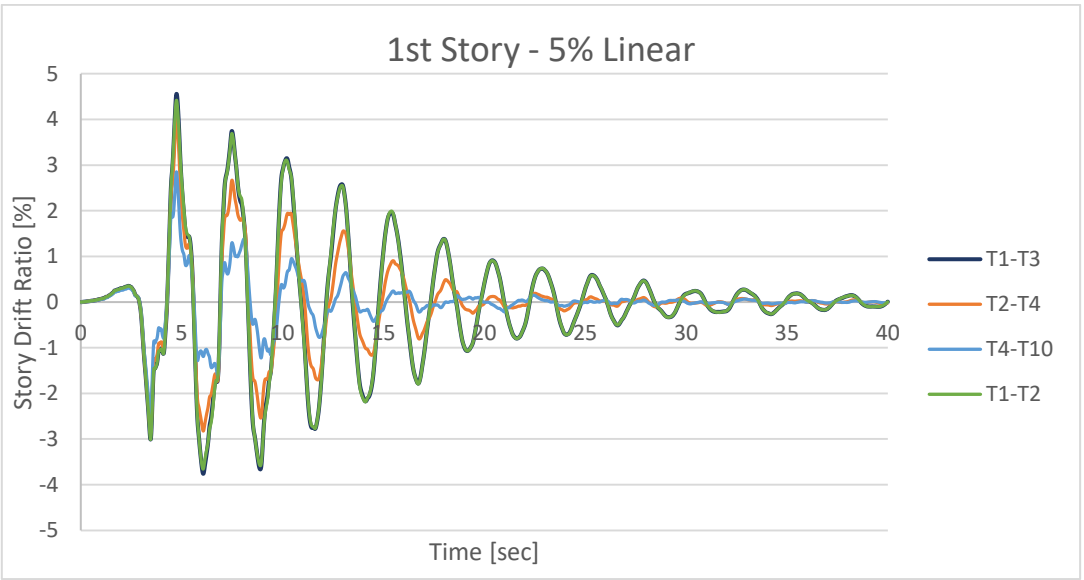

	T_1-T_2	T_1-T_3	T_2-T_4	T_4-T_{10}
Peak SDR (%)	4.421	4.558	4.059	2.852

A2. 5% Non-linear Analysis

The Peak SDR is on the 2nd level above the seismic base of the moment frame.

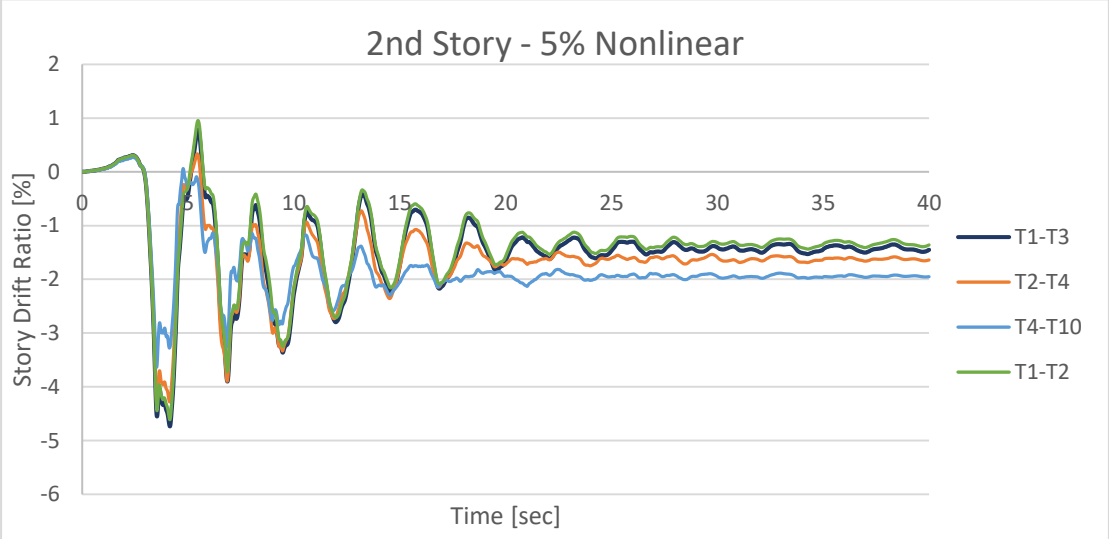

	T_1-T_2	T_1-T_3	T_2-T_4	T_4-T_{10}
Peak SDR (%)	4.611	4.734	4.316	3.635

B. Damping ratio 2%

B1. 2% Linear Analysis

The Peak SDR is on the 1st level above the seismic base of the moment frame.

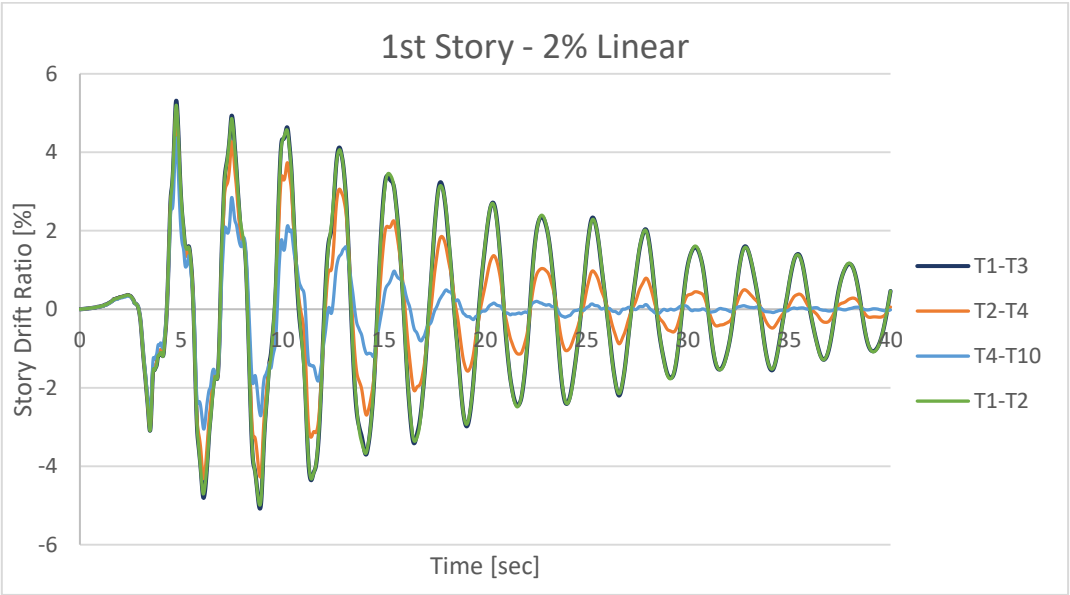

	T_1-T_2	T_1-T_3	T_2-T_4	T_4-T_{10}
Peak SDR (%)	5.000	5.314	5.094	4.365

B2. 2% Non-linear Analysis

The Peak SDR is on the 2nd level above the seismic base of the moment frame.

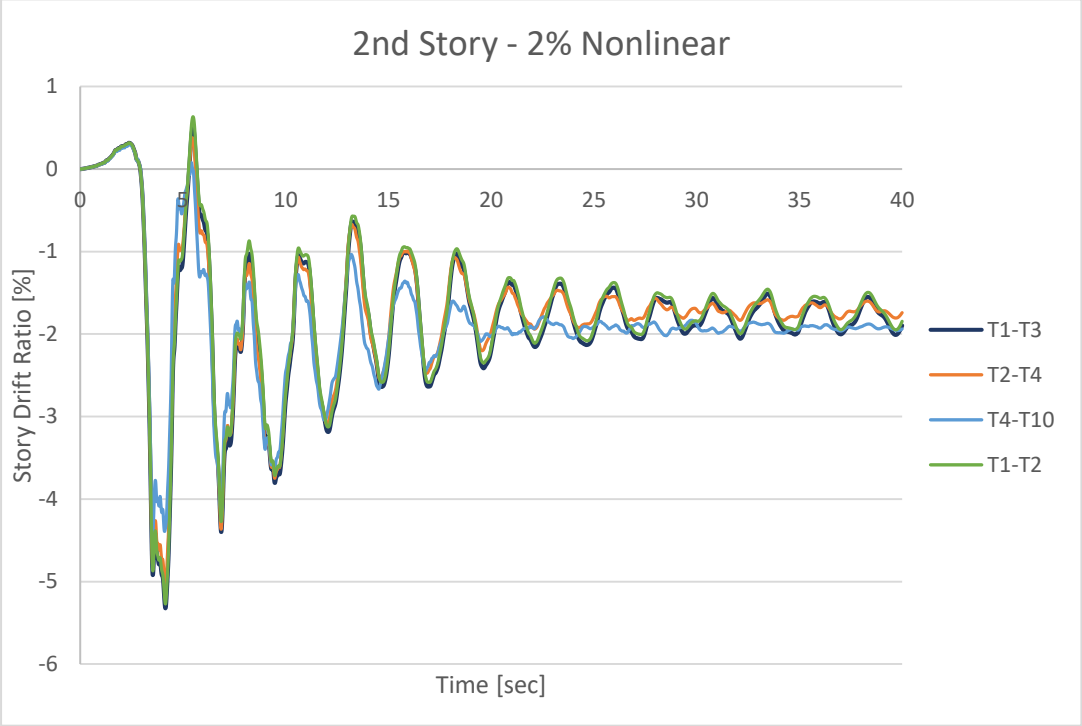

	T_1-T_2	T_1-T_3	T_2-T_4	T_4-T_{10}
Peak SDR (%)	5.271	5.323	5.066	4.439

Notes:

- In Linear analyses the Peak SDR is at the 1st level while in Non-linear analyses the peak SDR is at the 2nd level of the moment frame.
- The combination of **T_1-T_3** gives the largest value of Peak SDR in Linear and Non-linear cases while combination of **T_4-T_{10}** always gives the smallest value compared to the other combinations.
- As it was expected, the story drift ratio of the case of damping ratio of 2% is larger compared to damping ratio of 5%.
- Additionally, in both damping ratio cases, the SDR of Non-linear analysis is greater than the linear analysis value.

APPENDIX B: M-THETA COMPARISON UTILIZING GM02 – NORTHRIDGE 1994

Case 1:

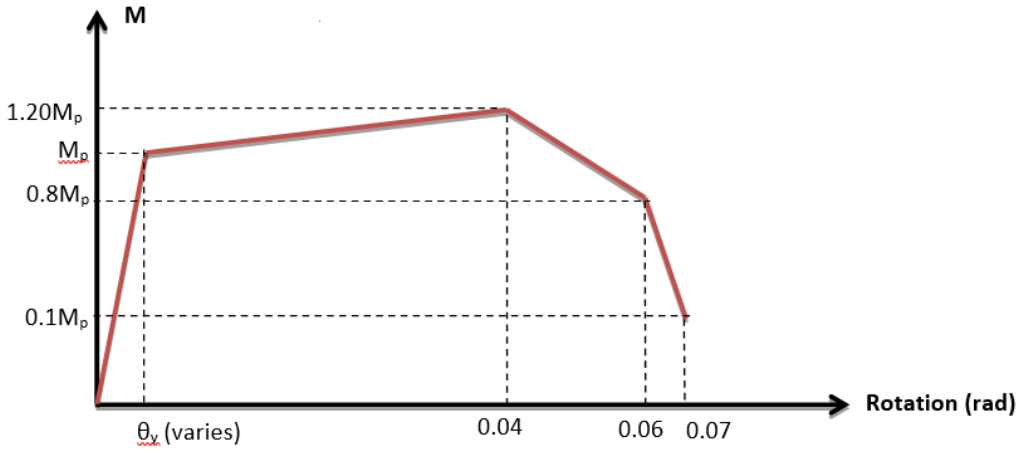

Case 2:

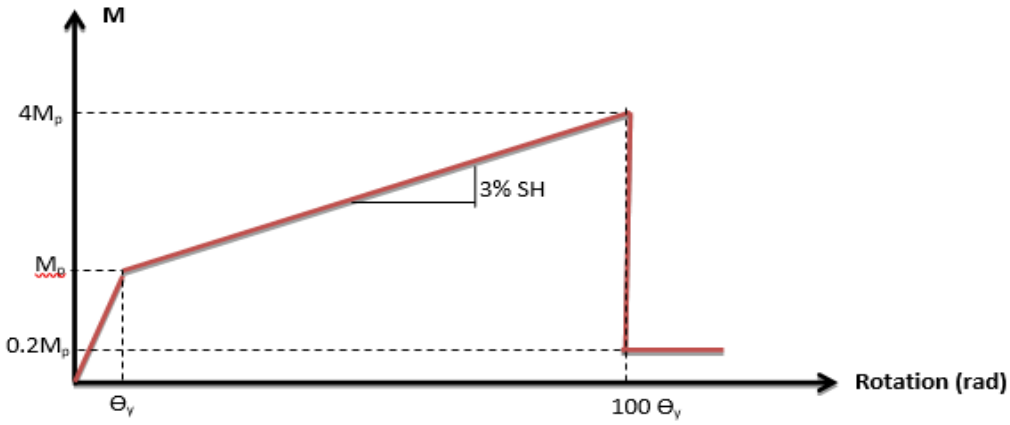

Case 3:

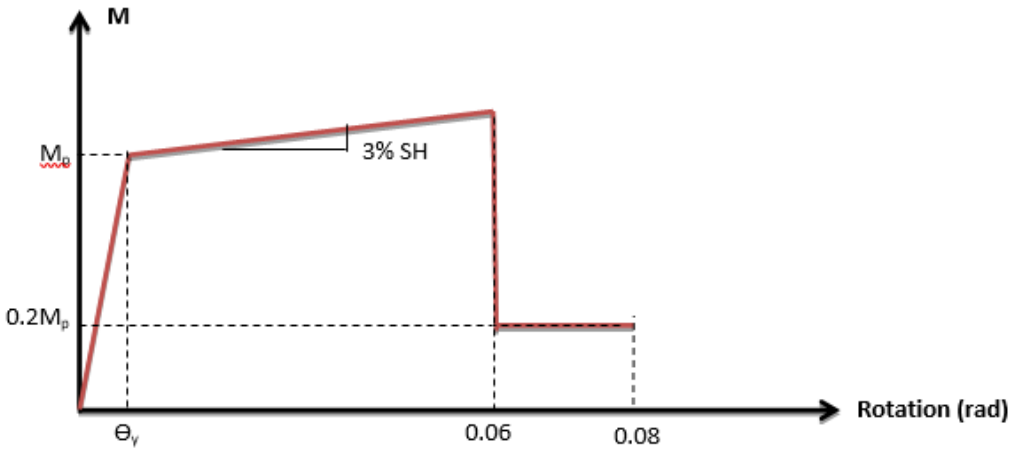

Case 4:

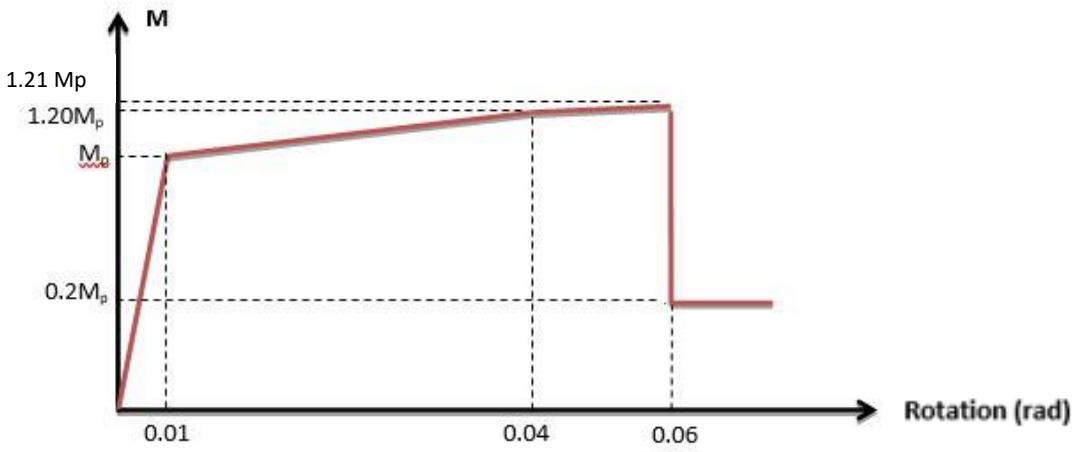

Case 5:

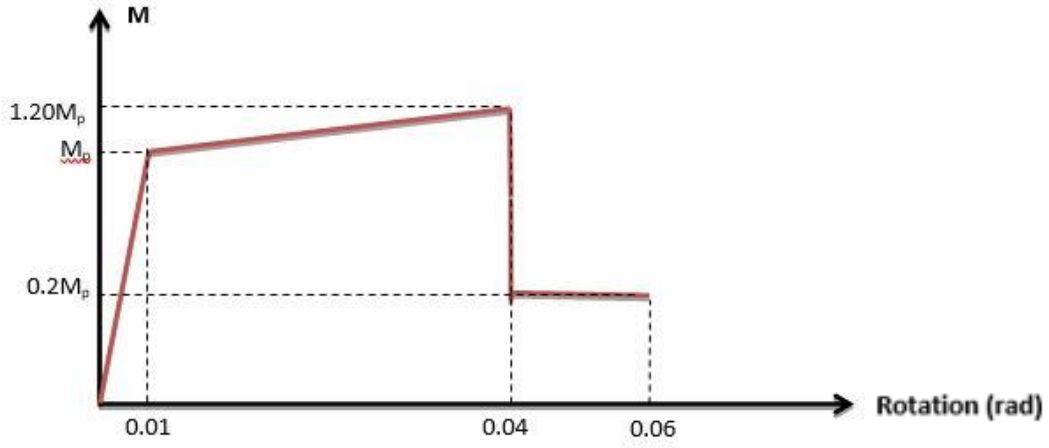

Analysis results indicate that Case 1 although it is the curve based on test data, it is not feasible to use for assessment on the plastic hinge rotation. SAP2000 was not able to handle the negative stiffness after the plastic hinge reached 0.04 radians.

Similarly, Case 5 results showed that it is not appropriate to use as it is expected that the plastic hinge will go beyond 0.04 rad when SDR is greater than 4% and negative stiffness is leading to numerical problems.

Case 2a(4%):

Peak SDR = 3.986% [2nd Story]

Peak PHR = 0.0358 [1st Story]

Moment at peak PHR: M = 3037.6 k-ft & Mp = 2544.89 k-ft → **1.19Mp**

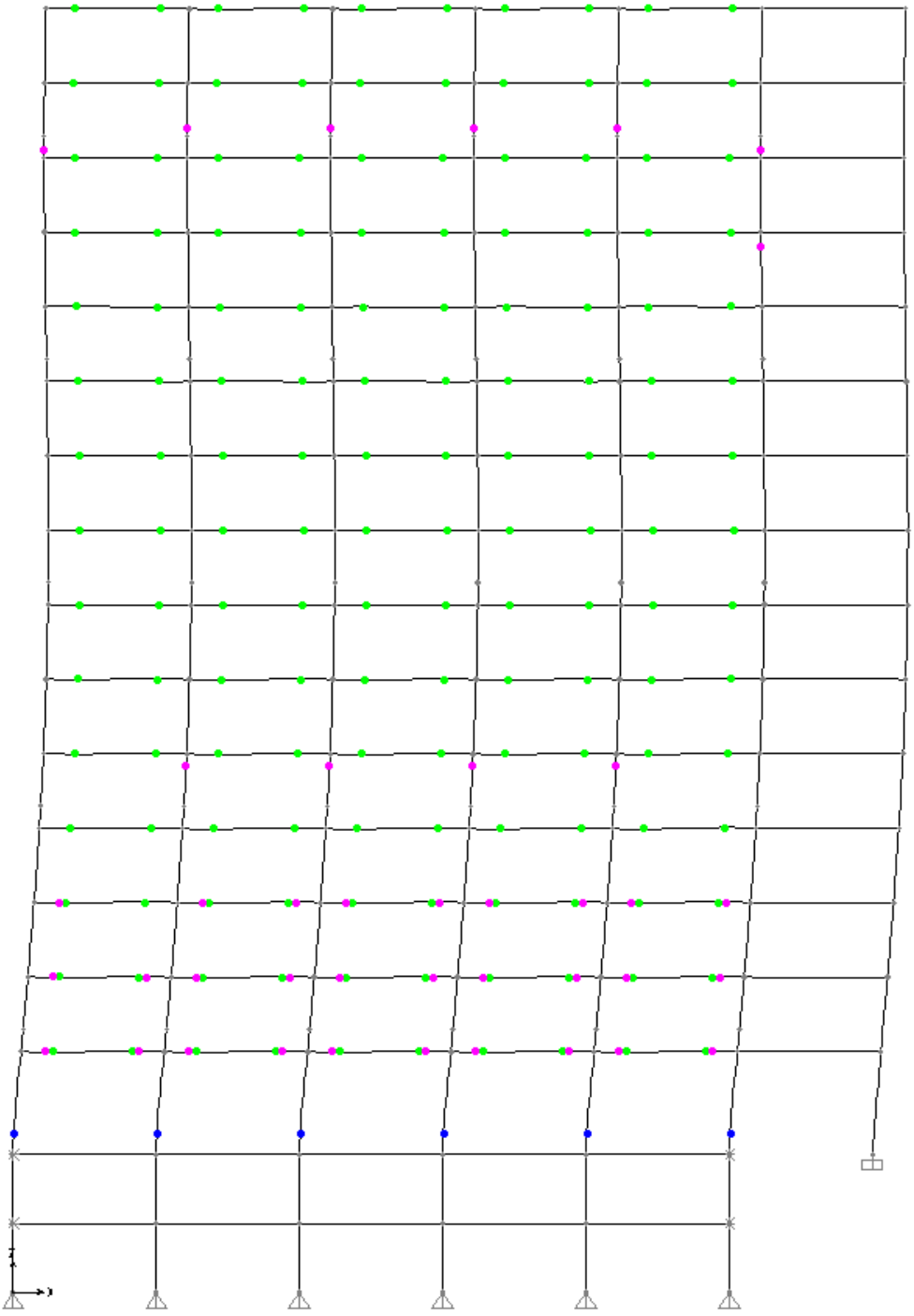

Figure B.1. Plastic hinge map at the end of excitation at 40 sec

Case 2b(6%):

Peak SDR = 5.997% [2nd Story] (the difference in SDR while the PHR is practically unchanged is due to the formation of plastic hinges in the columns. The fact that the beam strength is ever increasing, forges the plastic hinge formation in columns)

Peak PHR = 0.0362 [1st Story level]

Moment at peak PHR: M = 3043.6 k-ft & Mp = 2544.89 k-ft → **1.2Mp**

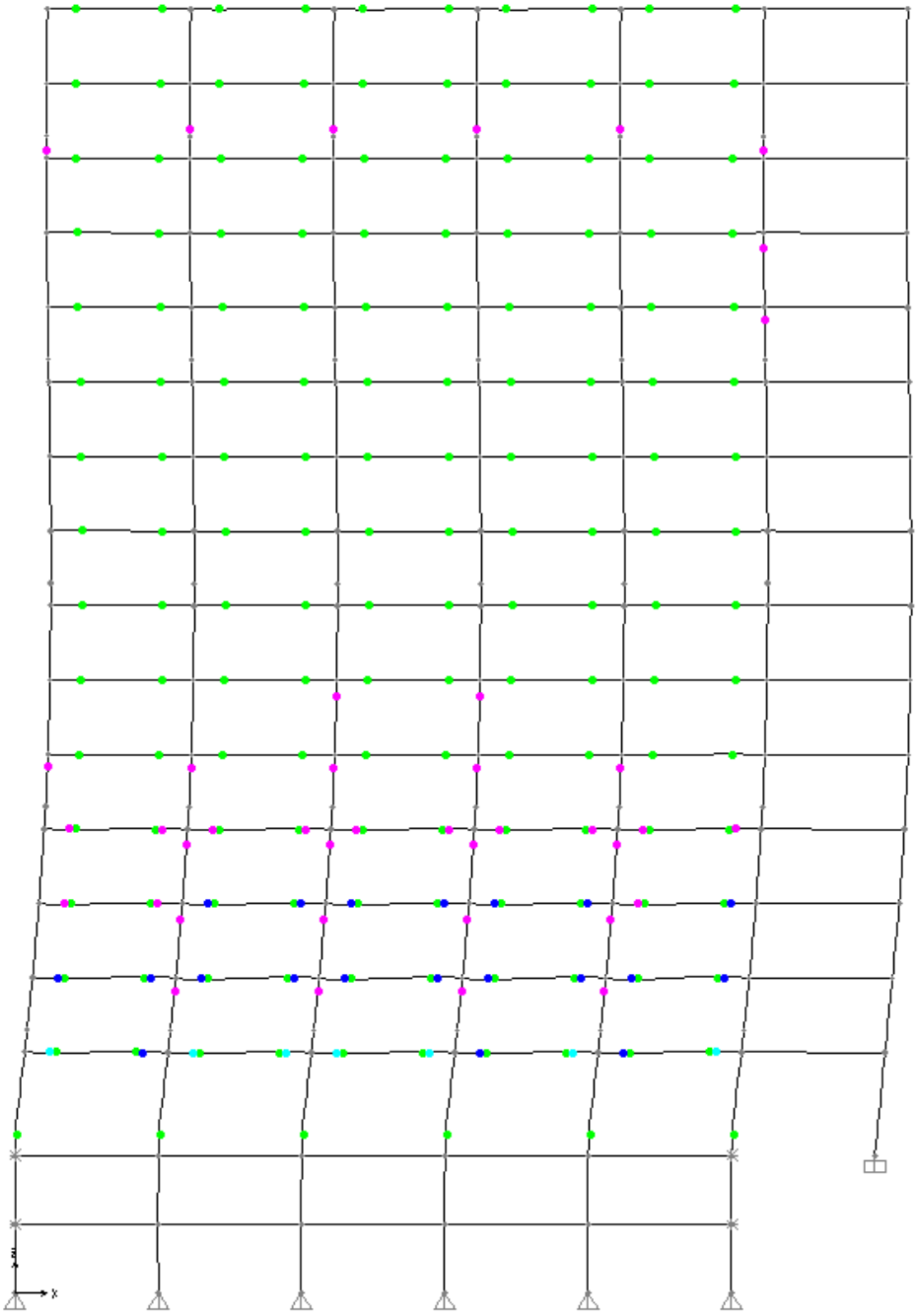

Figure B.2. Plastic hinge map at the end of excitation at 40 sec

Case 3a(4%):

Peak SDR = 4.029% [2nd Story]

Peak PHR = 0.0327 [1st Story]

Moment at peak PHR: M = 3038.4 k-ft & Mp = 2544.89 k-ft → **1.19Mp**

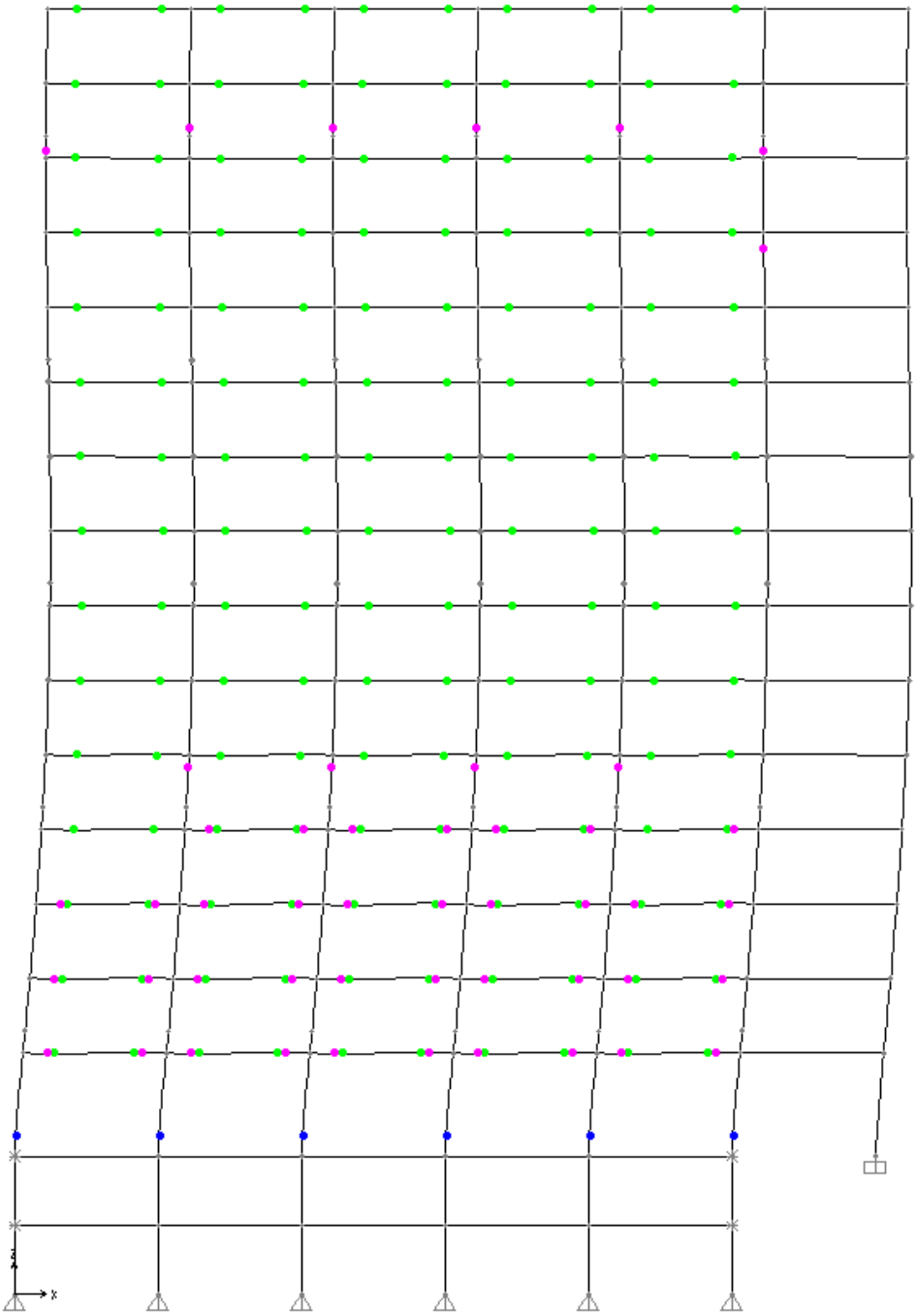

Figure B.3. Plastic hinge map at the end of excitation at 40 sec

Case 3b(6%):

Peak SDR = 6.078% [2nd Story]

Peak PHR = 0.0331 [1st Story]

Moment at peak PHR: M = 3044.6 k-ft & Mp = 2544.89 k-ft → **1.2Mp**

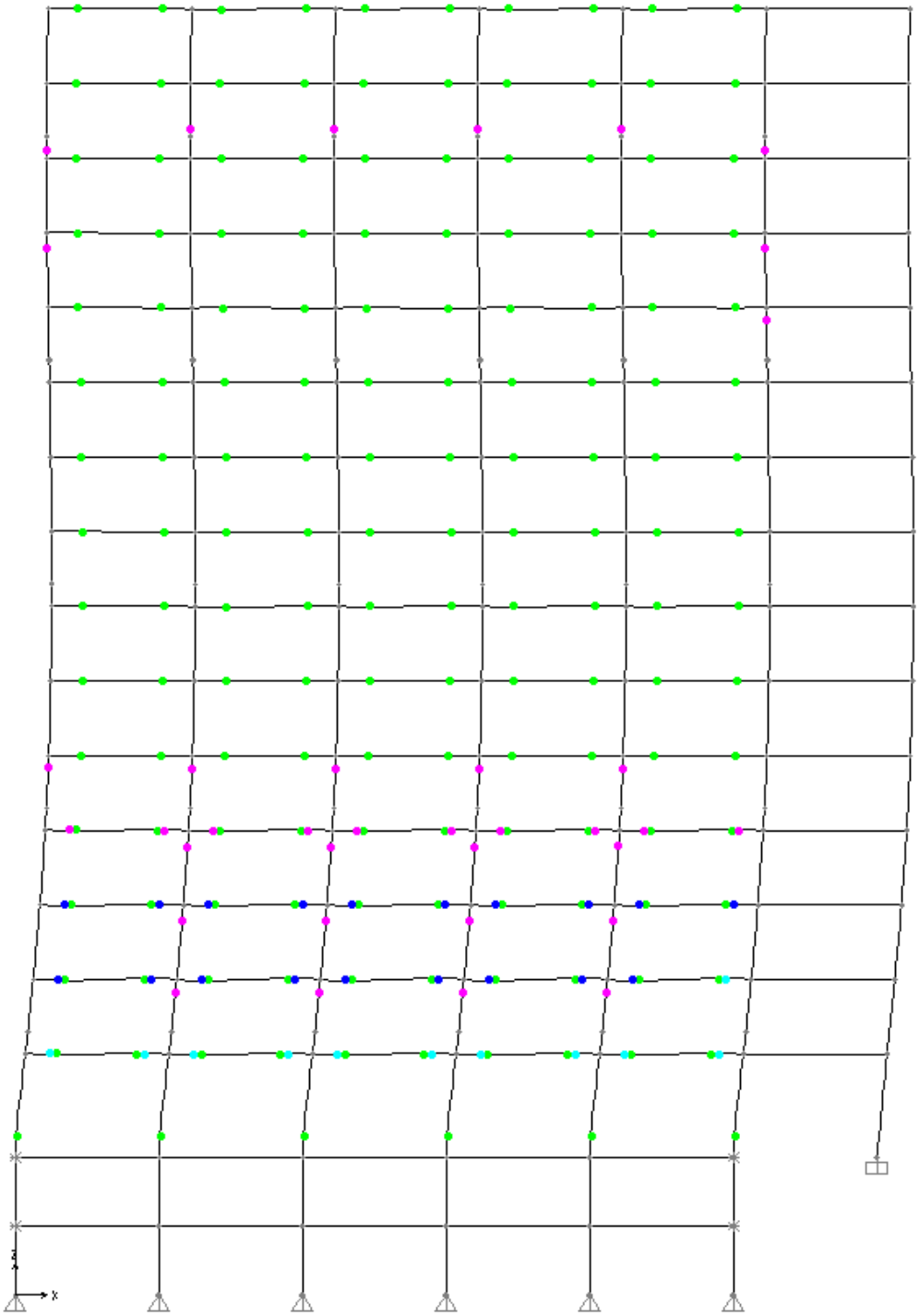

Figure B.4. Plastic hinge map at the end of excitation at 40 sec

Case 4a(4%):

Peak SDR = 4.00% [2nd Story]

Peak PHR = 0.0334 [1st Story]

Moment at peak PHR: M = 3038.3 k-ft & Mp = 2544.89 k-ft → **1.19Mp**

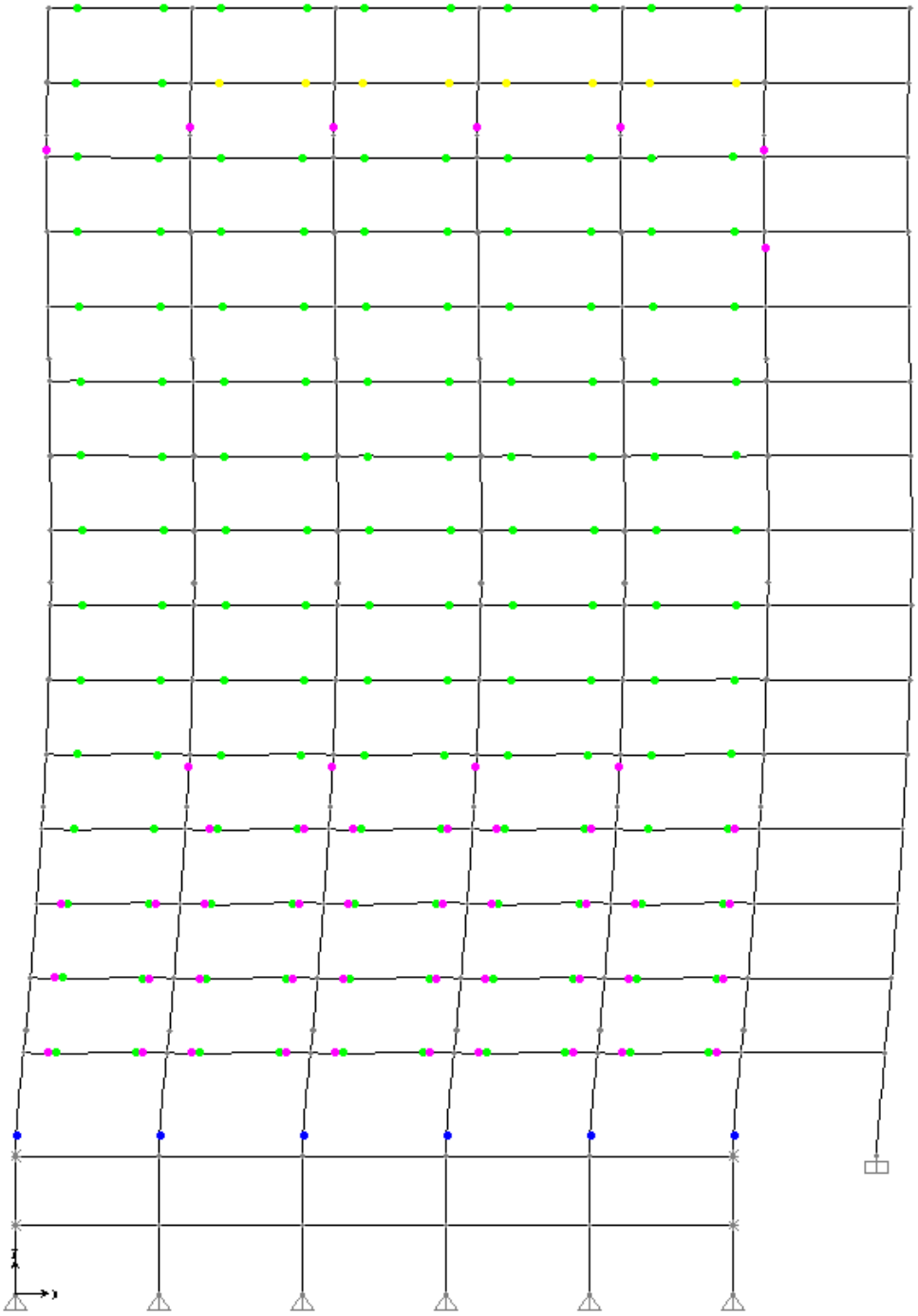

Figure B.5. Plastic hinge map at the end of excitation at 40 sec

Case 4b(6%):

Peak SDR = 6.02% [2nd Story]

Peak PHR = 0.0335 [1st Story]

Moment at peak PHR: M = 3044.3 k-ft & Mp = 2544.89 k-ft → **1.2Mp**

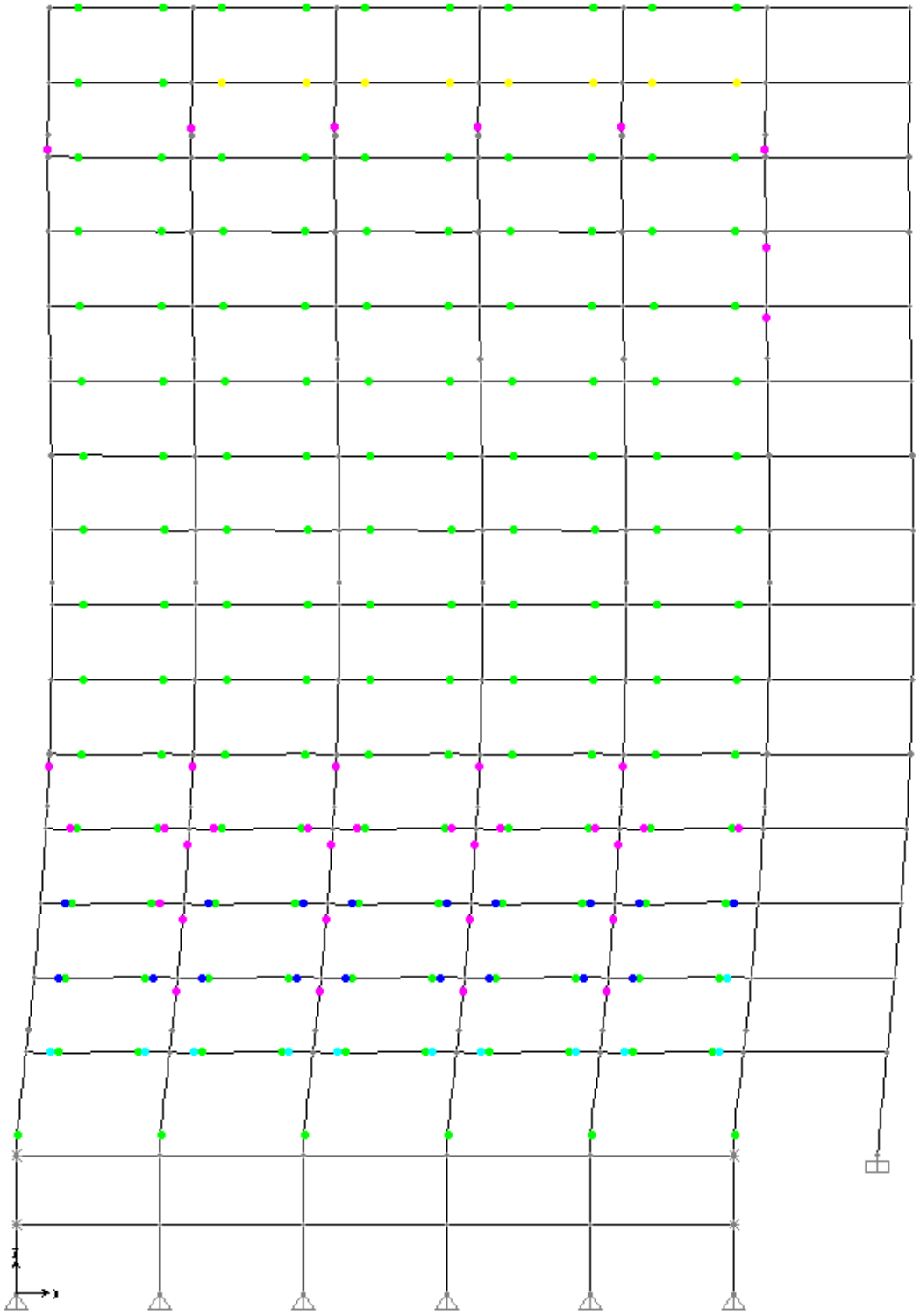

Figure B.6. Plastic hinge map at the end of excitation at 40 sec

Case 4a:

Peak SDR = 4.00% [2nd Story] & Peak PHR = 0.0334 [1st Story]

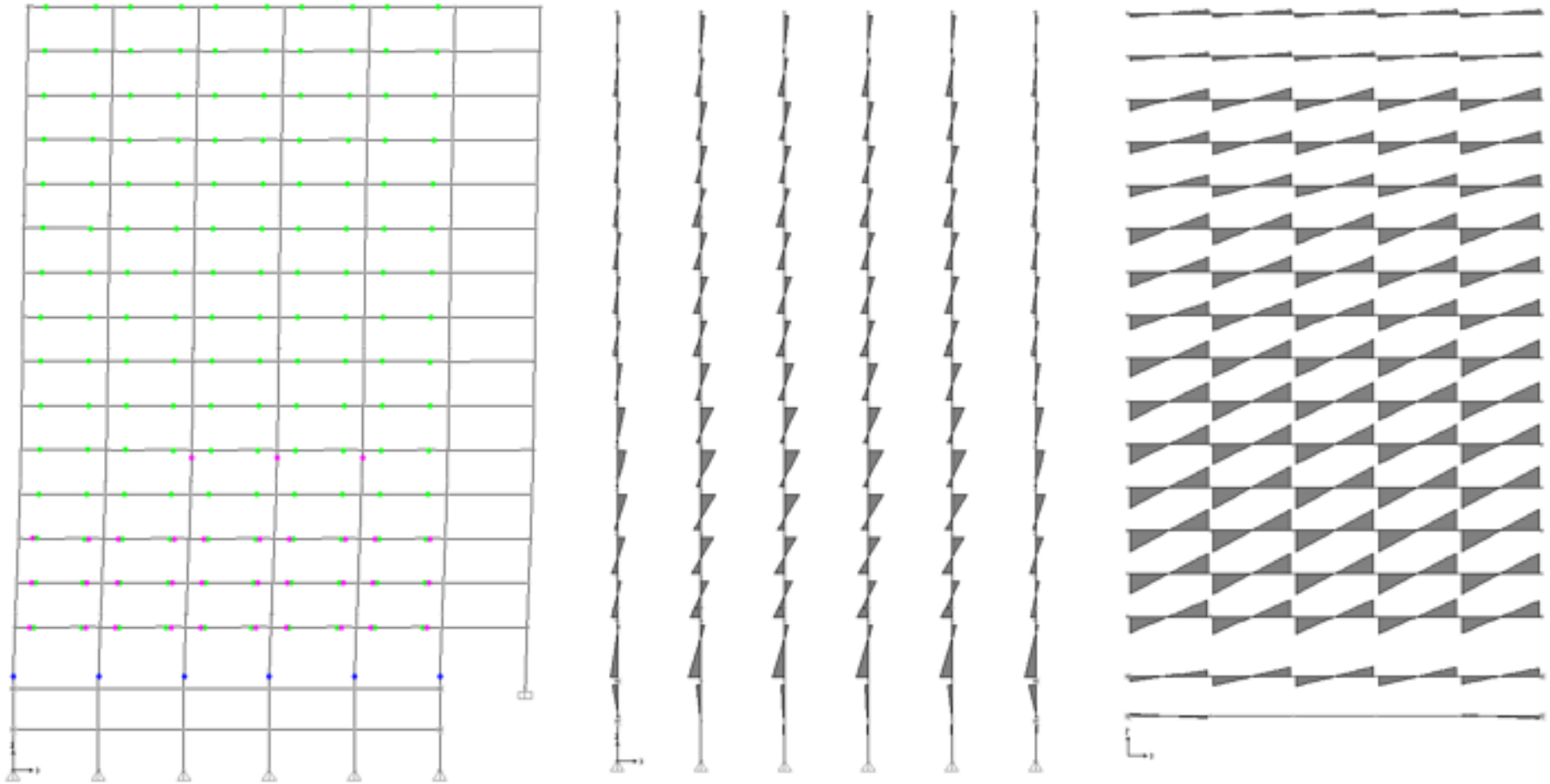

Figure B.7. 1st set of plastic hinge formation at 6.415 sec

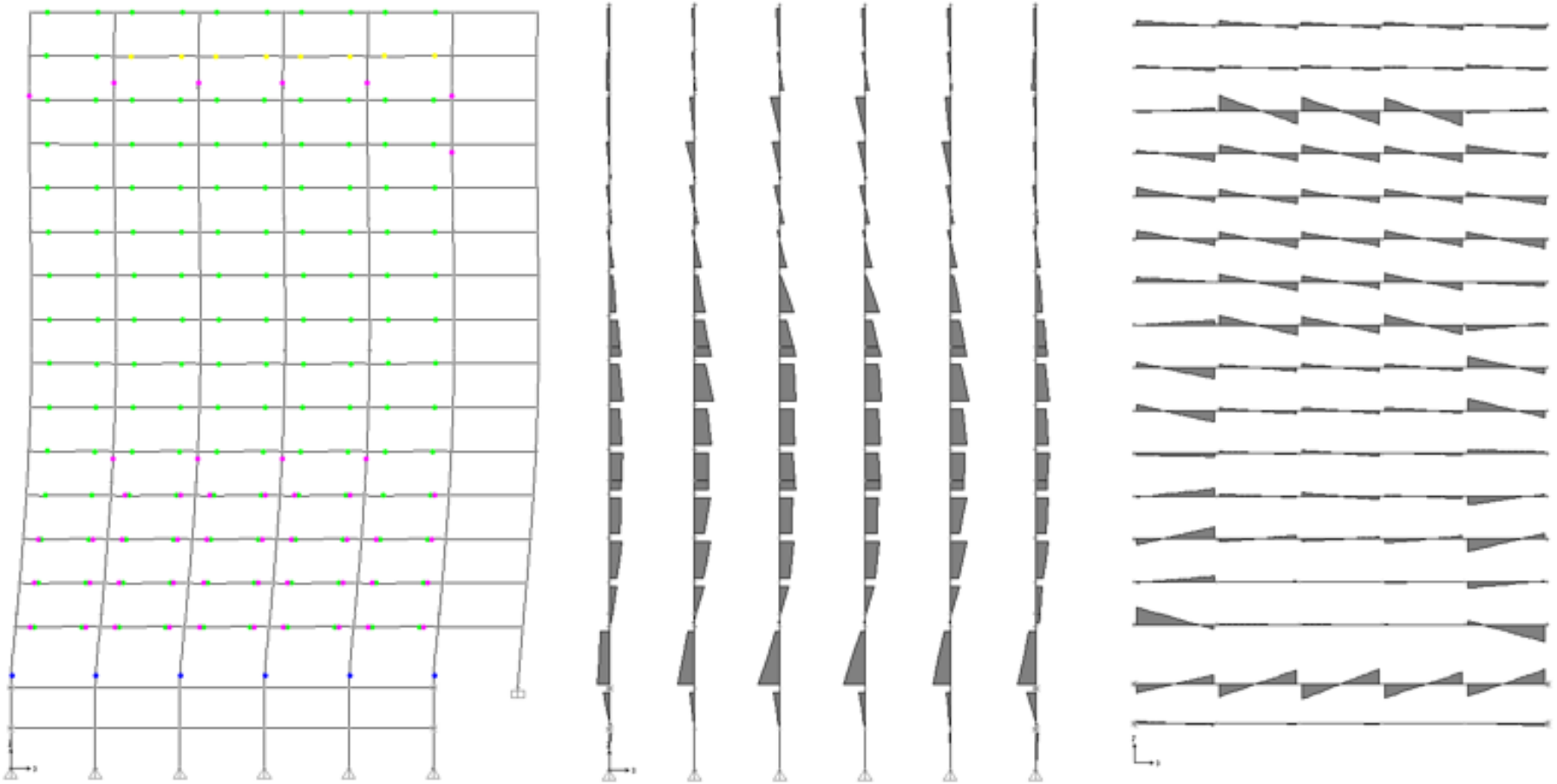

Figure B.8. At the end of excitation at 40 sec

Case 4b:

Peak SDR = 6.02% [2nd Story] & Peak PHR = 0.0335 [1st Story]

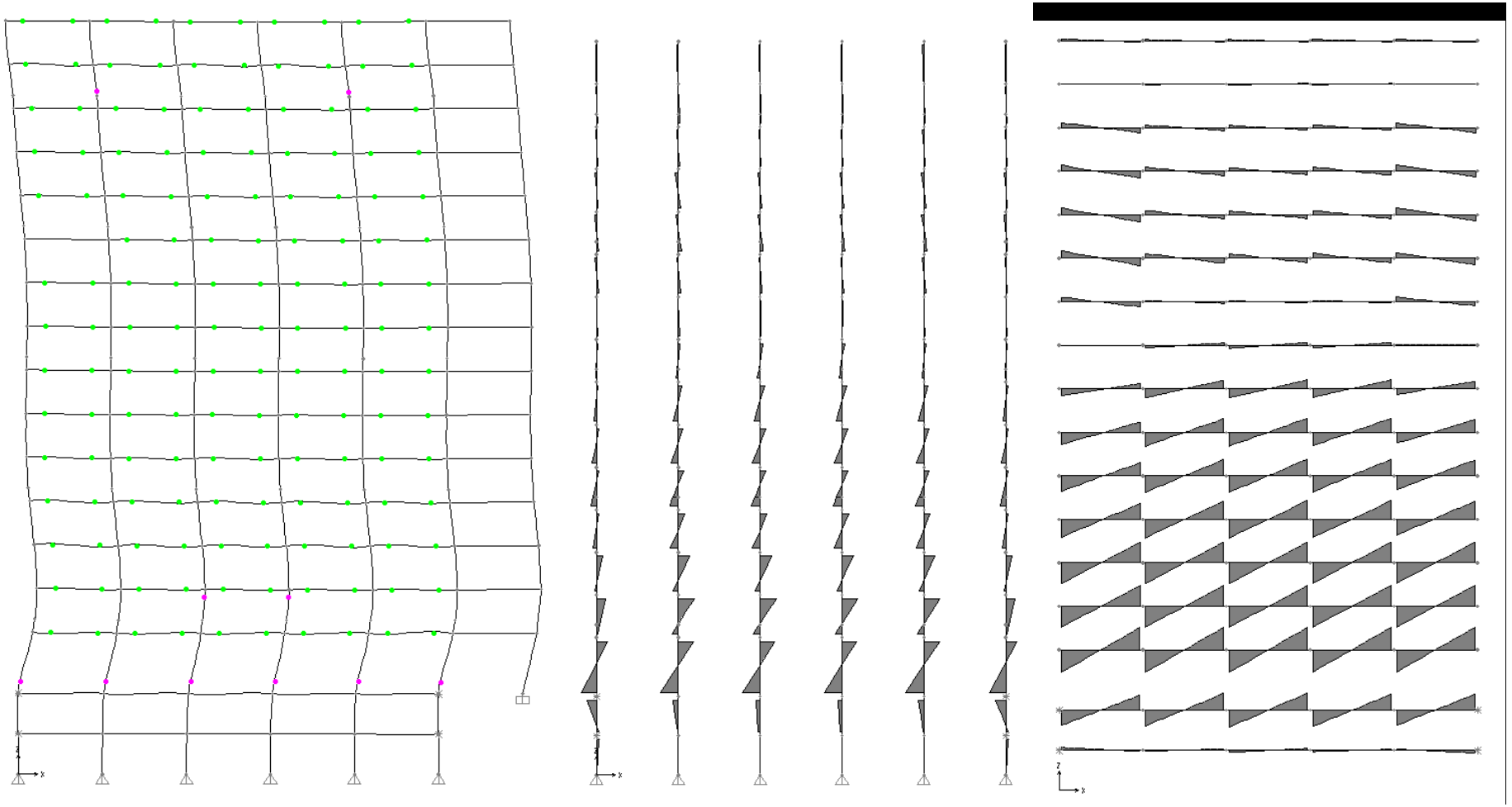

Figure B.9. 1st set of plastic hinge formation at 6 sec

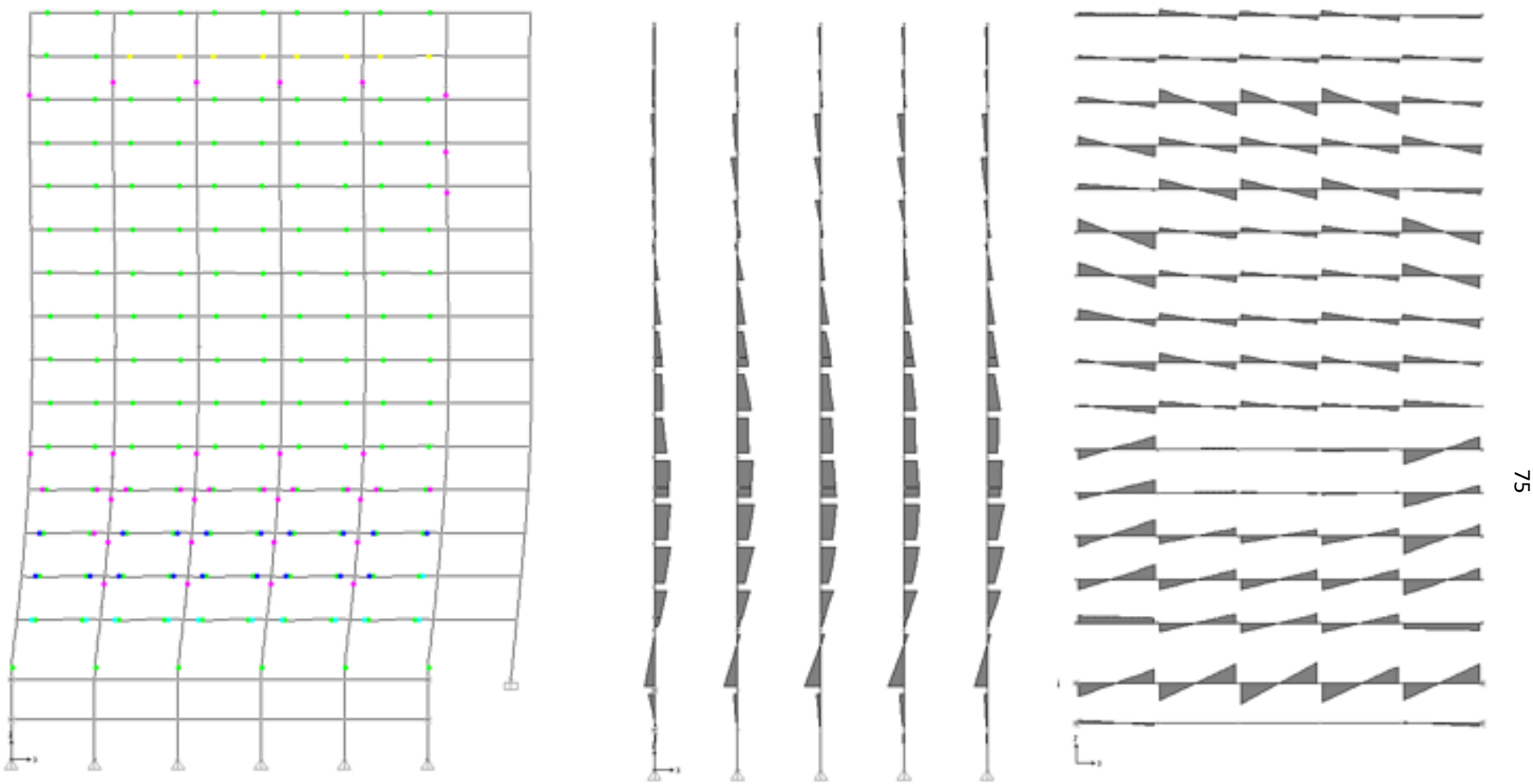

Figure B.10. At the end of excitation at 40 sec

APPENDIX C: BENDING MOMENT DIAGRAMS FOR GM02 – NORTHRIDGE 1994

M-theta curve:

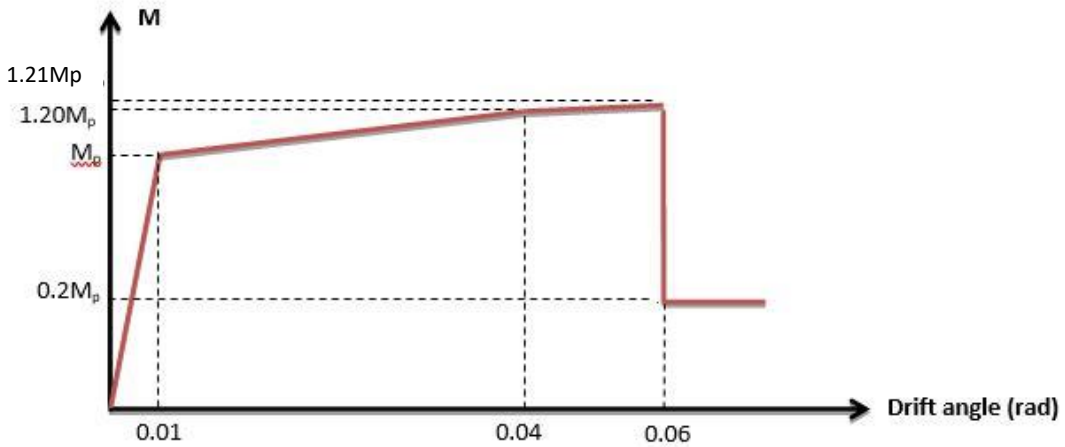

Ground motion time history:

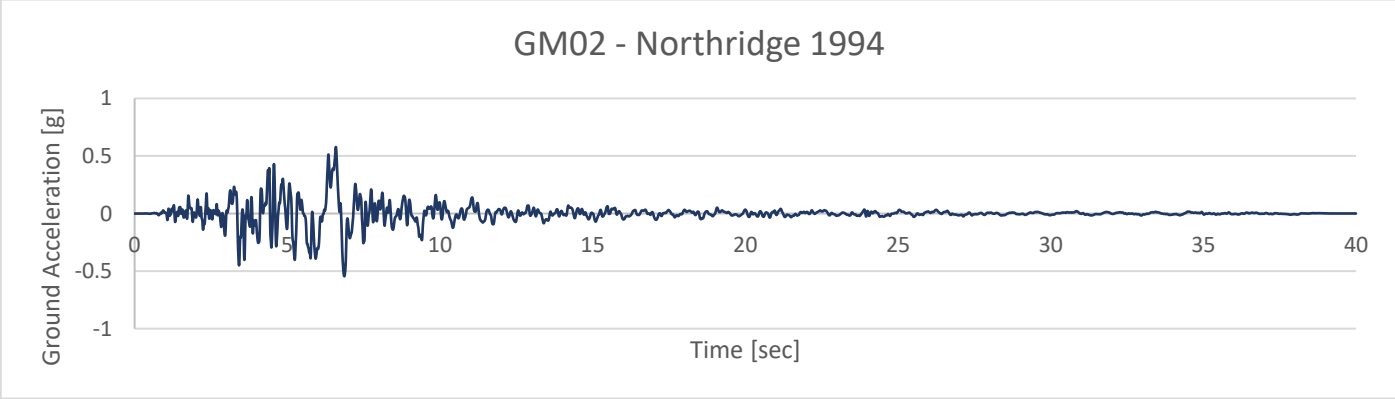

SDR 1%

Peak SDR -> 14th story

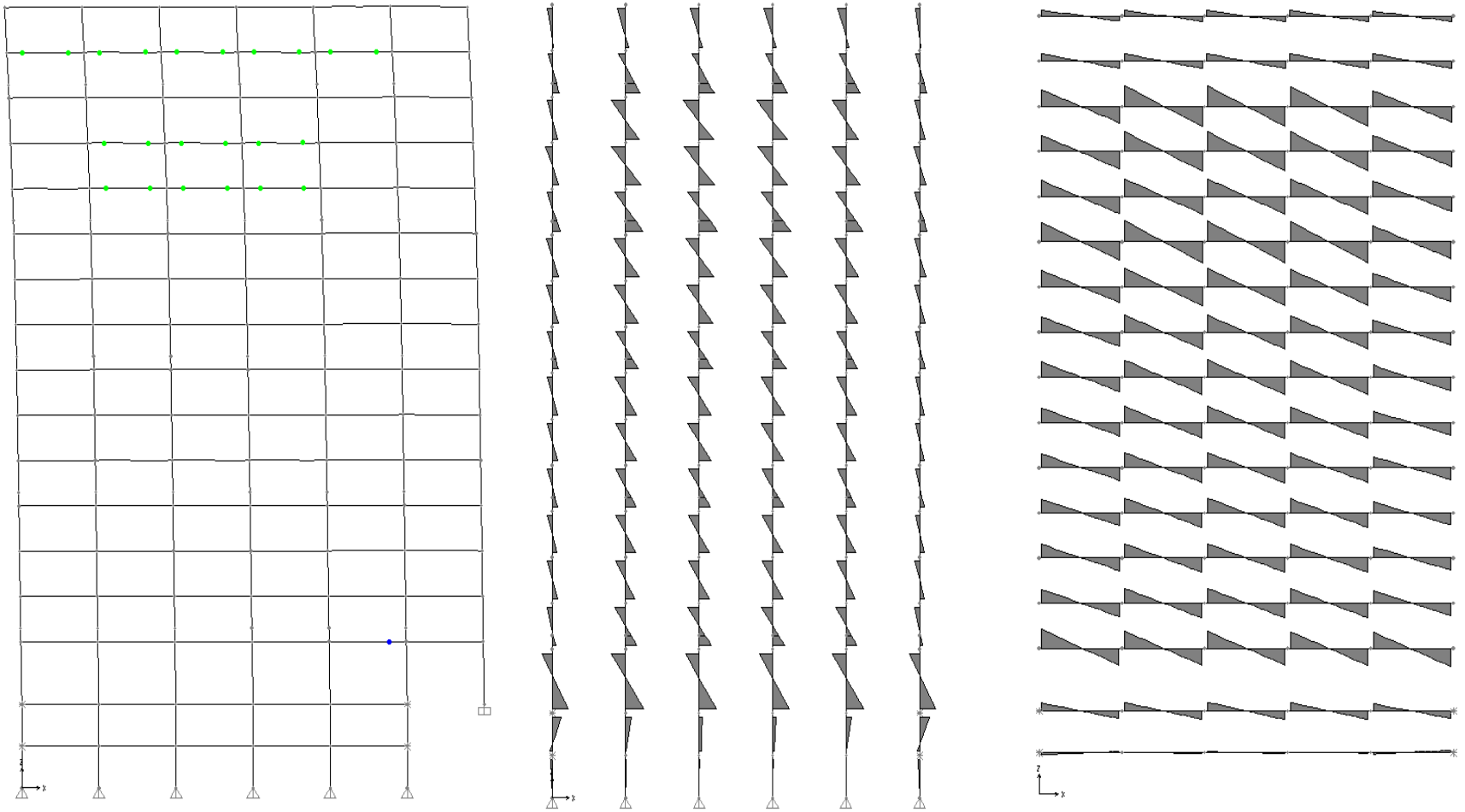

Figure C.1. Peak SDR at 7.265 sec

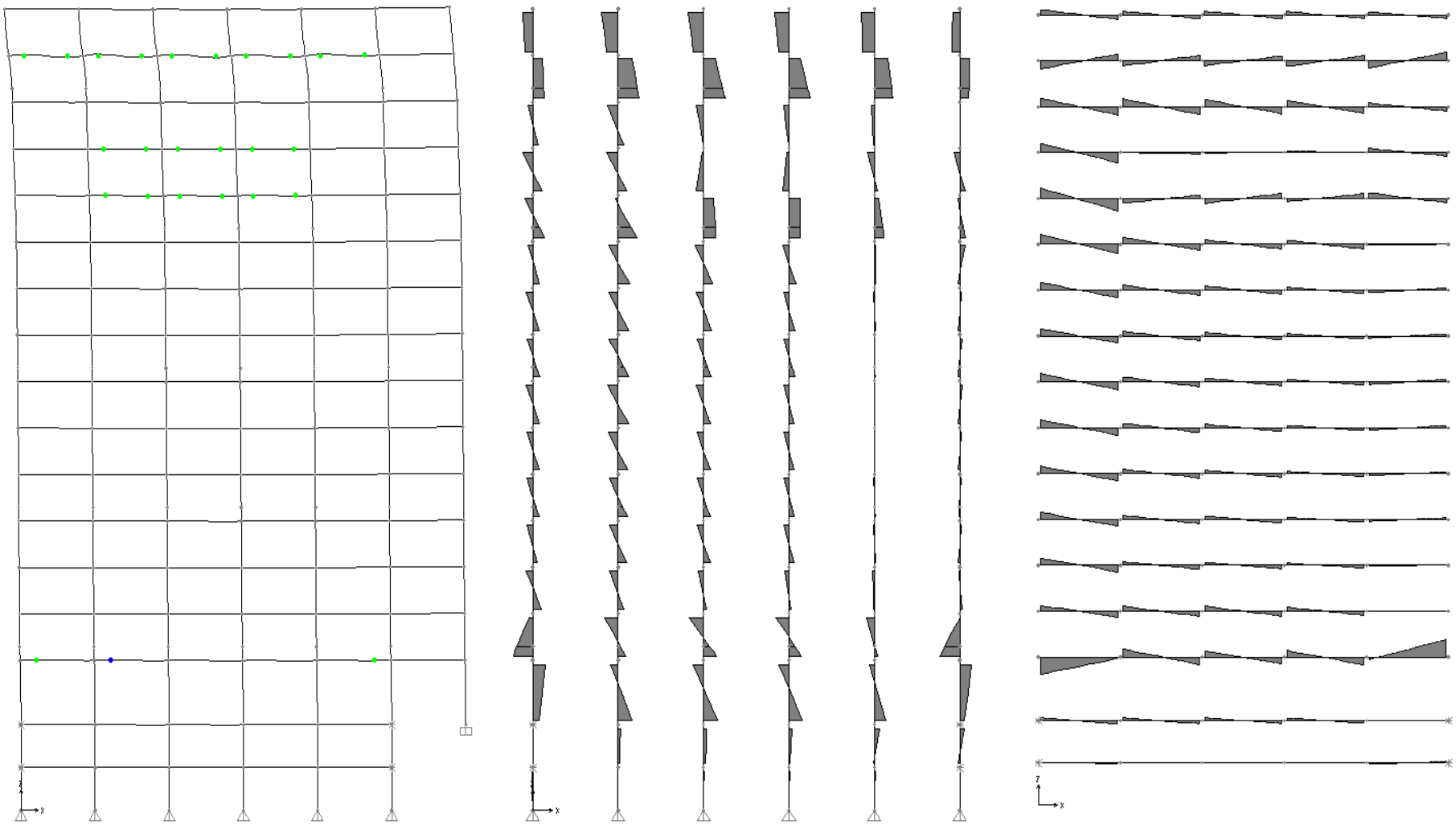

Figure C.2. At the end of excitation at 40 sec

SDR 2%

Peak SDR -> 4th story

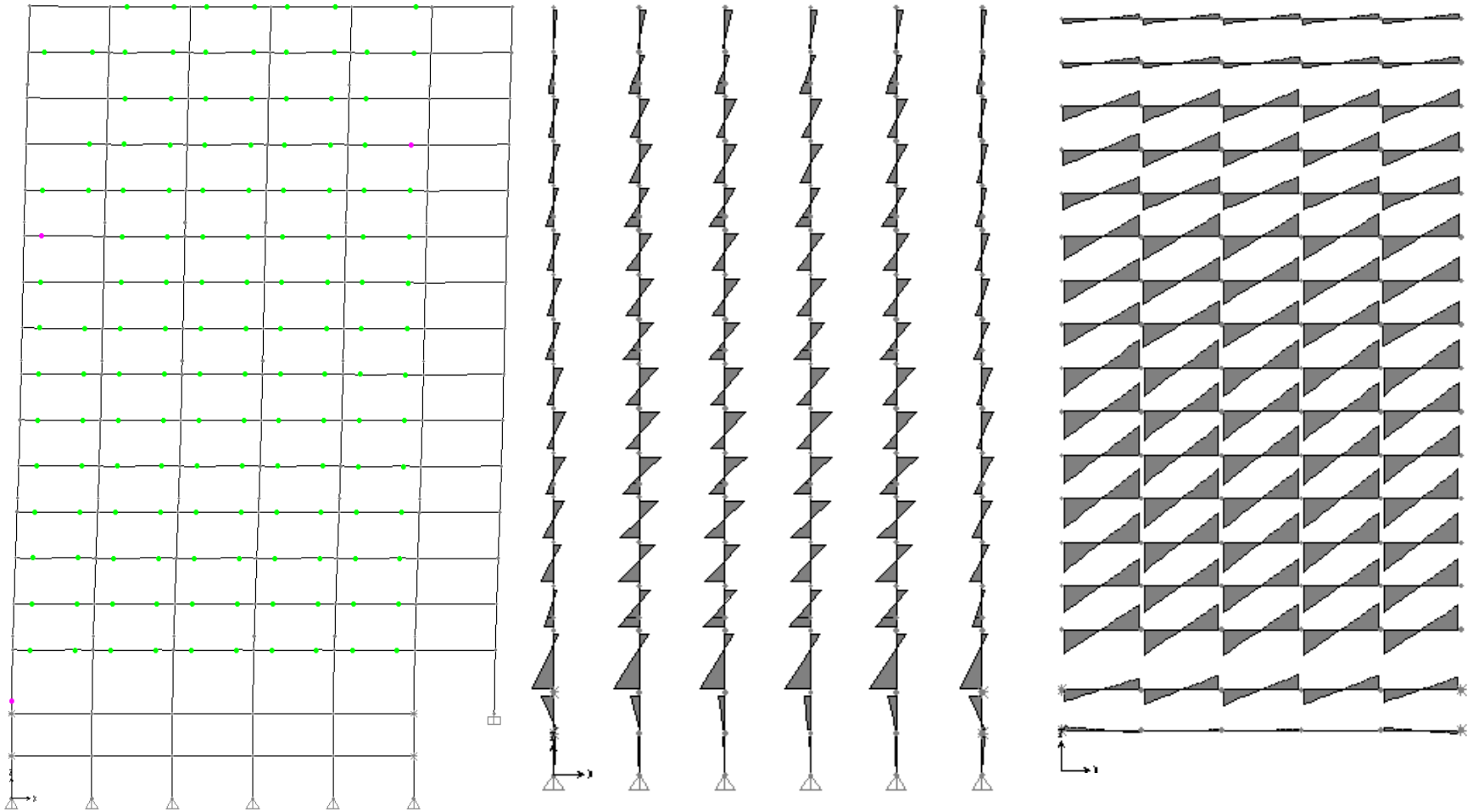

Figure C.3. Peak SDR at 6.435 sec

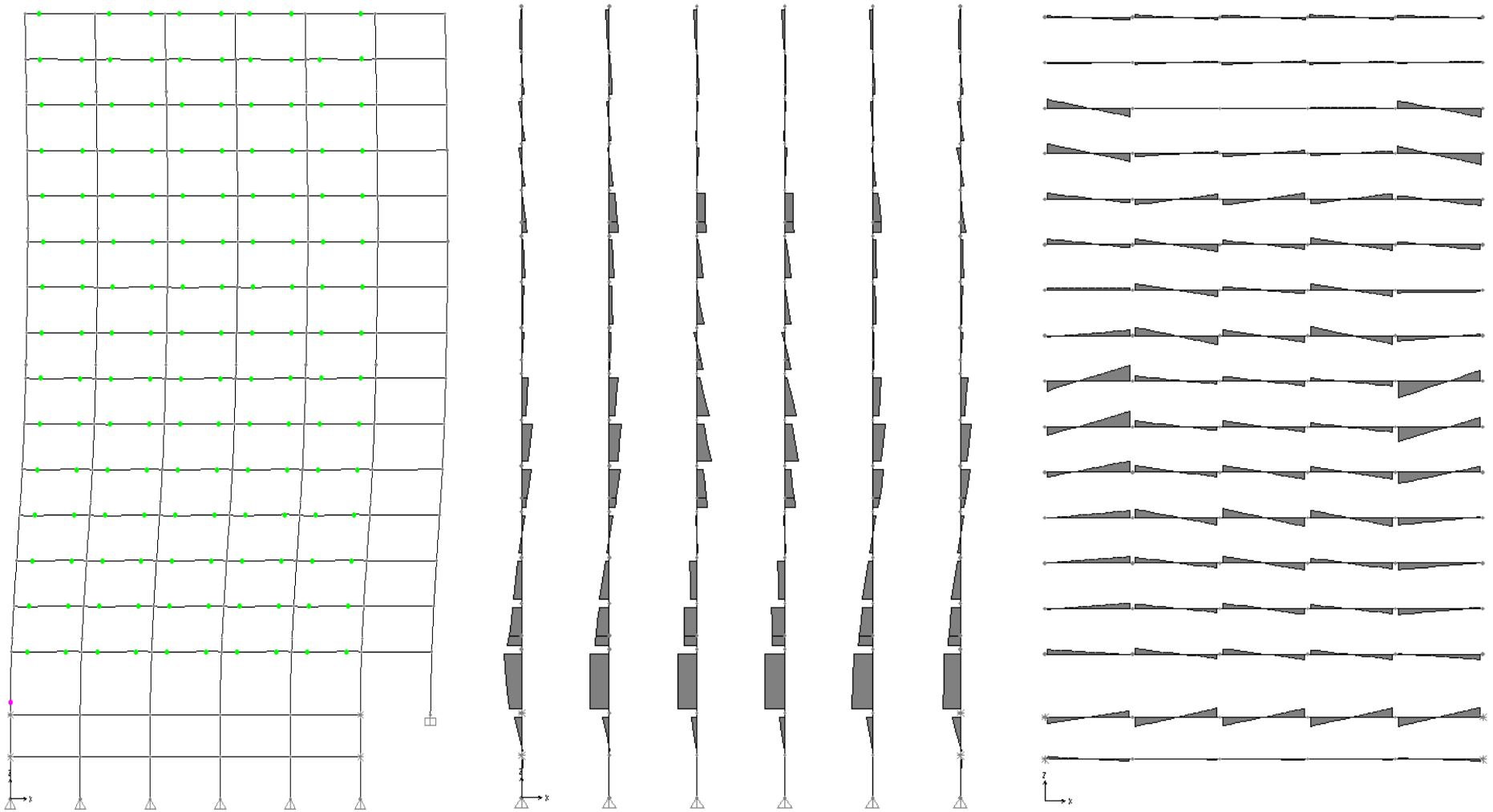

Figure C.4. At the end of excitation at 40 sec

SDR 3%

Peak SDR -> 3rd story

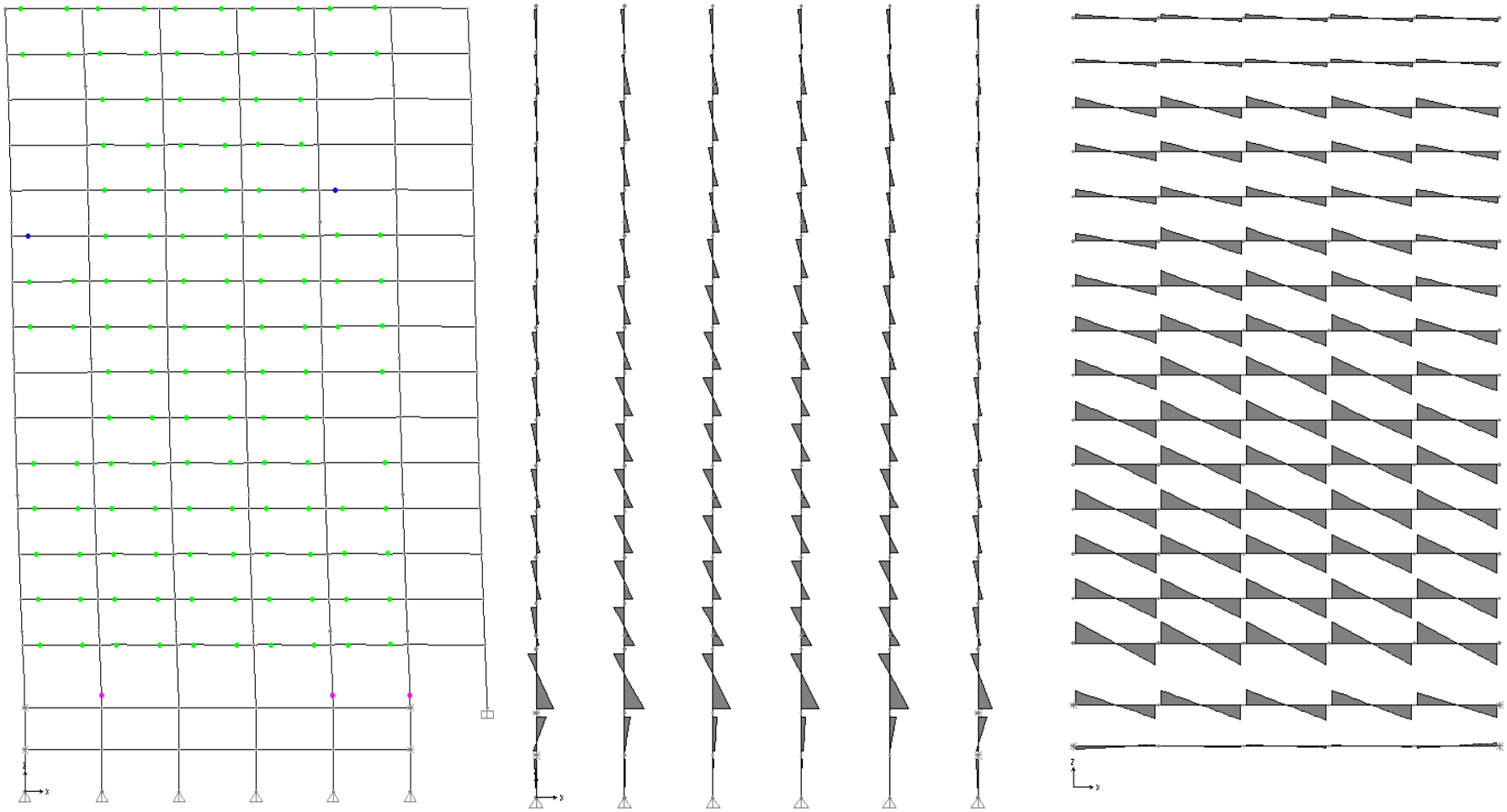

Figure C.5. 1st set of plastic hinges on 1st story columns at 5.12 sec

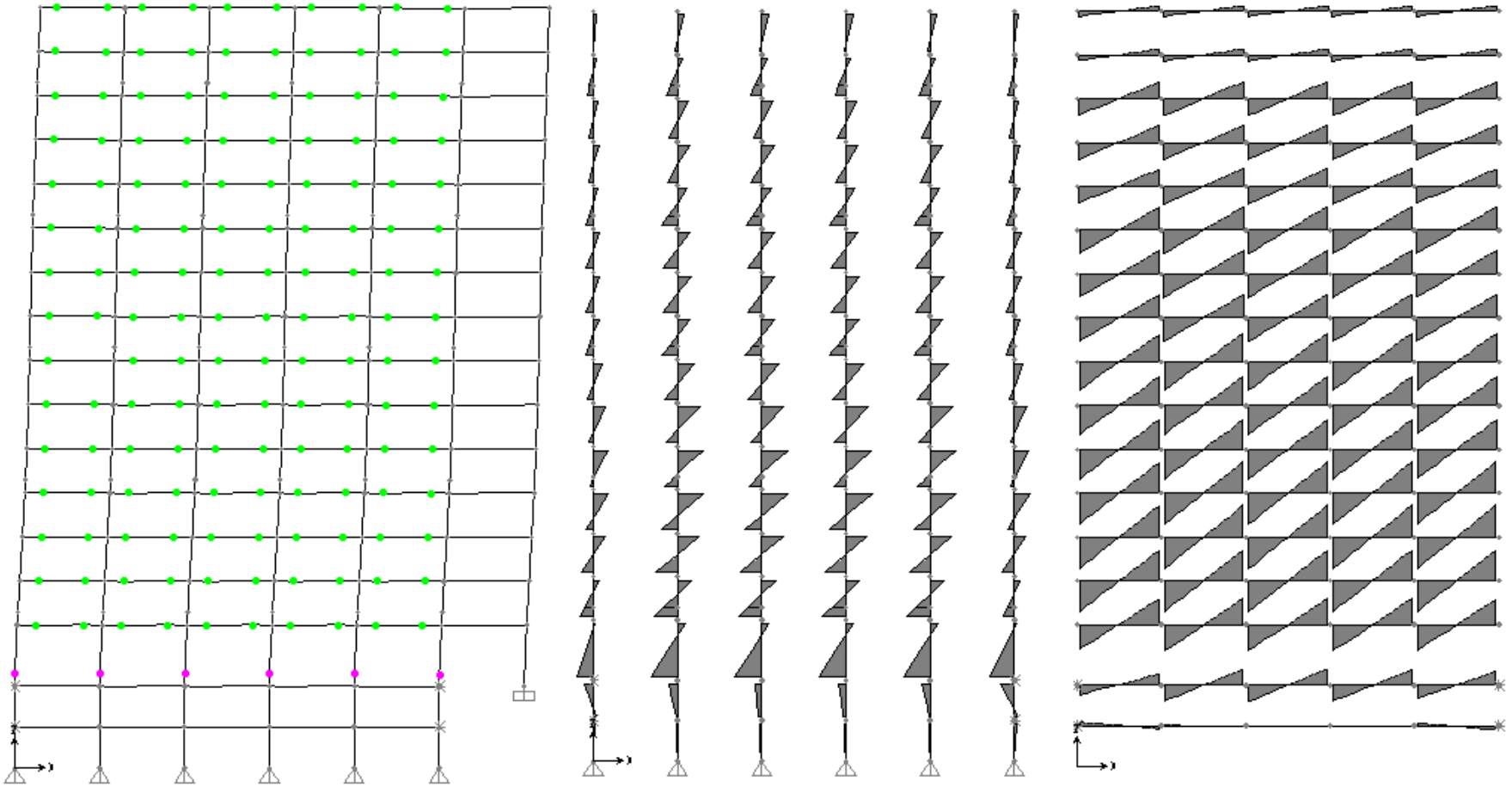

Figure C.6. Peak SDR at 6.405 sec

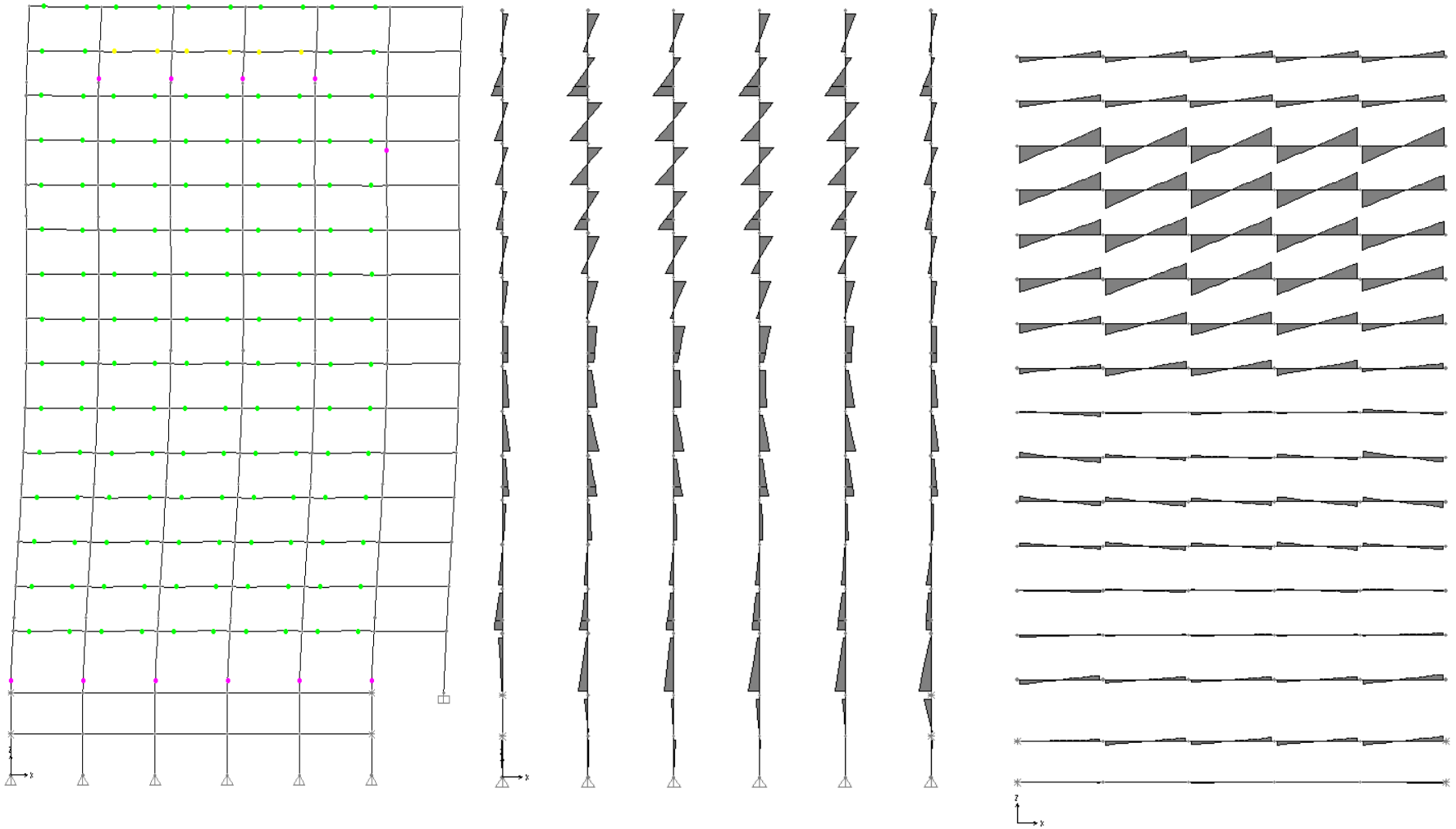

Figure C.7. 2nd set of plastic hinges on 14th story columns at 7.64 sec

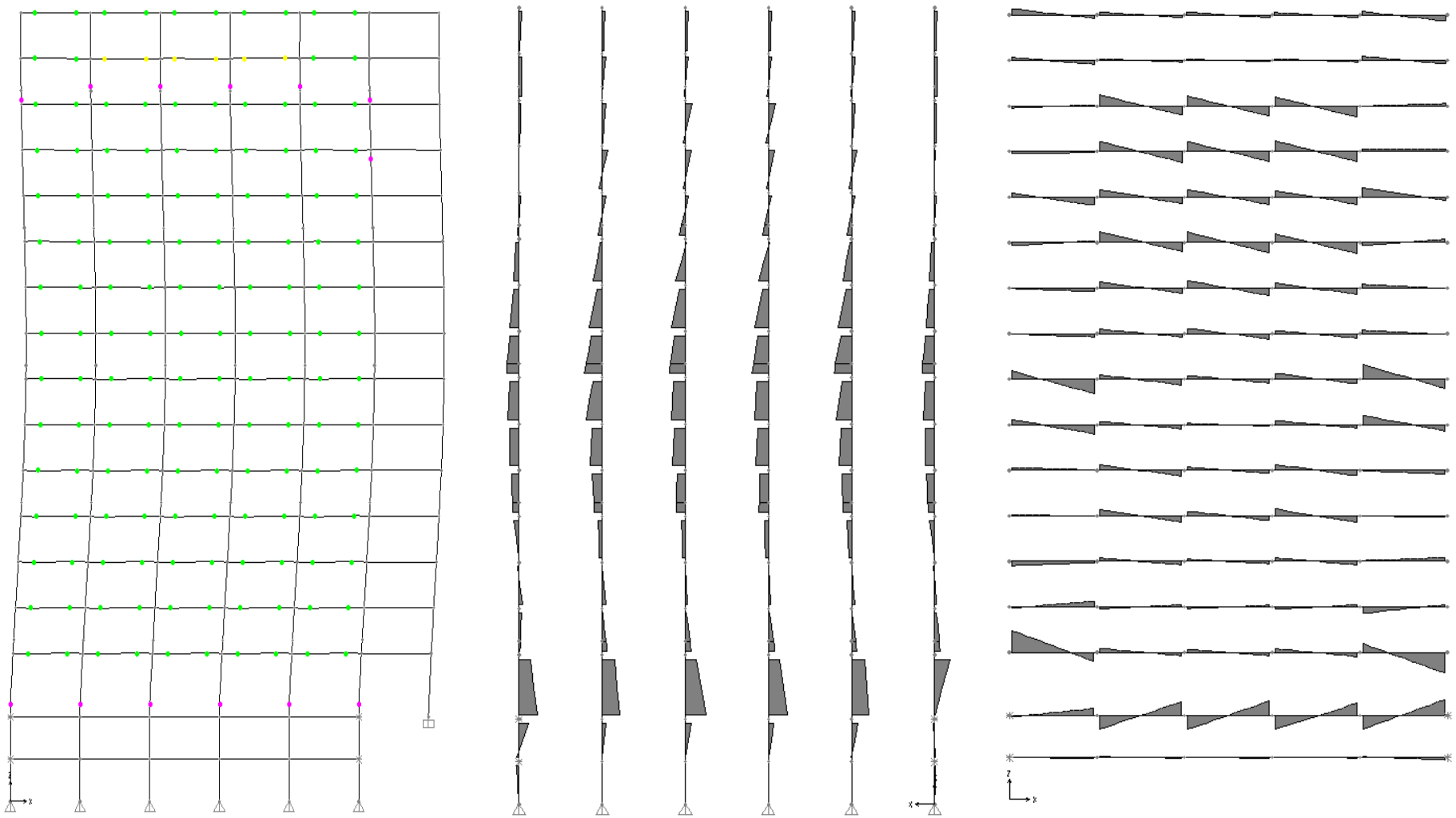

Figure C.8. At the end of excitation at 40 sec

SDR 4%

Peak SDR -> 2nd story

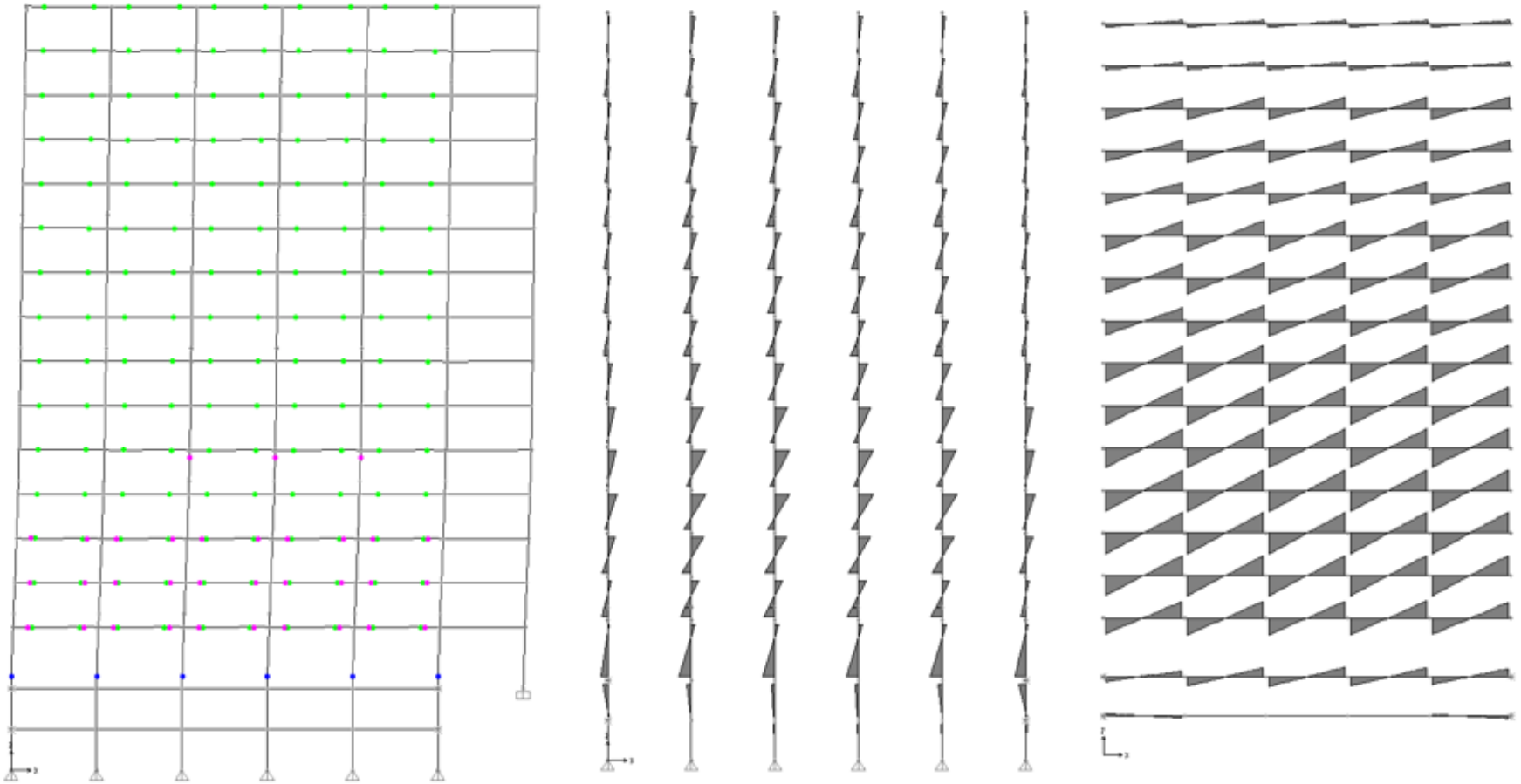

Figure C.9. 2nd set of plastic hinge formation on 5th story columns at 6.415 sec

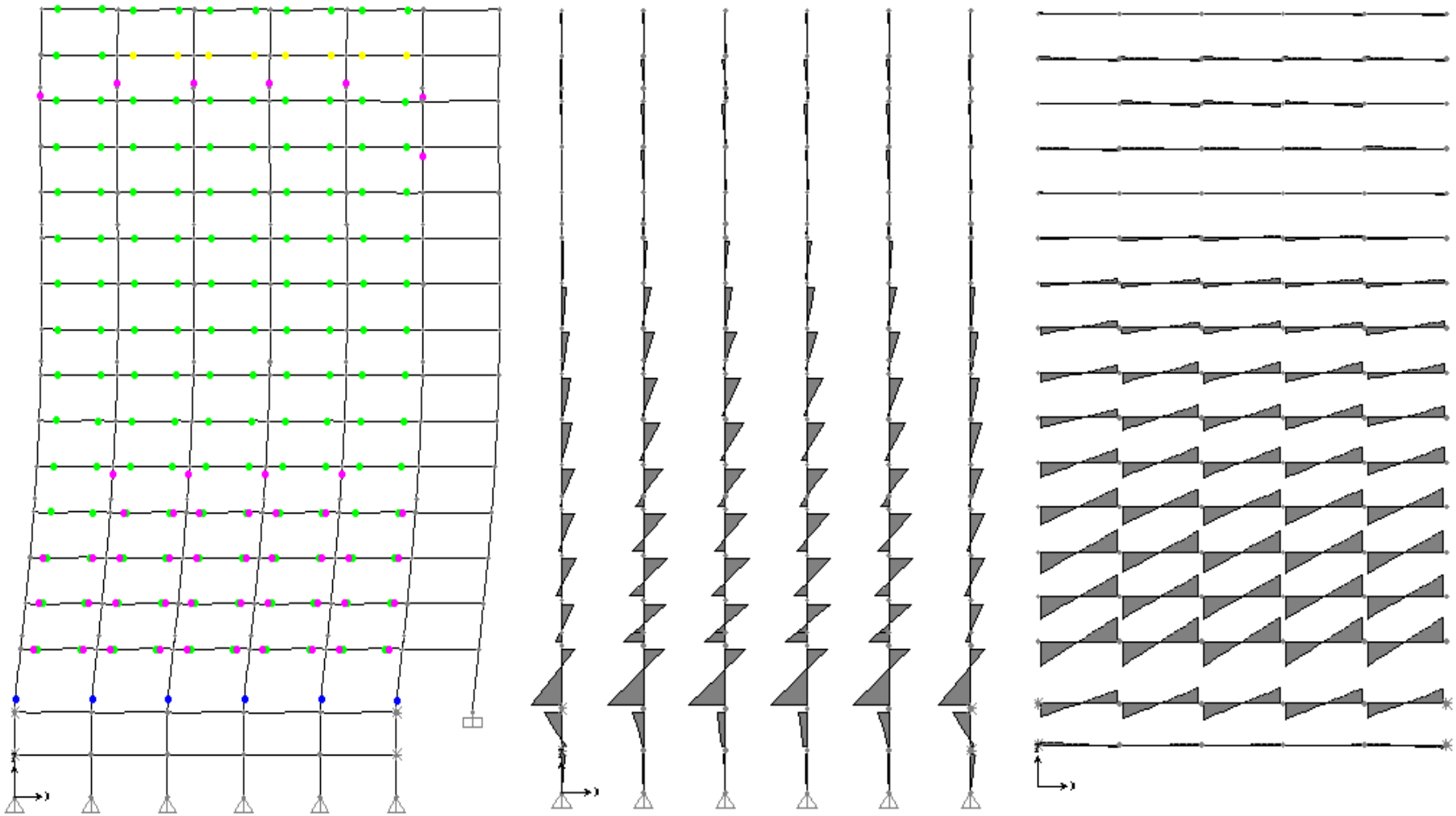

Figure C.10. Peak SDR at 12.675 sec

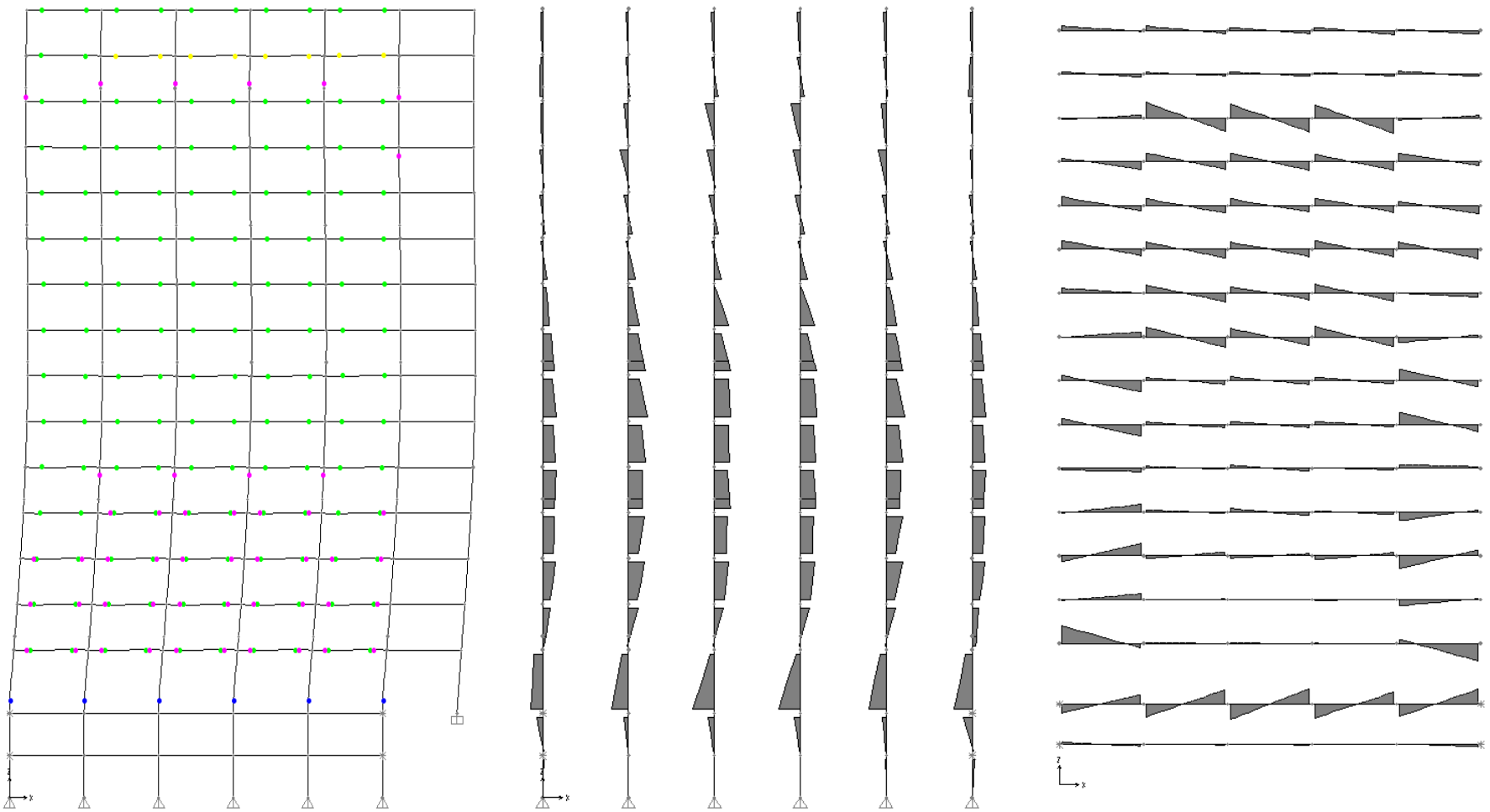

Figure C.11. At the end of excitation at 40 sec

SDR 6%

Peak SDR -> 2nd story

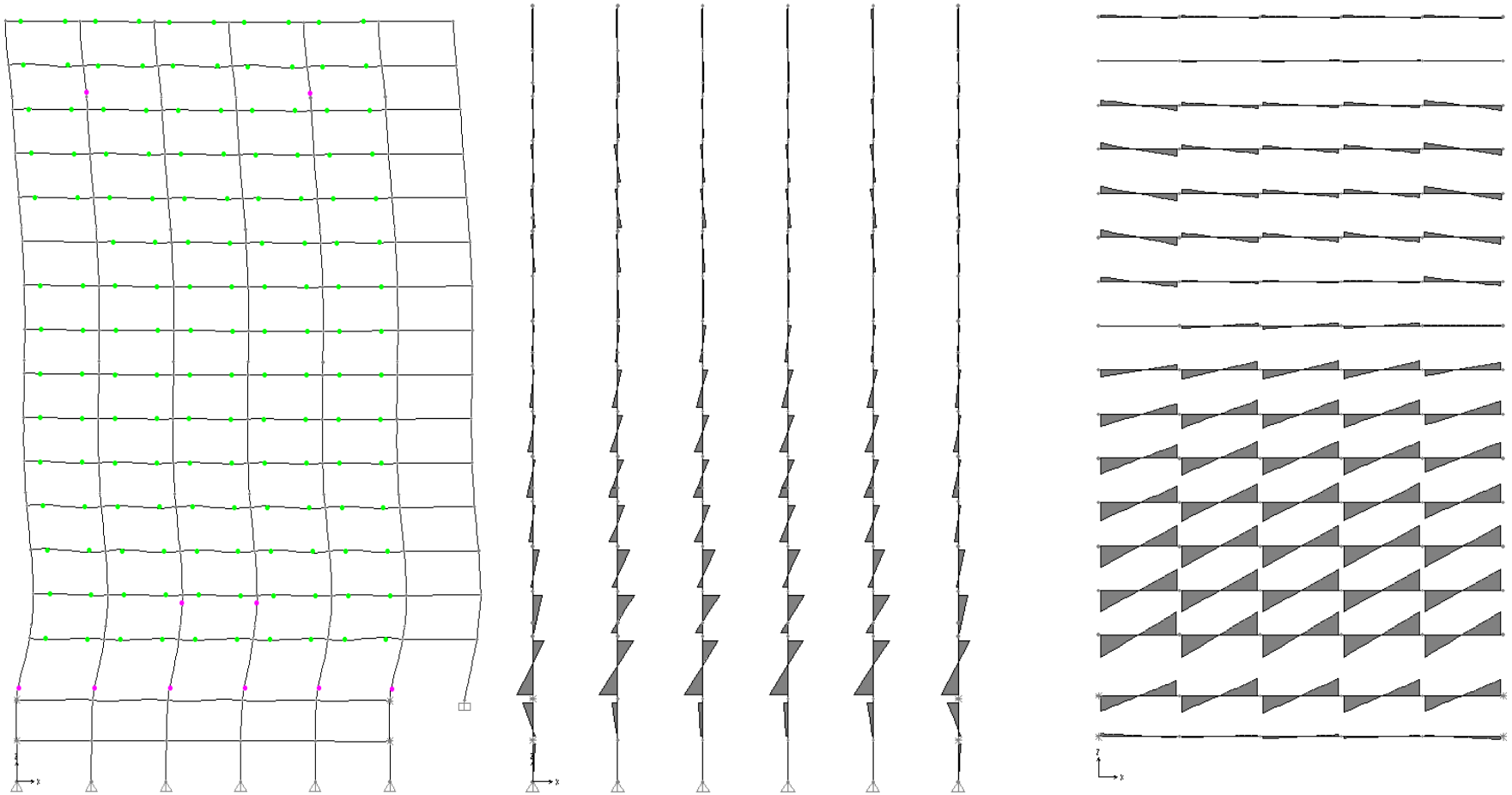

Figure C.12. 2nd set of plastic hinge formation on 2nd story columns at 6 sec

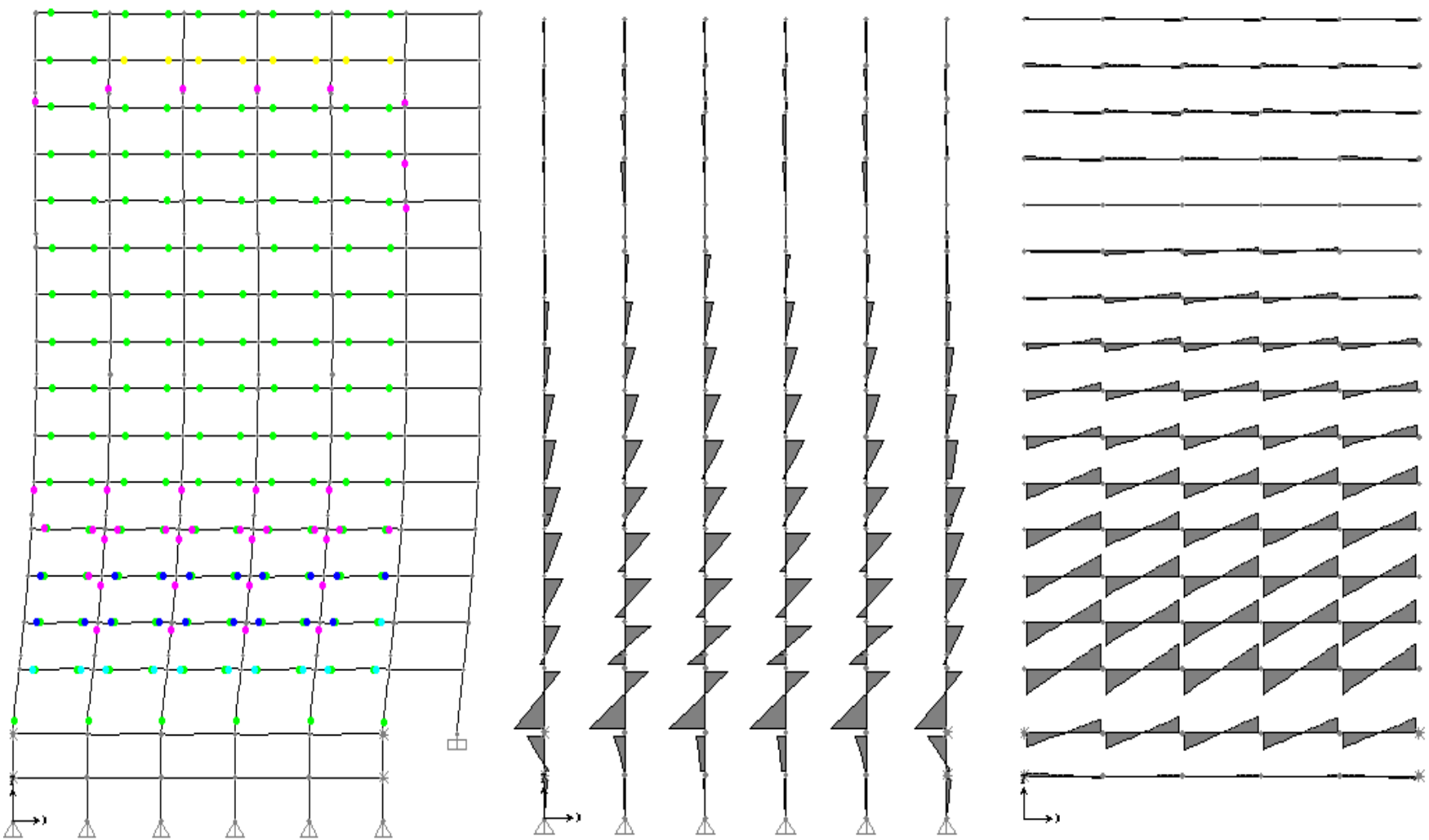

Figure C.13. Peak SDR at 12.73 sec

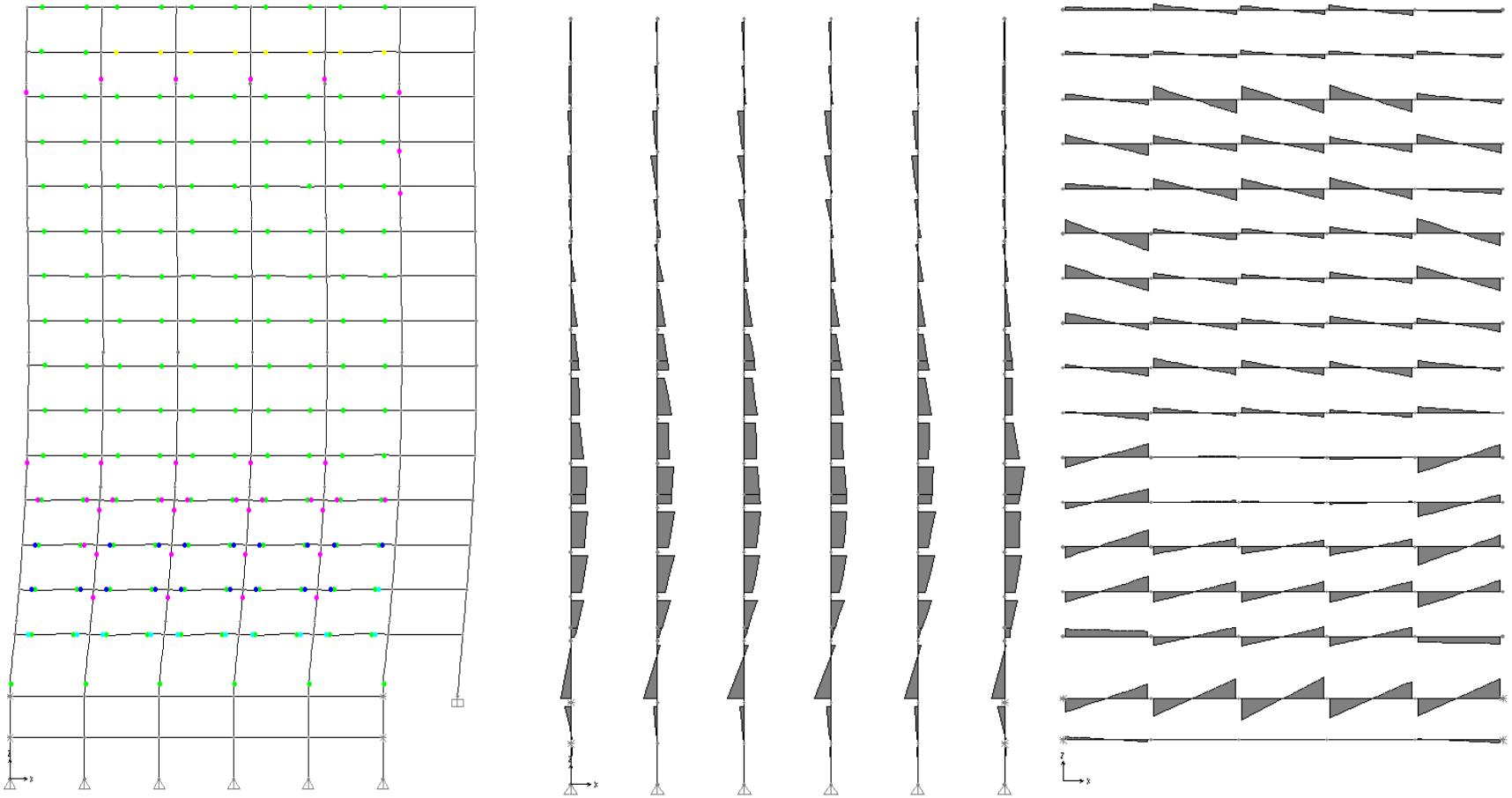

Figure C.14. At the end of excitation at 40 sec